TIBIOFEMORAL CONTACT AREAS AND CONTACT FORCES IN HEALTHY AND OSTEOARTHRITIC SUBJECTS

by

Ali ZEIGHAMI

MANUSCRIPT-BASED THESIS PRESENTED TO ÉCOLE DE TECHNOLOGIE SUPÉRIEURE IN PARTIAL FULFILLMENT OF THE REQUIREMENTS FOR THE DEGREE OF DOCTOR OF PHILOSOPHY Ph.D.

MONTREAL, 27 JUNE, 2018

ECOLE DE TECHNOLOGIE SUPÉRIEURE
UNIVERSITÉ DU QUÉBEC

BOARD OF EXAMINERS (THESIS PH.D.)

THIS THESIS HAS BEEN EVALUATED

BY THE FOLLOWING BOARD OF EXAMINERS

Prof. Rachid Aissaoui, Thesis Supervisor
Génie de la production automatisée, École de technologie supérieure

Prof. Raphaël Dumas, Thesis Co-supervisor
IFSTTAR, Université Claude Bernard Lyon 1

Prof. Yvan Petit, President of the Board of Examiners
Génie de la production automatisée, École de technologie supérieure

Prof. Jacques De Guise Member of the Jury
Génie de la production automatisée, École de technologie supérieure

Prof. Maxime Raison, External Evaluator
Département de génie mécanique, École Polytechnique de Montréal

THIS THESIS WAS PRENSENTED AND DEFENDED

IN THE PRESENCE OF A BOARD OF EXAMINERS AND PUBLIC

MAY 31ST, 2018

AT ÉCOLE DE TECHNOLOGIE SUPÉRIEURE

ACKNOWLEDGMENT

First, I would like to thank the members of the jury for having accepted to evaluate my manuscript and attend my defense.

I am sincerely grateful to Prof. Rachid Aissaoui for his continuous support, positive attitude which gave me the courage and confidence to persevere and progress in my research. Thank you for sharing with me your scientific expertise and your human qualities. My sincere gratitude to Prof. Raphael Dumas for his thoroughness and resourcefulness which helped me think in different perspectives and widen my horizons. Accomplishing this thesis would not have been possible without the assistance and feedback from both my supervisors.

I wish to thank Prof. Jacques de Guise, Prof. Nicola Hagemeister, Dr. Frédéric Lavoie for our fruitful collaboration on tibio-femoral contact zone project. An extra thanks to Jacques, Nicola, and Rachid for creating such an amazing environment of research and collaboration in Laboratoire de recherche en imagerie et orthopédie (LIO).

A special thanks to Gerald, Benoit, and Pierre-Oliver who crucially helped me on the technical aspects of this work and shared their valuable expertise with me. I am thankful to all members of LIO, especially Maria, Amir, Lulu, Thierry, Cheng, Michele, Julien, Lauranne, and Yousef. Working with such a smart, hard-working, and friendly group of people has been an amazing experience for me.

This dissertation is dedicated to my parents, Fatemeh and Yousef, who have always put my preference and comfort before theirs. No words can describe how much I love and respect you. Thank you to my brothers, Reza and Morteza for their precious moral support. I also wish to thank my parents-in-law, Sedigheh and Jamshid, for all the motivation and kind words I received from them. I am very lucky to have you all in my life.

A very special thank to the love of my life, Sara, who has been a great companion. Beside you, I always feel proud, happy, and strong. You had a significant contribution ($p<0.001$) to this accomplishment. Thank you for always being there for me!

Finally, I would like to thank the organizations that funded this Ph.D., NSERC, MITACS, the CRCHUM, and the École de Technologie Supérieure.

LES ZONES ET LES FORCES DE CONTACT TIBIO-FÉMORAL CHEZ LES SUJETS SAINS ET GONARTHROSIQUES

Ali ZEIGHAMI

RÉSUMÉ

La gonarthrose est un type courant d'incapacité musculo-squelettique, en particulier chez les personnes âgées. Des forces de contact excessives sur l'articulation, ou sur une partie spécifique des surfaces articulaires (par exemples sur le compartiment médial), ainsi que le déplacement des forces de contact vers les régions qui ne sont pas adaptées aux charges sont les facteurs mécaniques qui peuvent provoquer la gonarthrose. Par conséquent, il est crucial de comprendre les différences de ces paramètres mécaniques chez les sujets gonarthrosiques par rapport aux sujets sains. Le but de cette étude était de comparer les localisations des points de contact tibiofémoraux et les forces de contact chez les sujets gonarthrosiques et sains et d'examiner si les localisations des points de contact influencent la distribution des forces de contact dans l'articulation dans ces deux groupes.

La localisation des points de contact tibiofémoraux chez 10 sujets sains et 9 sujets gonarthrosiques au cours d'un mouvement de squat a été mesurée à l'aide d'une série d'images radiographiques biplanes. Une méthode manuelle de reconstruction et recalage 3D multi-vues a été utilisée pour reconstruire la forme et la position des os dans différentes positions et un calcul pondéré de la carte des distances os-à-os a été appliqué pour estimer la localisation des points de contact. Les résultats ont montré que les emplacements des points de contact des sujets gonarthrosiques sur les deux compartiments médial et latéral étaient décalés médialement par rapport aux emplacements du groupe sain. Dans les deux groupes, les points de contact ont montré une excursion postérieure sur le compartiment médial et des excursions postérieures et latérales sur le compartiment latéral. L'excursion sur le compartiment latéral était plus petite chez les sujets gonarthrosiques.

Afin d'estimer les forces de contact tibiofémorales, un modèle musculo-squelettique du membre inférieur avec l'intégration des points de contact personnalisés a été mise en œuvre. Le modèle estime les forces de contact pendant la marche aux points de contact spécifiques au sujet, tels que définis pendant le mouvement de squat. Le modèle de l'articulation fémoro-tibiale a ainsi été reformulé de telle sorte que les contraintes de l'articulation correspondent à la superposition des points de contact personnalisés tibial et fémoral en fonction de l'angle de flexion du genou. Les contraintes proposées sont adaptables aux points de contact dérivés des modèles articulaires classiques (par exemple, des mécanismes parallèles) ou ceux mesurés expérimentalement à partir des techniques d'imagerie 3D (par exemple, la fluoroscopie). Les forces de contact estimées à l'aide des points de contact personnalisés ont été comparées à celles estimées à partir des modèles classiques de l'articulation du genou chez 10 sujets sains. Les résultats ont montré que l'impact de la personnalisation des points de contact sur les forces de contact est très variable entre les sujets et que les déplacements des points de contact seuls

ne peuvent prédire la distribution des forces de contact entre les compartiments médial et latéral.

Pour évaluer la contribution des points de contact à la distribution des forces de contact, le modèle musculo-squelettique du membre inférieur avec les trajectoires de points de contact personnalisées a été utilisé pour estimer les forces de contact médiales et latérales de 12 gonarthrosiques et 10 sujets sains. Les forces de contact chez les sujets sains étaient légèrement plus élevées que chez les sujets gonarthrosiques. Cependant, aucune différence statistiquement significative n'a été notée dans les pics de force de contact médiaux, latéraux ou totaux. Les résultats d'une analyse de régression linéaire ont montré que le moment d'adduction du genou et le moment de flexion du genou étaient les principaux contributeurs au ratio de force de contact entre médial et total dans les deux groupes. Selon l'emplacement du point de contact dans deux directions anatomiques, seul l'emplacement du point de contact médial dans la direction médiale/latérale a eu une contribution significative au ratio de force chez les sujets gonarthrosiques. Cette étude a montré que le mécanisme de distribution de la force de contact dans l'articulation était différent dans les articulations arthrosiques où, contrairement aux personnes en bonne santé, l'emplacement du point de contact avait une contribution significative. De plus, le moment de flexion du genou a eu une plus grande contribution que le moment d'adduction du genou, alors que chez les sujets sains, le moment d'adduction du genou était le facteur le plus important.

Mots-clés : gonarthrose, points de contact tibiofémoraux, modèle musculo-squelettique du membre inférieur, forces de contact tibiofémoraux, distribution des forces de contact.

TIBIOFEMORAL CONTACT AREAS AND CONTACT FORCES IN HEALTHY AND OSTEOARTHRITIC SUBJECTS

Ali Zeighami

ABSTRACT

Knee osteoarthritis (OA) is a common type of musculoskeletal disability, particularly among the elderly population. Excessive contact forces on the joint, or on specific parts of it (e.g. medial compartment), or shifting the contact forces to the regions that are not adapted to loading are the mechanical factors which can trigger OA. Therefore, it is crucial to understand the differences of these mechanical parameters in OA subjects with respect to the healthy ones. The aim of this study was to the compare the tibiofemoral contact point locations and the contact forces in OA and healthy subjects and examine if the contact point locations influence the contact force sharing in both groups.

The tibiofemoral contact point locations in 10 healthy and 9 osteoarthritic (OA) subjects during a weight-bearing squat was measured using stand-alone biplane X-ray images. A manual multiple view 3D reconstruction/registration method was used to reconstruct the bones in different squat postures from the biplane radiographs and a weighted center of bone-to-bone proximity was applied to estimate the contact point locations. Results showed that the contact point locations of the OA subjects on the medial and lateral compartments were shifted medially compared to the healthy group. In both groups, contact points showed a posterior excursion on the medial compartment and posterior and lateral excursions on the lateral compartment, where the excursion on the lateral compartment was smaller in OA subjects.

To estimate the tibiofemoral contact forces, a custom musculoskeletal model of the lower limb with the integration of personalized contact points was provided to estimate contact forces at subject-specific contact points during gait. The tibiofemoral joint model was reformulated so that the constraints of the joint were formed by the superimposition of the personalized tibial and femoral contact points. The suggested constraints are adaptable to the contact points derived from the classical joint models or those experimentally measured from the 3D imaging techniques. The estimated contact forces estimated using the personalized contact points were compared to those estimated from the classical knee joint models in 10 healthy subjects. Results showed that the impact of personalization of contact points on the contact forces is very variable among the subjects and the shifts of the contact points alone cannot predict the distribution of contact forces in the medial and lateral compartments.

To evaluate the contribution of contact point locations to the contact force distribution the musculoskeletal model of the lower limb with the personalized contact point trajectories were used to estimate the medial and lateral contact forces of 10 healthy and 12 OA subjects. The contact forces in healthy subjects were slightly higher compared to the OA subjects. However, no statistically significant difference was noted in the peaks of medial, lateral or total contact forces. The regression analysis results showed that the knee adduction moment and knee flexion moment were the main contributors to the medial-to-total contact force ratio (MR) in

both groups. From the components of the contact point location, the medial contact point location in medial/lateral direction had a significant contribution to the MR in OA subjects. This study showed that the mechanism of load distribution was different in OA joints where contrary to the healthy ones the contact point location was a significant contributor to MR. In addition, the knee flexion moment had a higher contribution to MR than the knee adduction moment whereas in healthy subjects the knee adduction moment was the most significant contributor to the MR.

Keywords: osteoarthritis, tibiofemoral contact point locations, musculoskeletal model of the lower limb, tibiofemoral contact force, distribution of the contact forces.

TABLE OF CONTENTS

LIST OF TABLES

Page

LIST OF FIGURES

Page

LIST OF ABBREVIATIONS

OA	Osteoarthritis
ACLD	Anterior cruciate ligament deficiency, or deficient
ACLR	Anterior cruciate ligament reconstructed
MCL	Medial collateral ligamen
LCL	Lateral collateral ligament
ACL	Anterior cruciate ligament
PCL	Posterior cruciate ligament
ECM	Extracellular matrix
K-L	Kellgren-Lawrence OA grading system
NSAID	Nonsteroidal anti-inflammatory drugs
MRI	Magnetic resonance imaging
CT-scan	Computed tomography-scan
RMS	Root mean square
SSM	Statistical shape model
MSK	Musculoskeletal
TKA	Total knee arthroplasty
BW	Body weight
DOF	Degrees of freedom
MR	Medial-to-total contact force ratio
KFM	Knee flexion moment
KAM	Knee adduction moment
Fmed	Medial contact force
CPz	Medial/lateral contact point location
CPx	Anterior/posterior contact point location
CPzmed	Medial/lateral contact point location on the medial compartment
CPzlat	Medial/lateral contact point location on the lateral compartment
CPxmed	Anterior/posterior contact point location on the medial compartment
CPxlat	Anterior/posterior contact point location on the lateral compartment
EMG	Electromyography

FE	Finite element
CRCHUM	Centre de recherche, centre hospitalier de l'Université de Montréal
ÉTS	École de technologie supérieure de Montréal
CP	Contact point
ANOVA	Analysis of variance
BMI	Body mass index (BMI)
KOOS	Knee injury and Osteoarthritis Outcome Score
LCP	Linear CP trajectory
SPP	Sphere-on-plane trajectory
PCP	Personalized CP trajectory
RF	Rectus femoris
VL	Vastus lateralis
VM	Vastus medialis
TA	Tibialis anterior
GM	Gastrocnemius medialis
GL	Gastrocnemius lateralis
ST	Semitendinosus
BF	Biceps femoris
PSA	Power spectrum analysis
BSIP	Body segment inertial parameters

LIST OF SYMBOLS

$\mathbf{E}_{3\times3}$	Identity matrix
i	Index for segment
j	Index for skin or virtual marker (in inverse kinematics) or muscle (in inverse dynamics)
$\mathbf{u}_i$, $\mathbf{v}_i$, $\mathbf{w}_i$	Anterior, superior and lateral axes of the segment
$\mathbf{r}_{P_i}$, $\mathbf{r}_{D_i}$	Positions of the proximal (P_i) and distal (D_i) endpoints
$\left(P_i, \mathbf{u}_i, \underbrace{\left(\mathbf{r}_{P_i} - \mathbf{r}_{D_i}\right)}_{\mathbf{v}_i}, \mathbf{w}_i\right)$	Non-orthonormal segment coordinate system
$(P_i, \mathbf{X}_i, \mathbf{Y}_i, \mathbf{Z}_i)$	Orthonormal segment coordinate system
$\mathbf{B}_i$	Transformation matrix from the non-orthonormal to the orthonormal segment coordinate system
α_i, β_i, γ_i	Constant angles between the axes of the non-orthonormal segment coordinate system
L_i	Segment length (between proximal and distal endpoints)
$\mathbf{Q}_i$	Natural coordinates (2 position and 2 direction vectors)
$\mathbf{\Phi}_i^r$	Rigid body constraints
$\mathbf{r}_{M_i^j}$, $\mathbf{r}_{V_i^j}$	Position of skin or virtual marker (M_i^j or V_i^j)
$(n_i)_u$, $(n_i)_v$, $(n_i)_w$	Coordinates in the non-orthonormal segment coordinate system
$\mathbf{N}_i$	Interpolation matrix
$\mathbf{\Phi}^k$	Kinematic constraints
θ	Tibiofemoral extension/flexion angle
$\mathbf{\Phi}^m$	Driving constraints
$\mathbf{G}$	Generalised mass matrix
$\mathbf{Q}$, $\dot{\mathbf{Q}}$, $\ddot{\mathbf{Q}}$	Vectors of generalized positions, velocities and accelerations for all segments
$\mathbf{K}$	Jacobian matrices of the constraints

$\boldsymbol{\lambda}$	Vectors of Lagrange multipliers
$\mathbf{R}$	Vector of generalized ground reaction forces and moments
$\mathbf{Z}_{\mathbf{K}_2^T}$	Orthogonal basis of the null space of $\mathbf{K}_2^T$(corresponding to a subset of the constraints)
$\mathbf{P}$	Vector of generalized weights
$\mathbf{L}$	Matrix of generalized muscular lever arms
$\mathbf{F}$	Vector of musculo-tendon forces
f, J	Objective functions in inverse kinematics and inverse dynamics
$\mathbf{W}$	Matrix of optimisation weights

INTRODUCTION

Knee osteoarthritis (OA) is a degenerative joint disease characterized by loss or deterioration of articular cartilage. It happens when the cartilage is unable to normally repair itself resulting in the breakdown of the cartilage tissue and the subchondral bone. OA primary clinical manifestations include swelling, pain, stiffness, and decreased range of motion. Known treatments are not effective to stop or slow down OA progression, but they rather address the symptoms of the disease. OA affects more than 10% of Canadian adults and is one of the main causes of chronic musculoskeletal disabilities worldwide. As the population ages, a growing number of OA disability is expected in the future.

There are two types of factors which are known to be responsible for OA initiation and progression: systematic factors such as gender, age, genetics, and racial characteristics and biomechanical factors such as joint overloading, obesity, joint deformity, and joint injury. Systematic factors are believed to establish the foundation of cartilage properties whereas the biomechanical factors determine the location and severity of cartilage degeneration (Arokoski 2003). Biomechanical abnormalities can be detrimental to the tissue by exposing the cartilage to excessive contact forces or by changing the contact point locations from the frequently loaded regions to the regions that are not usually loaded. Subtle kinematic abnormalities triggered by conditions such as anterior cruciate ligament deficiency (ACLD), shift the contact point locations from the frequently loaded regions and causes cartilage thinning which is an early sign of OA initiation (S Koo et al., 2007).

High levels of contact forces could also damage the cartilage. While some level of repetitive loading is required for the nutrient distribution through the cartilage and regeneration of the tissue structure, excessive contact forces could damage cartilage by killing the cartilage living cells (chondrocytes), which regenerate and maintain the tissue structure (Clements et al., 2001). In the knee joint, the medial compartment carries a bigger proportion of the contact forces and is more likely to be affected by OA than the lateral compartment. The larger forces on the medial compartment are due to the line of ground reaction force which falls medial to

the knee joint center creating an external adduction moment in the frontal plane. However, studies have argued that other parameters such as knee flexion moment, knee frontal plane alignment, gait speed have also a significant contribution to the contact force distribution (Adouni et al., 2014; Esculier et al., 2017; Kumar et al., 2013; Kutzner et al., 2013). In addition, since the external knee moments are counterbalanced partially by the medial and lateral contact forces, the contact point locations would also contribute to the contact force distribution (Lerner et al., 2015; Saliba et al., 2017b).

According to what was discussed above, the knee contact point locations and contact forces are the two main biomechanical parameters in understanding the pathomechanics of OA. Thus, it is crucial to understand the patterns of contact points and contact forces and also, the relationship between these two parameters in OA and healthy subjects. This latter requires knowledge of the personalized contact points and the inclusion of these personalized contact points in the contact force estimations. Until now, the literature has not provided a quantitative description of the contact points in OA subjects in comparison with healthy controls. Moreover, the attempts to personalize the knee kinematic models in OA subjects does not address directly the contact points (Clément et al., 2017; Lerner et al., 2015). None of knee kinematic models introduced in musculoskeletal model currently allow evaluating the impact of the pathology distinct patterns of contact points on the contact force estimations.

The general objective of this thesis is to evaluate the tibiofemoral contact locations and the contact forces in OA subjects and to analyze the differences with respect to the healthy subjects. Chapter 1 provides an introduction on the function and anatomy of the knee joint, the mechanisms of OA and discusses the current body of the literature on the tibiofemoral contact points and contact forces in normal and pathological knees and the methodological aspects of estimating these parameters and their limitations. Chapter 2 lists the problematics, aims and specific objectives of the current work. Chapter 3 introduce a method to estimate the personalized contact points during a weight-bearing squat activity from a set of biplane X-ray images and a 3D/2D registration techniques. The contact point locations in OA and healthy subjects are compared to examine the existence of a shift in the contact point locations of OA

joints with respect to the healthy ones. Chapter 4 provides the preliminary results on evaluating the effectiveness of a valgus knee orthosis in changing the contact point locations of severe OA subjects during squat. This gives a clinical example of the use of contact point locations as a novel metric for assessing the effectiveness of the interventions planned to improve the ambulatory function of subjects with OA. Chapter 5 introduces a method for the integration of the personalized contact points in the musculoskeletal model of the lower limb when estimating the contact force. Chapter 6 uses the musculoskeletal model with the personalized contact points to compare the medial and lateral contact forces in OA and healthy subjects. We also evaluated the contribution of contact point trajectories in the medial-to-total contact force ratio in the knee joint and determined the parameters with the highest contribution in OA and healthy subjects. Chapter 7 presents a general discussion summarizing the results of the four studies and remind the various limitations of the project and makes recommendations for the further projects. Finally, a general conclusion with the principal contributions ends this thesis.

CHAPTER 1

LITERATURE REVIEW

1.1 Structure and anatomy of the knee joint

The knee represents one of the most voluminous joints and surely one of the most complex of the human body. It is composed of two main joints, one being the junction between the two main long bones of the lower limb, i.e. the femur and the tibia (tibiofemoral joint), and the second between the femur and the patella (patellofemoral joint) (Figure 1-1). Although these two articulations are anatomically and functionally related, this project will focus on the tibiofemoral articulation.

1.1.1 Structure and components of the tibiofemoral joint

The tibiofemoral joint is a double load carrying joint. The articulation (Figure 1-2) is composed of the femoral and tibial condyles which are located at the medial distal and lateral distal ends of the femur and at the proximal medial and proximal lateral ends of the tibia respectively. The convex shape of the femoral condyles articulates with the slightly concave surface of the tibial condyles granting significant mobility to the knee in the six degrees of freedom. The articulating surfaces are covered by a thin layer of articular cartilage allowing an efficient lubrication. The low congruence of the joint surfaces leaves limited contact surface that may be the cause of high contact pressures. This is, however, attenuated by the presence of two menisci attached to the peripheral edges of the tibial condyles. The crescent-shaped menisci with fibrocartilaginous structure, make it possible to distribute articular pressures over a larger contact area. The medial meniscus is narrow and long in shape of a "c" while the lateral meniscus is wider as well as shorter in the shape of an "0" (Figure 1-3). The menisci are slightly deformable structures during movement, but they remain firmly anchored at the joint surfaces by the meniscal attachments.

A set of ligaments provide stability to the tibiofemoral joint. Medial collateral ligament (MCL), Lateral collateral ligament (LCL), Anterior cruciate ligament (ACL), and Posterior cruciate ligament (PCL) are the four main knee joint ligaments.

Collateral ligaments are necessary to prevent rotation in the frontal plane around the anteroposterior axis when the knee is in extension, while cruciate ligaments help to prevent anteroposterior translation of the articular surfaces by connecting the tibia and femur.

Meniscus and ligament pathology are in some cases primary to OA. A long-term change in the dynamics of knee loading due to ligament or meniscus injury is associated with a very high risk of OA development (Lohmander et al., 2007).

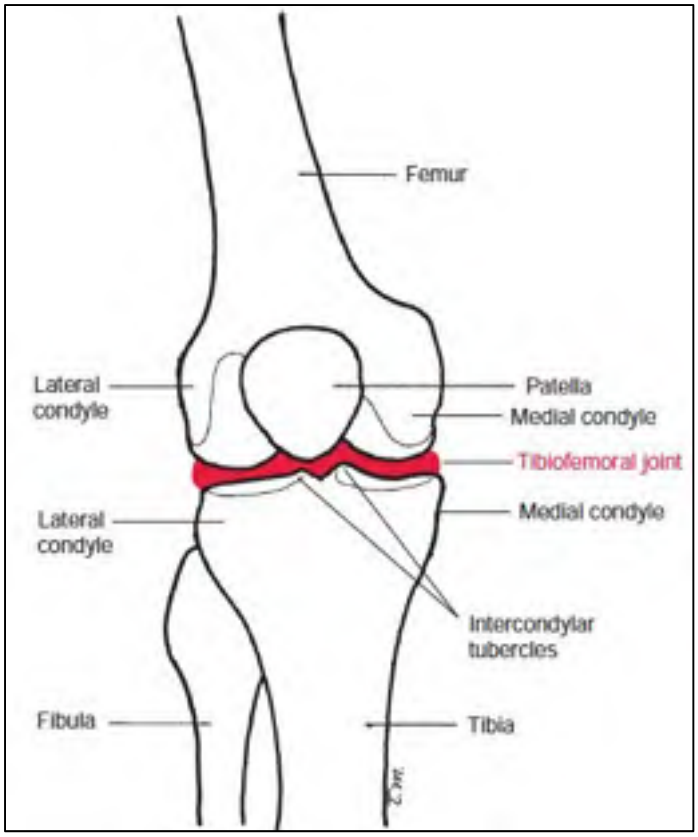

Figure 1-1 Anatomy of the knee and the tibiofemoral joint. Figure adapted from Norkin et al. (2016).

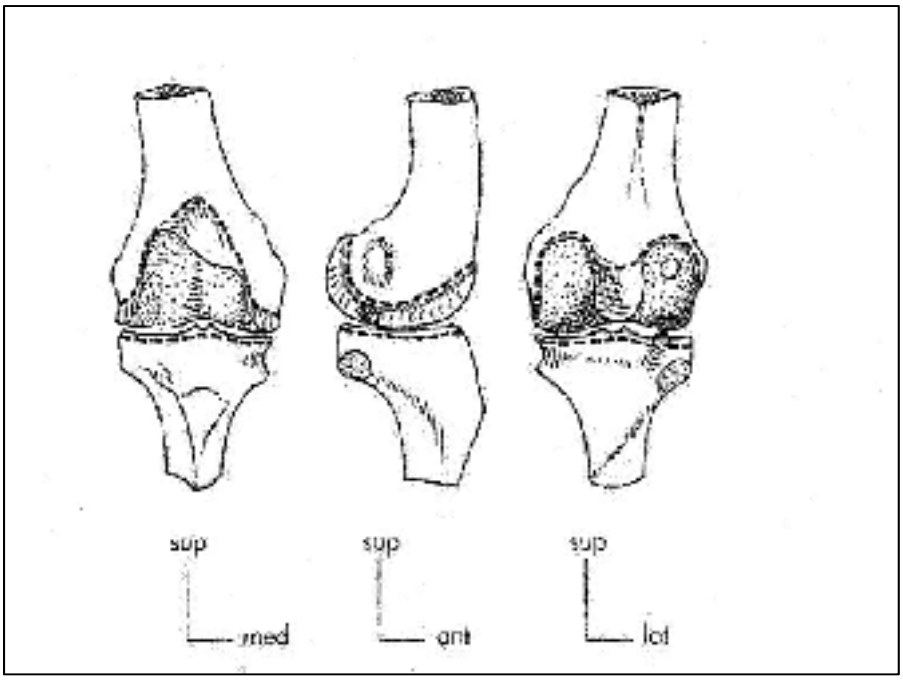

Figure 1-2 Tibiofemoral articulation viewed from anterior (left) lateral (middle) and posterior (right) directions, allowing to illustrate the shape of the femoral and tibial condyles, adapted from Dufour (2007).

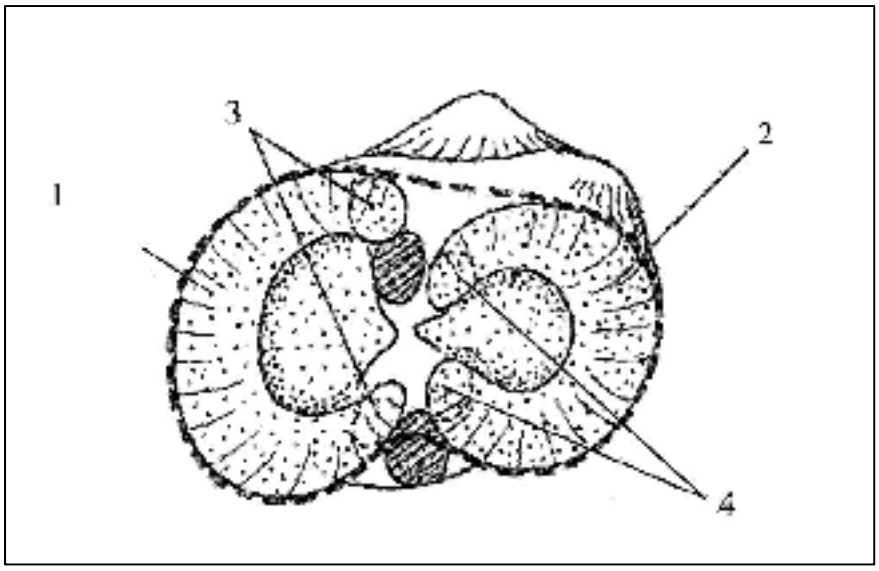

Figure 1-3 Top view of the tibial plateau showing the shape of the medial (1) and lateral (2) menisci and their corresponding attachments (3,4). The figure is adapted from (Dufour, 2007).

1.1.2 Structure and composition of articular cartilage

Knee articular cartilage is a thin layer of hyaline cartilage specialized to provide a smooth and efficient lubrication between the joint surfaces. This tissue has no nerves, blood vessels, or lymphatics. It rather consists of an extracellular matrix (ECM) structure in which a type of cells called chondrocytes is scarcely distributed. The ECM structure is principally formed from collagen and proteoglycans and retains a substantial amount of water (Sophia Fox et al., 2009). This water is gently released under pressure and provides cartilage its unique lubrication properties under dynamic loading. The components of the cartilage are briefly described in the following.

1.1.2.1 Water

Water accounts for about 65 % - 80% of the wet weight of articular cartilage in deep and superficial zones respectively (Baykan, 2009). Water has two main roles in the cartilage being the distribution of nutrients and giving special mechanical properties to the cartilage. Unlike other organs and tissues, cartilage is devoid of nutrient carrying blood vessels. The nutrients to chondrocyte cells are transported through the flow of fluid in and out of the cartilage. Articular cartilage has the ability to withstand significant loads while maintaining minimal friction thanks to the interstitial fluid in its structure. Under loading, the fluid inside the cartilage which cannot escape easily from the surface is pressurized and transfers a major proportion of the load. Meanwhile, the water flow minimizes the solid-to-solid friction and makes the cartilage very efficient in lubrication.

1.1.2.2 Collagens

Type II collagen molecules represent ~75% of the dry weight of the cartilage. Collagen molecules form small fibrils and larger fibers distributed throughout the cartilage with depth-dependent dimension and orientation. The specific architecture of the collagen fibrils

contributes to the stability of the ECM and provides cartilage with important shear and tensile properties. In the superficial zone, collagen fibrils are packed tightly and aligned parallel to the surface to better resist shear and tensile forces imposed by articulation. They are oriented obliquely in middle zone and perpendicularly in the deep zone to provide the highest resistance to the compressive forces (Figure 1-4).

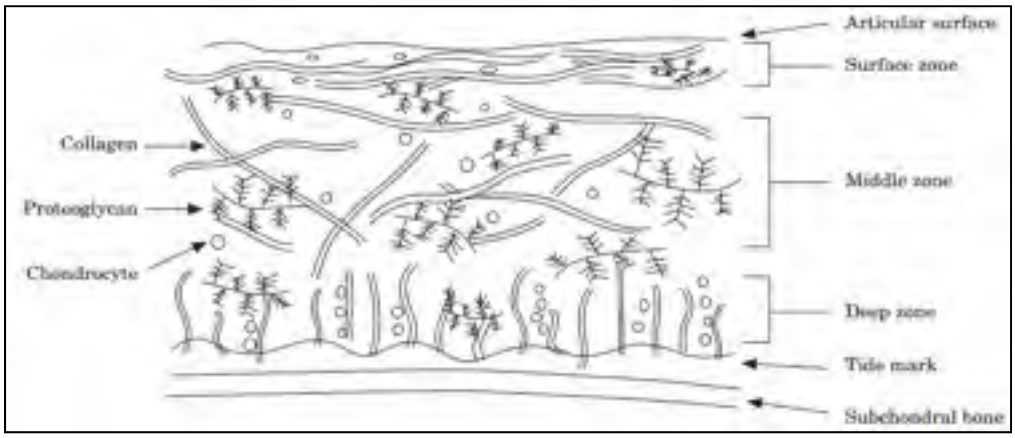

Figure 1-4 Scheme of articular cartilage structure, adapted from Fox et al. (2009)

1.2 Cartilage loading and OA progression

Progression of OA occurs during a long period of time. However, due to the lack of nerves in the cartilage tissue the symptoms appear towards the end stages. At this point, OA cannot be stopped or reversed. Therefore, it is crucial to understand the initiation and progression mechanisms. These mechanisms are largely unknown. But, it is generally thought that the initiation and progression of OA are associated to the mechanical properties and structure of cartilage on one hand and the joint loading on the other hand (Herzog et al., 2006).

1.2.1 Mechanical loading effect on cartilage

Mechanical loading has a double effect on the cartilage tissue. Given the nature of nutrient distribution with the fluid flow throughout the cartilage, loading has a great impact on the

synthesis of proteoglycan molecules. Normal cyclic loading of the cartilage promotes proteoglycan synthesis and makes it stiffer. It is reported that a cartilage regularly exposed to some levels of stress contains a higher amount of proteoglycans (Arokoski et al., 2000). On the other hand, continuous high-stress levels in the cartilage diminish proteoglycan synthesis and result in damages to the tissue through necrosis. Clements et al. (2001) suggested a threshold over which the chondrocytes would dye under cyclic loading. In a bovine cartilage experiment, they reported this threshold to be 6 Mpa. Over this threshold, the chondrocyte viability was negatively correlated to the magnitude of applied stress (Figure 1-5).

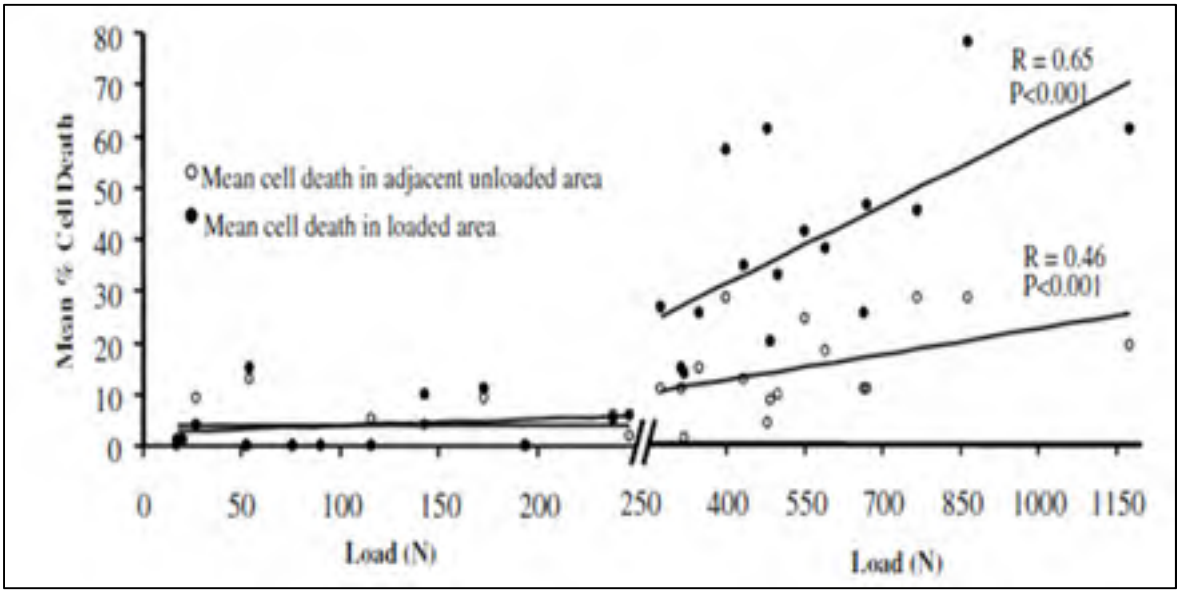

Figure 1-5 cyclic loading over 6 Mpa kills the chondrocytes in bovine cartilage. Figure adapted from (Clements et al., 2001)

Decreased proteoglycan concentration, disorganization of the collagen network, and softening of cartilage are the early signs of OA and cartilage injury (Figure 1-6). It is believed that once the integrity of the superficial zone of cartilage is lost, the underlying tissue would experience abnormally high strains. Thereafter, the degenerations would extend into the deeper zones of cartilage (Figure 1-6) (Arokoski et al., 2000). In the initial stage, the cartilage loses volume and becomes more vulnerable to damage under excessive load. The subchondral bone thickens

and fluid-filled cysts may appear near the joint. Eventually, broken bone or cartilage particles may float in the joint triggering further mechanical damage.

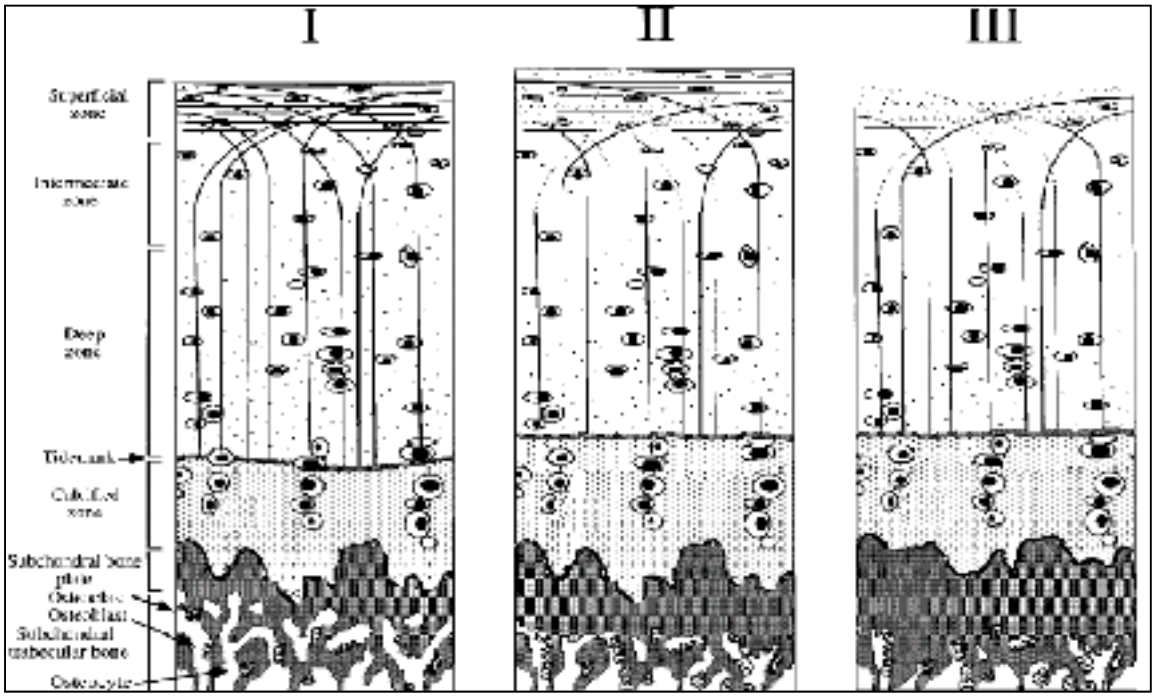

Figure 1-6 Articular cartilage structure. Chondrocytes (ovals), proteoglycans (dots) and collagen fibrils (curved lines). The normal histology of the cartilage (left). The onset of OA (middle): Depletion of proteoglycans and disorganization of collagen fibrils in the superficial zone. Point of no return (right): Fibrillation of the superficial zone, additional loss of proteoglycans, and subchondral bone sclerosis, adapted from (Arokoski et al., 2000).

1.2.2 Mechanical behavior of cartilage as an indicator of OA

Following the histopathological and structural changes of cartilage due to OA progression, its mechanical characteristics change as well. Softening of cartilage in the initial stage is reported in some papers. In a study on different parts of cartilage collected during total knee arthroplasty, Kleemann et al. (Kleemann et al., 2005) found a meaningful correlation between OA severity and the reduction in the cartilage stiffness.

Other studies showed that in artificially made OA through ACL transaction shear, tensile, compressive and other mechanical behaviors of cartilage are considerably changed (Setton et

al., 1999). It indicates that the mechanical, structural, and histological changes of cartilage during OA are interrelated. The results indicated a relation between structural, mechanical and histological changes in all stages of the degeneration. With increasing grade, the cartilage stiffness, which is primarily influenced by the integrity of the extracellular matrix, decreases and so are other mechanical properties.

1.3 OA demonstrations and grading of the disease

Regarding the histopathological changes in cartilage different scoring and grading methods are presented to classify the development of disease (Collins, 1939; Mainil-Varlet et al., 2003; Mankin et al., 1971). A histopathological grade assessment guide is presented in Table 1-2 based on Pritzker's method (Pritzker et al., 2005) to indicate what generally represents the step by step OA progression in different stages.

The mainstay tool for diagnosis and monitoring of OA is plain radiography. Therefore, the classification of the disease is commonly performed using the manifestations observed in radiographic images. Kellgren-Lawrence (K-L) is among the most popular OA classification tools which describe the severity of OA based on a 0 to 4 grading system (Kellgren et al., 1957; Schiphof et al., 2008). The K-L grading system was used in this thesis to discriminate the severe OA subjects and healthy controls.

Table 1-1 Kellgren-Lawrence OA grading system and each grade characteristics. Adapted from Kohn et al. (2016).

Kellgren-Lawrence scale grades	***Characteristics***
Grade 0	No Joint space narrowing or reactive changes
Grade 1	Doubtful joint space narrowing, possible osteophytic lipping
Grade 2	Possible joint space narrowing, definite osteophytes.
Grade 3	Definite joint space narrowing, moderate osteophytes, some sclerosis, possible bone-end deformity
Grade 4	Marked joint space narrowing, large osteophytes, severe sclerosis, definite bone ends deformity

Table 1-2 Pritzker's histopathological grade assessment guide indicating the histopathological changes of cartilage during OA progression. Adapted from (Pritzker et al., 2005).

OA cartilage histopathology grade assessment—grading methodology

Grade (key feature)	Associated criteria (tissue reaction)
Grade 0: surface intact, cartilage morphology intact	Matrix: normal architecture Cells: intact, appropriate orientation
Grade 1: surface intact	Matrix: superficial zone intact, oedema and/or superficial fibrillation (abrasion), focal superficial matrix condensation Cells: death, proliferation (clusters), hypertrophy, superficial zone Reaction must be more than superficial fibrillation only
Grade 2: surface discontinuity	As above +Matrix discontinuity at superficial zone (deep fibrillation) ±Cationic stain matrix depletion (Safranin O or Toluidine Blue) upper 1/3 of cartilage ±Focal perichondronal increased stain (mid zone) ±Disorientation of chondron columns Cells: death, proliferation (clusters), hypertrophy
Grade 3: vertical fissures (clefts)	As above Matrix vertical fissures into mid zone, branched fissures ±Cationic stain depletion (Safranin O or Toluidine Blue) into lower 2/3 of cartilage (deep zone) ±New collagen formation (polarized light microscopy, Picro Sirius Red stain) Cells: death, regeneration (clusters), hypertrophy, cartilage domains adjacent to fissures
Grade 4: erosion	Cartilage matrix loss: delamination of superficial layer, mid layer cyst formation Excavation: matrix loss superficial layer and mid zone
Grade 5: denudation	Surface: sclerotic bone or reparative tissue including fibrocartilage within denuded surface. Microfracture with repair limited to bone surface
Grade 6: deformation	Bone remodelling (more than osteophyte formation only). Includes: microfracture with fibrocartilaginous and osseous repair extending above the previous surface

II. Grade = depth progression into cartilage.

1.4 Altered gait and anatomy characteristics in patients with OA

The gait differences in OA subjects has been the subject of previous studies. Symptomatic OA subjects experience pain performing daily activities. This may result in adopting compensating gait strategies to reduce joint loading and the resultant pain (Stauffer et al., 1977). Reduced range of knee flexion is a remarkable pattern in the gait of OA patients (Schnitzer et al., 1993; Stauffer et al., 1977). Kaufman et al. (2001) reported 6° reduced range of motion and significantly lower gait speed in OA patients. The stride characteristics were also altered in OA group. Stride length was significantly smaller in OA subjects whereas cadence increased with respect to healthy controls (Kaufman et al., 2001). Knee varus alignment is another typical feature in OA and is believed to make the joint more vulnerable to the adverse effects of obesity and joint overloading (Sharma et al., 2000).

External moments, and in particular adduction moment has been found to be associated with OA in many studies. Baliunas et al. (2000) observed increased peak of adduction moment in OA subjects. Adduction moment has been found to correlate with severity (Schnitzer et al., 1993) or progression (Miyazaki et al., 2002) of OA. Adduction moment was also found to be correlated with the bone density of the proximal tibia (Hurwitz et al., 2002) and the outcome of tibial osteotomy surgery (C. Prodromos et al., 1985; Wang et al., 1990). Knee flexion moments is also one of the altered characteristics of gait in OA subjects. The peak of knee flexion moment decreased in OA subjects with respect to healthy controls (Baliunas et al., 2000; Kaufman et al., 2001).

The mechanism behind the biomechanical alterations in OA is not fully understood. It is known that mitigating knee joint pain in some subjects can reverse some of these changes. For instance, following 4 weeks of treatment with nonsteroidal anti-inflammatory drugs (NSAID), the maximum adduction moment and quadriceps moment (measured on ergometer) increased due to the joint pain reduction (Schnitzer et al., 1993). However, some biomechanical alterations are attributed to the morphological changes such as joint space narrowing in OA knees which permanently change the configuration of the joint and, as a result, the dynamics of the joint. Relieving the pain, in this case, would not make a difference. In a study on medial

compartment OA subjects and healthy controls, Andriacchi et al. (2004) reported that the varus alignment and the adduction moment were similar between healthy and moderate OA subjects whereas they were significantly different in severe OA patients who had a remarkable joint space narrowing in the medial compartment. Andriacchi et al. (2004) hypothesized that the change in the varus alignment and the adduction moment are a result of the change in the morphology of the joint in severe OA.

1.5 Altered tibiofemoral contact point in patients with OA

Along with the morphological changes of the joint, the tibiofemoral joint surface interpositions change as well. It is assumed that the initiation of OA begins with a change in the contact locations of the joint to the regions where it is not frequently loaded (Andriacchi et al., 2004). This shift could follow a traumatic or chronic condition such as meniscus or ligament injury. Loading the regions that are not conditioned to carry high frequent loads is detrimental to the cartilage tissue resulting in fibrillation of the surface and further damage to the tissue. Surface fibrillation causes an increase in the surface friction which induces further damage to the cartilage and accelerates the progression of the disease (Figure 1-7). However, the experimental data supporting this hypothesis on the pathomechanics of the knee OA is scarce.

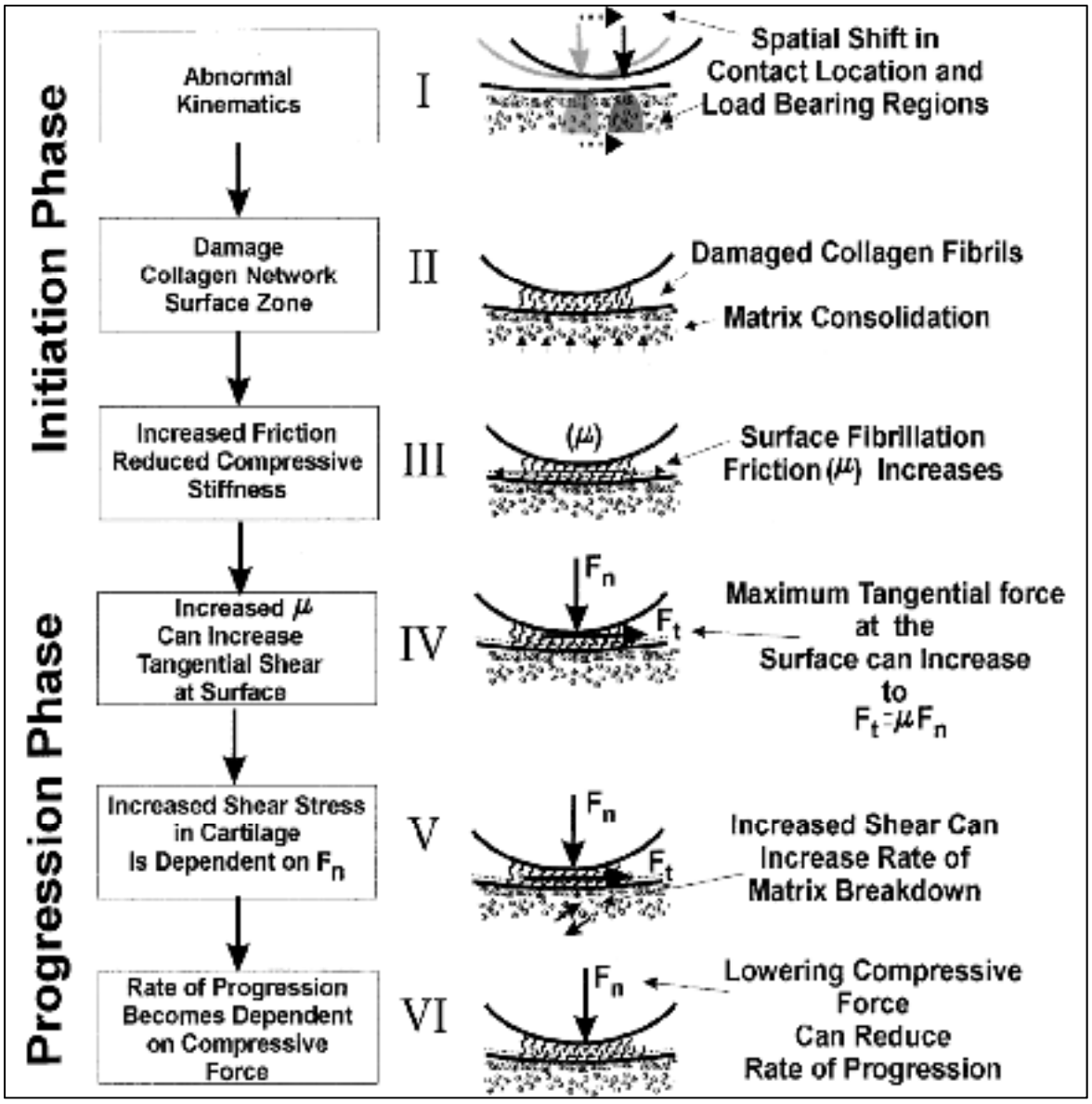

Figure 1-7 A hypothetical framework for the initiation and progression of OA. OA initiation begins with a change in the contact locations of the joint. Cartilage in the less loaded regions Show signs of damage and surface fibrillation under the higher-than-normal loading conditions. Increased friction due to damage to the cartilage causes more severe degeneration of the tissue stimulating the progression of the cartilage breakdown. Figure adapted from (Andriacchi et al., 2004)

Using dual fluoroscopy, Farrokhi et al. (2014) found that in OA subjects with self-reported instability the excursion and velocity of the medial compartment contact points were

significantly increased with respect to the healthy controls. In a later study, they showed that the increased velocity and excursion of contact points in OA group was associated with the increased frontal plane alignment. Increased contact point (CP) excursion in OA was therefore considered as a measure of mechanical instability of the affected joint (Farrokhi et al., 2016). In this regard, in the biomechanical analysis of the knee joint in OA, it is important to consider the configuration of the joint and the interaction of the articulating bones along with the other parameters of gait. This will help to better understand the parameters contributing to the pathomechanics of OA.

1.6 Tibiofemoral contact point estimation

Estimating the *in vivo* tibiofemoral contact points provides precious information that is valuable in understanding the initiation and progression mechanism of OA. It is hypothesized that the initiation of cartilage degeneration is triggered by a shift in the tibiofemoral contact point locations from the frequently loaded parts of the joint close to the tibial plateau centerlines towards the less loaded regions (T. P. Andriacchi, 2004). Positioning the contact point is also important in designing total knee arthroplasties and developing the customized or personalized musculoskeletal models (Lerner ZF, 2015 Feb 26).

Identification of joint contact parameters utilizing casting and pressure sensitive films are only practical in cadaver models (Ahmed et al., 1983; Walker et al., 1985). Magnetic resonance techniques normally scan the knee joint statically in supine posture and have technical limitations in studying naturally loaded joints and large ranges of motion (Johal et al., 2005; Yao et al., 2008). Therefore, 3D/2D registration techniques have been widely used to track the *in vivo* 3D motion of the bones in load-bearing conditions. The bone is generally reconstructed from magnetic resonance imaging (MRI) or computed tomography (CT)-scan with or without the cartilage layer, and then rigidly moved to match the 2D fluoroscopic or X-ray images recorded during movements. Tibiofemoral contact points are then estimated using the proximity of the articulating surfaces.

1.6.1 Reconstruction of subject-specific bone using imaging techniques

The geometry of the knee joint for analysis of the joint is usually reconstructed from a stack of images obtained from MRI or CT-scan of the joint. The MRI is typically preferred for the soft tissues reconstruction, whereas CT images are widely used for hard tissues i.e., bones (Kazemi et al., 2013). MRI does not emit ionizing radiation that makes it minimally detrimental to the patient. Both imaging methods provide segmentation accuracy with a root mean square (RMS) error below twice the pixel size. For a 1.5T MRI, this accuracy is less than 1mm. However, MRI is relatively costly, time-consuming in each acquisition and is normally performed only in supine position. CT-scan, on the other hand, exposes the subject to high levels of ionizing radiations making it potentially detrimental particularly in larger scale reconstructions such as the whole lower body.

1.6.2 Reconstruction of subject-specific bone using X-ray images

The radiographic images are the most clinically available data in assessing OA subjects and they show hard tissue boundaries with a very good resolution. The ability to reconstruct the 3D patient-specific surface model of a bone from a limited number of 2D X-ray images (2 or more) would be clinically valuable. Various manual, semi-automatic and automatic solutions were proposed for this purpose. One solution is using a statistical shape model of the bone and adapting it to the personalized biplane X-ray of the subject to approximate the individual 3D geometry (G. Zheng et al., 2009).

Another solution was proposed using EOS® system (EOS imaging, Paris, France) biplane X-ray images and a generic model of the bone. The EOS® system simultaneously captures 2 perpendicular images of the whole (or lower) body of standing subject in a single scan with a 1:1 vertical scaling. Generating the geometric models of the bone structures of the knee with the EOS® system requires segmenting the bone contour in the biplane radiographs (Chav et al., 2009). Then, a generic bone model is deformed semi-automatically until it is superimposed

on the contours segmented in the previous step (Thierry Cresson et al., 2010; Cresson et al., 2008) (Figure 1-9).

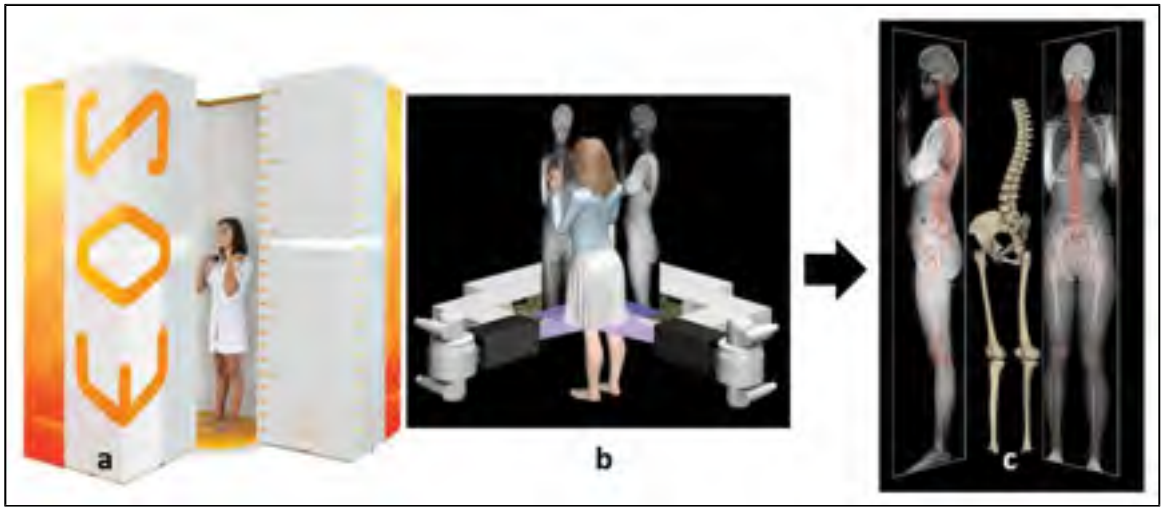

Figure 1-8 EOS® low-dose imaging system and the reconstruction of the 3D geometry of the bones using a pair of biplane X-ray images. Adopted from http://www.eos-imaging.com, 2016

A major advantage of the EOS® system is its low emission of ionizing radiation; at the level of the spine, it has been estimated 8 to 10 times less than that of conventional radiography, and 800 to 1000 times less than CT-scan (Deschênes et al., 2010; Dubousset et al., 2005). The main drawback of this procedure is that segmentation of soft tissue and cartilage is not possible. Only hard tissues are well visualized in X-ray images.

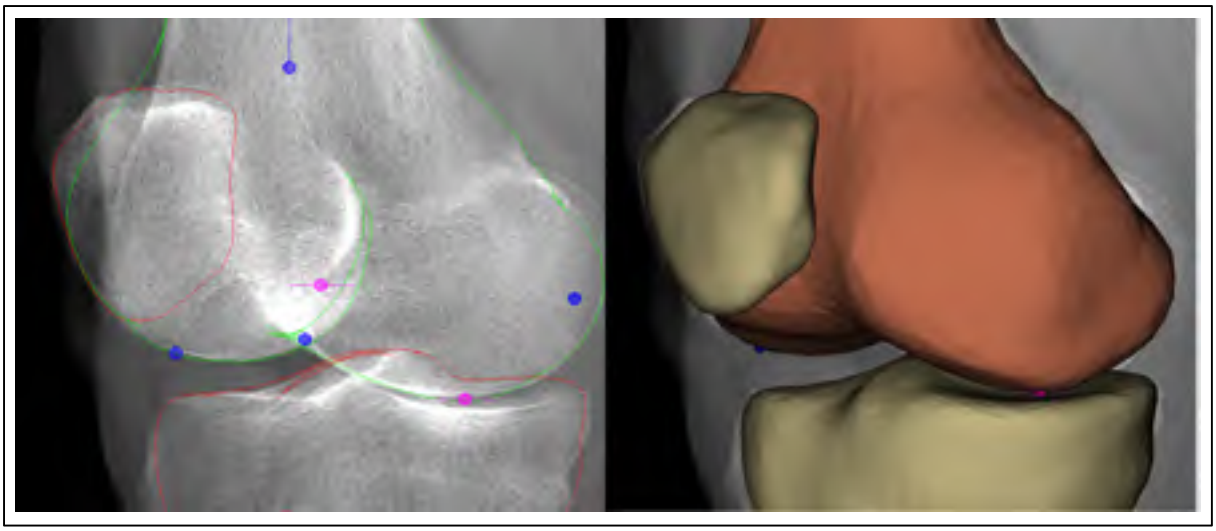

Figure 1-9 Reconstruction of the bone using EOS® biplane X-ray images.

1.6.3 3D kinematics tracking of bones using biplane images

The techniques to study *in vivo* 3D knee kinematic include a 3D reconstruction of the geometry using CT-scan, MRI, or biplane radiographs (EOS®) and then matching the model to the 2D projections of the joint captured during joint movement. Tashman et al. (2003) used a combination of CT and high-speed biplane radiography to measure the joint motion. (G Li et al., 2001) performed a computational analysis on the cartilage with the cartilage contact calculated using a reconstruction of bone and cartilage from MRI and movement tracking by 2D fluoroscopic images.

In the current project, we use the 2D images captured in EOS® in a standing position to reconstruct the shape of the bone. For the kinematics tracking, the 3D reconstructed geometry is matched to the biplane EOS® images of the subject taken at different flexion angles. The reconstruction/registration procedure is performed in IdefX software through the steps as described in (Chaibi et al., 2010). Further technical details are provided in chapter 3.
Previous studies have been conducted on kinematics tracking using EOS® images. In a cadaveric study, Azmy et al. (2010) combined EOS® 3D reconstructions with an

optoelectronic motion capture system for measuring tibiofemoral and patellofemoral pseudo-kinematics. They reported the overall rotational and translational uncertainty below 0.4° and 1.8 mm for the tibiofemoral and 0.4° and 1.2 mm for the patellofemoral kinematics respectively.

Other studies used stand-alone EOS® X-ray images for both geometry reconstruction and motion registration processes to study squat task (Clément et al., 2015, 2017). Some studies developed automated techniques for the 3D/2D registration step while others used manual registration. Südhoff et al. (2007) used EOS® reconstruction/registration as a reference to compare three attachment systems and harnesses designed to measure the 3D kinematics of the knee. All three were installed on subjects during pseudo-dynamic squats in the EOS® system. Thus, the tibiofemoral kinematics measured by the attachment systems and harnesses could be compared to that from EOS® system as a reference. Jerbi et al. (2011) employed an automated registration process based on the frequency domain to track the motion of the bone in healthy and prosthetic subjects. In this case, the manual registration was considered as the gold standard and the registration error was reported 1.5 mm and 1.5° for the healthy group and 0.5 mm 0.8° for the prosthetic group. Michèle Kanhonou (2017) used an iterative closest point algorithm for the 2D/3D registration process and reported the reproducibility of the method 0.4 mm and 0.5°. They also checked the sensitivity of the method to the 3D reconstruction and found the translational and rotational sensitivities to be 1.7 mm and 1.4° respectively.

1.7 Gait Analysis

1.7.1 3D kinematics: Marker tracking using KneeKG™ system

In 3D kinematic studies by marker tracking, reflective or light-emitting markers are attached to the skin surface of the segments whose movements are to be tracked. Their movements are recorded by cameras during a dynamic activity and the 3D kinematics is deduced by processing these data. However, the measured kinematics suffers from measurement inaccuracy induced due to soft tissue artefact, i.e. the sliding of the soft tissues between the markers and the bones.

This soft tissue artefact has been quantified by several teams. By comparing the kinematics calculated using skin markers with respect to the actual movement of the bones measured with fluoroscopy. The errors could reach up to 12 ° and 20 mm for the 3D rotations and displacements respectively (Ganjikia et al., 2000; Sati et al., 1996; Tsai et al., 2015). Others compared the 3D kinematics obtained using skin markers with that calculated using bone embedded implants during walking. Here, maximum mean differences of about 4 ° and between 10.5 mm and 13.7 mm have been reported for the angular and linear displacements (Michael S Andersen et al., 2010; Benoit et al., 2006).

To reduce measurement errors associated with soft tissue artefact, the exoskeleton attachment systems were developed to measure the 3D kinematics of the knee. They exploit the fact that some areas of the lower limb are less prone to movement than others. In the current project, we used the KneeKG ™ system (Emovi inc., Laval, Quebec, Canada) which is an exoskeleton system developed with the objective of providing a reliable analysis of the lower limb kinematics while minimizing the soft tissue artefact (Figure 1-10). The femoral arch of the exoskeleton is installed between the tendons of the biceps femoris and iliotibial band on the lateral side. On the medial side, it is placed between vastus medialis and sartorius tendon. For the tibial portion, the rigid portion of the exoskeleton is attached along the anterior tibia.

Figure 1-10 Anterior view of a right knee fitted with the KneeKG ™ system. Secure fixation to the thigh and calf minimizes skin motion artifact.

Sati et al. (1996) evaluated how the Knee KG ™ harness reduces the influence of soft tissue movement in 3D kinematics measurements. Three subjects instrumented with KneeKG ™ system performed a dynamic flexion. Radiopaque markers were placed on the skin and the KneeKG ™ system. The markers movement was recorded by a monoplane fluoroscopy. It was observed that the harness reduced skin movement artifact from 11 mm RMS to 1.7 mm RMS at the medial condyle and from 8.5 mm RMS to 2.9 mm RMS at the lateral condyle. By analyzing KneeKG™ under fluoroscopy and biplane radiography, Ganjikia et al. (2000) and then Südhoff et al. (2007) assessed its stability during movement. In this latter study, 3 attachment systems were tested on 6 subjects. It was estimated that the KneeKG ™, the most stable of the three, allowed accurate angular measurement in the sagittal and frontal planes, with an average measurement accuracy of less than 1.4 °. In a recent study, the 3D kinematics measured from KneeKG™ system in obese and non-obese subjects was compared to the kinematics obtained from EOS® radiographs to quantify the soft tissue artefact in both groups (Clément et al., 2018). The soft tissue artefact at the femur ranged 1.4° – 8.0° for the rotations and from 5.2 mm – 9.1 mm for the displacements in the non-obese group and ranged from 1.2° – 3.0° for the rotations and 4.4 mm – 8.9 mm for the displacements in the obese group. At

tibia, the soft tissue artefact impact was smaller, ranging 0.3° - 2.4° and 1.1 mm – 3.3 mm in non-obese group, and ranging 0.6° - 4.5° and 0.9 mm – 5.8 mm in the obese group (Clément et al., 2018). In addition, Hagemeister et al. (2005) estimated the reproducibility of angular measurements between 0.4 ° and 0.8 ° and those of translational measurements between 0.8 mm and 2.2 mm, during walking in 15 subjects.

In sum, despite some measurement errors, KneeKG™ remains a reliable measurement tool when considering the use of markers for kinematics measurement; reproducibility is high and accuracy sufficient to study the biomechanical behavior of the knee following a degenerative pathology (Lustig et al., 2012).

1.8 Tibiofemoral contact force estimation

1.8.1 Musculoskeletal models of the lower limb

A direct *in vivo* measurement of joint loads is not currently practical in natural human tissue. While instrumented implants can provide measurements in total knee arthroplasty subjects, musculoskeletal (MSK) models are currently the only means of comparing joint loadings of OA and healthy subjects in the natural knee joint. Some of the previous studies providing estimations for the tibiofemoral joint contact forces using instrumented implants or musculoskeletal models in healthy or pathologic subjects are listed in (Table 1-3).

The external joint moments acting on the joints can be reliably estimated using the motion data and an inverse dynamics analysis. Transformation of these external (or internal) moments into individual muscle forces needs to overcome the muscular redundancy problem. It could be resolved by regrouping muscles and build a very simplistic model of the lower limb or by solving an optimization problem.

Various approaches were used in the literature to solve the redundancy problem (Chèze et al., 2015; Erdemir et al., 2007). In this thesis, we used a 3D MSK model of the lower limb allowing

musculo-tendon and joint contact force simultaneous estimations in a one-step optimization procedure (Florent Moissenet et al., 2014). The computational framework of the MSK model computing the musculo-tendon, joint contact and ligament forces from experimental data is illustrated in Figure 1-11.

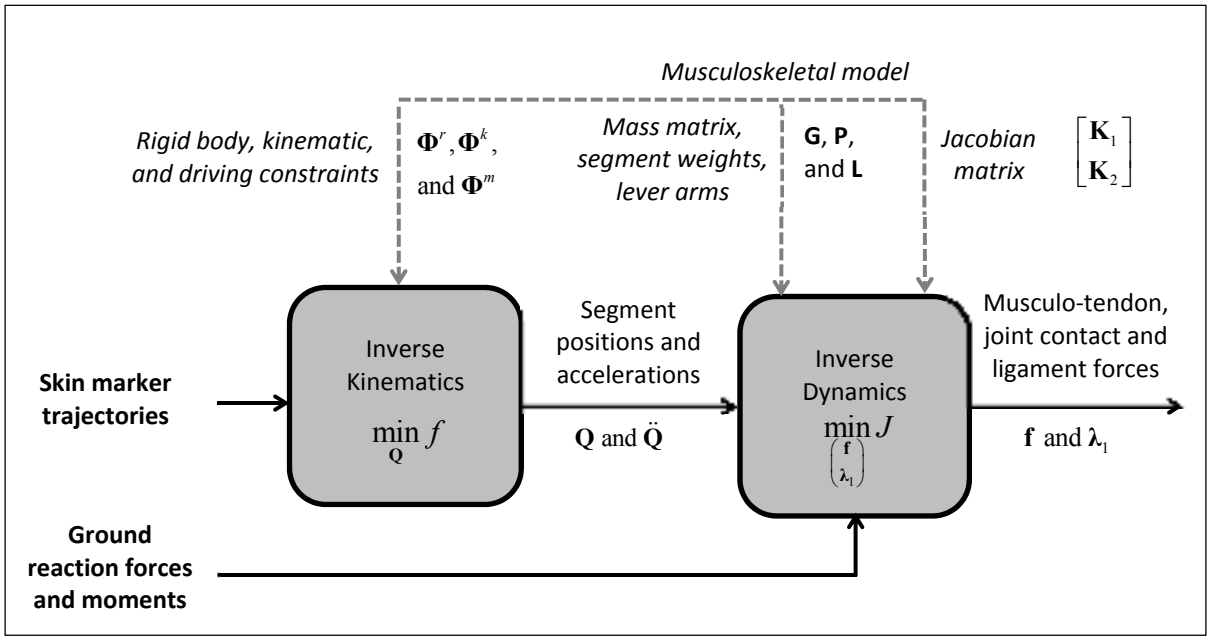

Figure 1-11 Computational framework of the MSK model used to calculate the musculotendon and contact forces. All variables are defined in the following text. Adapted form (Raphael Dumas et al., 2018)

This model is parametrized with natural coordinates to describe the position and orientation of segments in space (R. Dumas et al., 2007). Each segment (i) is defined with two position vectors for the proximal and distal endpoints ($\mathbf{r}_{Pi}$, $\mathbf{r}_{Di}$) and two unitary direction vectors ($\mathbf{u}_i$, $\mathbf{w}_i$) (Figure 1-11).

$$\mathbf{Q}_i = \begin{pmatrix} \mathbf{u}_i \\ \mathbf{r}_{P_i} \\ \mathbf{r}_{D_i} \\ \mathbf{w}_i \end{pmatrix} \tag{1.1}$$

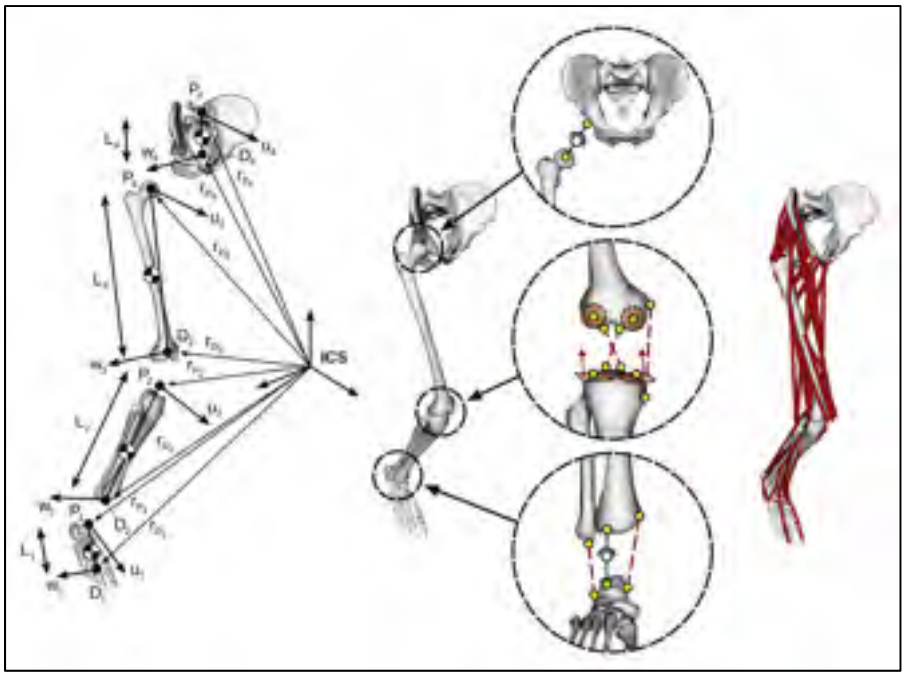

Figure 1-12 Lower limb parametrization with natural parameters (left). The kinematic constraints for the hip knee and ankle joints. Figure adapted from (Florent Moissenet et al., 2012)

Each segment is characterized with 12 parameters for 6 degrees of freedom (DOFs) representing an overabundant system. 6 rigid body constraints per segment ($\mathbf{\Phi}^r$) with the corresponding Jacobean matrix, $\mathbf{K}^r$complete the system for further kinematics and dynamics analyses (Duprey et al., 2010).

The joints are defined, each with kinematic constraints, ($\mathbf{\Phi}^k$) and the corresponding Jacobean matrix, $\mathbf{K}^k$. The hip joint is modeled as a ball and socket (3 DOFs) and ankle joint as a parallel mechanism (1 DOF). In a generic model of the knee, it is also modeled as a parallel mechanism with sphere-on-plane contacts and isometric ligaments (1 DOF) (Florent Moissenet et al., 2012, 2014) (Figure 1-12). In this thesis ,we presented a novel technique to replace the generic model of the knee joint with personalized kinematic constraints deduced directly from the tibial and femoral contact point trajectories estimated from the biplane EOS® images. The different

mechanisms used to model the knee joint are provided in the next section. The integration of personalized contact point trajectories into the MSK model is further explained in chapter 5.

Once the kinematic chain is completed with all the joints and segments, a constrained multibody kinematics optimization is performed with the objective of minimizing the sum of squared differences between measured and model-derived skin marker trajectories (Begon et al., 2018). The aims of this first optimization, sometimes, called inverse kinematics step, are to compensate for the skin motion artefact and find consistent accelerations $\ddot{\mathbf{Q}}$, velocities $\dot{\mathbf{Q}}$, and positions $\mathbf{Q}$ for the dynamic computation step.

In the dynamics step, the dynamics equation of the lower limb is formulated as follow:

$$\mathbf{G}\ddot{\mathbf{Q}} + \mathbf{K}^{\mathrm{T}}\boldsymbol{\lambda} = \mathbf{R} + \mathbf{P} + \mathbf{L}\mathbf{f} \tag{1.2}$$

With $\mathbf{G}$ being the generalized mass matrix, $\ddot{\mathbf{Q}}$ the generalized accelerations, $\mathbf{K} = \begin{bmatrix}\mathbf{K}^{\mathrm{k}} & \mathbf{K}^{\mathrm{r}}\end{bmatrix}$ the Jacobian matrix of both joint kinematic and rigid body constraints, $\boldsymbol{\lambda}$ the Lagrange multipliers, $\mathbf{R}$ the ground reaction forces and moments, $\mathbf{P}$ the weight vector, $\mathbf{L}$ the generalized muscular lever arms and $\mathbf{f}$ the musculo-tendon forces. The unknowns are the musculotendon forces $\mathbf{f}$, and the Lagrange multipliers $\boldsymbol{\lambda}$ which represent the forces associated to kinematics and rigid body constraints. Among these Lagrange multipliers some, of them have important biomechanical interpretation including the contact, ligament, and bone forces.
The dynamics equation above is an under-constrained problem which should be solved through optimization. The optimization criterion was minimizing the sum of squared musculo-tendon forces ($\mathbf{f}$) and a number of joint contact and ligament forces (a subpart $\boldsymbol{\lambda}_{\mathbf{l}}$ of the Lagrange multipliers $\boldsymbol{\lambda}$). Since not all of the Lagrange multipliers are of interest in the optimization, a partial parameter reduction is performed (De Jalon et al., 2012; Florent Moissenet et al., 2014) to keep only the Lagrange multipliers of interest in the objective function.

Therefore, the objective function (J) is formulated as below taking into account the musculo-tendon forces and the contact and ligament forces that are included in the optimization ($\boldsymbol{\lambda}_1$).

The constraints consist of the dynamic equation and the fact that the musculotendon and contact forces are bounded (typically, the musculotendon forces are positive).

$$\min_{\begin{pmatrix}\mathbf{f}\\ \boldsymbol{\lambda}_1\end{pmatrix}} J = \frac{1}{2}\begin{pmatrix}\mathbf{f}\\ \boldsymbol{\lambda}_1\end{pmatrix}^T \mathbf{W}\begin{pmatrix}\mathbf{f}\\ \boldsymbol{\lambda}_1\end{pmatrix} \tag{1.3}$$

$$\text{subject to } \begin{cases} \mathbf{Z}_{\mathbf{K}_2{}^T}\begin{bmatrix}\mathbf{L} & -\mathbf{K}_1{}^T\end{bmatrix}\begin{pmatrix}\mathbf{f}\\ \boldsymbol{\lambda}_1\end{pmatrix} = \mathbf{Z}_{\mathbf{K}_2{}^T}\left(\mathbf{G}\ddot{\mathbf{Q}} - \mathbf{P} - \mathbf{R}\right) \\ \begin{pmatrix}\mathbf{f}_{\min}\\ \boldsymbol{\lambda}_{1\,\min}\end{pmatrix} \le \begin{pmatrix}\mathbf{f}\\ \boldsymbol{\lambda}_1\end{pmatrix} \le \begin{pmatrix}\mathbf{f}_{\max}\\ \boldsymbol{\lambda}_{1\,\max}\end{pmatrix} \end{cases}$$

$\mathbf{W}$ is the optimisation weights matrix, and $\mathbf{Z}_{\mathbf{K}_2{}^T}$ is the projection matrix (i.e. for the partial parameter reduction). A more detailed description of the equations, assigned weights, and the model could be found in (Florent Moissenet et al., 2014).

Table 1-3 1st and 2nd peak of tibiofemoral medial (Med pk1-pk2), lateral (Lat pk1-pk2), and total (Total pk1-pk2), contact forces (per BW) in healthy, OA, total knee arthroplasty (TKA), ACL-deficient(d), or ACL-reconstructed(r) subjects (subj) in studies within the past 20 years.

Study	***subj***	***Condition***	***OA status***	***Total (pk1-pk2)***	***Medial (pk1-pk2)***	***Lateral (pk1-pk2)***
Strithan 2017	19	Model	Healthy	2.3-3.5	2.0-3.0	0.3-0.52
Strithan 2017	39	Model	OA	2.32-3.8	2.12-3.25	0.3-0.59
Dell'Isola 2017	18	Model	Healthy	3.50	2.13	1.44
Dell'Isola 2017	10	Model	Medial OA with varus	3.25	2.30	1.00
Dell'Isola 2017	12	Model	Bilateral OA with varus	3.10	1.97	1.13
Dell'Isola 2017	17	Model	OA normally aligned	3.40	2.07	1.34
Bergmann 2014	8	Prosthetic Treadmill	TKA	2.9-3.4		
Marouane 2016	1	FE Model	Normal	4.1-3.7	3.2-3.0	2.6-0.8
Lemieux 2016	1	Model	Healthy		1.53-1.72	0.94-1.03
Lemieux 2016	1	Model	Healthy		1.30-.091	0.91-1.1
Marouane 2016	1	FE Model	OA	3.3-3.5	2.7-3.0	1.8-0.7

Study	subj	Condition	OA status	Total (pk1-pk2)	Medial (pk1-pk2)	Lateral (pk1-pk2)
Meireles 2016	23	OpenSim Model	OA	4.5-3.7		
Meireles 2016	16	OpenSim Model	Early OA	4.1-3.6		
Meireles 2016	20	OpenSim Model	Healthy	4.0-3.7		
Harding 2016	80	2D 3muscle Model	Healthy	1.99-1.61		
Harding 2016	115	2D 3muscle Model	Moderate OA	1.81-1.52		
Moissenet 2016	1	Model	TKA	1.8-1.1	1.3-0.6	0.5-0.5
Lerner 2015	1	OpenSim Model	TKA	2.3-2.8	1.3-1.5	1.0-1.3
Moissenet 2014	4	Model	TKA	2.2-2.9	1.5-2.0	0.7-0.9
Kumar 2013	16	EMG-driven Model	healthy	3.7-2.2	2.4-1.8	1.3-0.5
Kumar 2013	12	EMG-driven Model	OA	3.5-2.2	2.6-2.1	0.9-0.1
Manal 2013	10	EMG-driven model	ACLr	4.1	2.3	1.8
Kutzner 2011	3	Prosthetic overground	TKA	2.1–2.5	1.5–2.0	0.5–0.9
Richards 2010	14	OpenSim Model	Healthy	4.36-4.40		
Richards 2010	10	OpenSim Model	Moderate OA	4.17-3.9		
Richards 2010	2	OpenSim Model	Severe OA	4.45-3.67		
Catalfamo 2010	1	Model	Healthy, ACLd	8.1		
Lin 2010	1	Model	TKA	1.8–3.6	1.4–2.7	0.4–0.9
Erhart 2010	1	Prosthetic overground	TKA	2.6	1.7	0.9
Kutzner 2010	5	Prosthetic overground	TKA	2.2–3.0		
Lundberg 2009	1	Model	Prosthetic	3.5	2.5	1
Wehner 2009	1	Model	Healthy	3.3		
Winby 2009	1	Model	Healthy	3.0–4.4	2.0–3.0	1.0–1.4
Fregly 2009	1	Prosthetic overground	TKA	2.3	1.8	0.5
Heinlein 2009	2	Prosthetic overground	TKA	2.1–2.8		
Kim 2009	1	Model	TKA	2.0–2.6	1.2–1.8	0.8–0.8
D'Lima 2008	3	Prosthetic treadmill	TKA	1.8–2.5		
Zhao 2007	1	Prosthetic treadmill	TKA	2.2	1.2	1
D'Lima 2006	1	Prosthetic overground	TKA	2.4		

Study	subj	Condition	OA status	Total (pk1-pk2)	Medial (pk1-pk2)	Lateral (pk1-pk2)
D'Lima 2006	1	Prosthetic overground	TKA	2.3		
Shelburne 2006	1	Model	Healthy	2.7	2.2	0.5
D'Lima 2005	1	Prosthetic overground	TKA	2.8		
D'Lima 2005	1	Prosthetic treadmill	TKA	2		
Shelburne 2005	1	Model	Healthy	2.9	2.4	0.5
Thambyah 2005	10	Model	Cadaveric	2.9–3.5		
Taylor 1998	1	Prosthetic overground	TKA	2.5		

1.8.2 Knee joint models

Accurate estimation of the skeleton kinematics from the skin markers requires defining joint constraints in order to produce movements similar to the natural kinematics of the joint and minimize the effect of soft tissue artefact. Especially in case of MSK models, the soft tissue artefact has a negative impact on the estimation of the muscle lever arms. There are several kinematic constraints used to describe the knee joint kinematics (Begon et al., 2018; Leardini et al., 2017). A short review of the associated mechanisms will be provided in this section.

Ball and socket: The knee is modeled as a spherical joint with 3 DOFs (Charlton et al., 2004; Lu et al., 1999). No study listed in Table 1-3 used this model at the knee joint.

Hinge: The knee is modeled as a hinge (also known as revolute or pin) joint with 1 DOF around flexion/extension axis (Michael Skipper Andersen et al., 2009). No study listed in Table 1-3 except the one of Dell'Isola et al., 2017 used this model at the knee joint but some of them used a 2D model that considers only flexion extension.

Parallel mechanism: This model describes the articulation as two sphere-on-plane contacts, guided by three isometric ligaments acting as connecting links. The system has 5 constraints leaving 1 DOF (Feikes et al., 2003; Florent Moissenet et al., 2014). The parameters of this

model could be personalized according to the anatomical measures from imaging techniques (Clément et al., 2015, 2017; da Luz et al., 2017) . From Table 1-3, (Florent Moissenet et al., 2014, 2016b) used the parallel mechanism model.

Coupling curves: In this case, the coupling between the degrees of freedom defines the 6 DOFs knee joint motion. Coupling curves could be obtained from techniques such as registration in cadaveric joints (Sholukha et al., 2006). A special case, limited to the sagittal plane, is sometimes described as a sliding hinge. This sliding hinge is used in most of the study listed in Table 1-3.

In this study, we present a novel approach to derive the knee joint constraints directly from the femoral and tibial personalized contact point trajectories. Interestingly, the contact point trajectories deriving from parallel mechanisms or coupling curves can be also modeled this way. The impact of the personalization on the kinematics and dynamics of the joint will be further discussed in chapter 6.

1.8.3 Medial and lateral contact force distribution

In knee OA, the medial compartment is often much more affected compared to the lateral compartment. The systematic risk factors of OA such as age, gender, and genetics affect both compartments equally. Therefore, the excessive loading on the internal side of the joint could be the reason for higher prevalence of the medial compartment OA. Studies have shown that more than 60% of the contact force is transferred through the medial compartment. This highlights the need to better understand (1) the contact force distribution between medial and lateral in knees affected by OA with respect to the normal knees to investigate the possible contact force distribution abnormalities in OA and (2) to identify the crucial parameters affecting the contact force distribution to find better interventions to lower the chances of accelerated OA progression. (Table 1-4) list the previous studies reporting the parameters contributing to the knee medial contact force. The medial-to-total contact force ratio (MR) has been an essential variable studied in the literature.

Table 1-4 The studies reporting the medial and lateral knee contact forces and the parameters contributing to the higher medial contact forces (Fmed) or the medial-to-total contact force ratio (MR), and impulse of medial contact force (Med impulse). Independent variables consist of external knee adduction moment (KAM),external knee flexion moment (KFM), frontal plane alignment, EMG of muscles, body weight (BW), gait speed (speed), medial/lateral contact point location (CPz), and joint laxity.

Study	***Subjects***	***Dependent variable***	***Predictors***	***Statistics***	***Remarks***
Dell'Isola 2017	39 OA 18 Healthy	Fmed, Med impulse	Frontal plane alignment	Regression analysis	Med impulse was correlated to frontal plane alignment only in subjects with bilateral OA and varus malalignment.
Saliba 2017	14 healthy 9 OA	Fmed, Flat	Frontal plane alignment, CPz	Linear regression and monte-carlo	CPz can lead to lateral condyle unloading.
Smith 2016	1 prosthetic	Fmed, MR	Frontal plane alignment, ligaments	Mont-carlo simulation and pearson's correlation	Frontal plane alignment influences the MR but not the F_{med}
Manal 2015	10 ACLr	Fmed	KAM, KFM	Linear regression analysis	Peak KAM is a good predictor of Fmed (adj. R^2=63%), peak KFM accounts for an additional 22% of the variance.
Creaby 2015	review article	Fmed	KAM, KFM		KAM and KFM should be considered together.
Lerner 2015	1 Prosthetic	Fmed, Flat	Frontal plane alignment, CPz	Regression analysis	gradients are 51N per degree for frontal plane alignment and 41N per mm for CPz.

Study	*Subjects*	*Dependent variable*	*Predictors*	*Statistics*	*Remarks*
Adouni 2014	1 FE	MR	KAM, Frontal plane alignment		Fmed mainly correlated to fontal plane alignment
Trepczynski 2014	9 prosthetics	Fmed, MR	KAM, KFM	Mixed effect regression	KAM is generally a good indicator of Fmed, R^2 varies considerably across subjects.
Meyer 2013	1 prosthetic	Fmed, Flat, Ft	Frontal plane alignment, KFM, EMG	Linear regression analysis	KAM explains up to 60% of Fmed variation. External loads and EMG are weak indicators of Fmed. KAM was more strongly correlated to MR than Fmed.
Kumar 2013	16 OA 12 Healthy	Fmed	BW, Frontal plane alignment, laxity, quadriceps muscle, KAM	Multiple linear regression	Best predictor: 1st peak: BW, KEM, KAM - 2nd peak: Frontal plane alignment.
Kutzner 2013	9 prosthetics	Fmed, MR	Gait speed, KAM, Frontal plane alignment	Linear and arctan regression	Predictions are strong only during early stance. High inter-subject variation.
Erhart 2010	1 prosthetic	Fmed	KAM	Linear regression analysis	F_{med} was correlated to KAM with $R^2 = 0.67$.
Johnson 1981	72 OA	Fmed	Frontal plane alignment	No statistics. Variable coefficient in equation	Fmed drops by a rate of 2% per valgus degree.

CHAPTER 2

RESEARCH PROBLEMATICS AND OBJECTIVES

2.1 Problematic 1:

According to what has been discussed in the previous chapter, the shift of the tibiofemoral contact points was hypothesized to initiate the cartilage damage process in OA. However, the current body of the literature does not provide a clear description of the regions of contact in OA joints and in what sense/direction they are different from the healthy ones.

The first aim of this thesis was to assess the contact point kinematics in OA and healthy joints and quantify the location and direction of the contact point shift in pathological knees.

Objective 1: Develop a validated 3D/2D reconstruction/registration technique to accurately measure the 3D kinematics of the knee joint from EOS® biplane X-ray images.

Objective 2: Measure the tibiofemoral contact points from the bone-to-bone proximity

Objective 3: Measure the contact point locations during a quasi-static squat task in healthy and OA subjects

Objective 4: Measure the contact point locations of OA subjects during a quasi-static task with and without wearing a valgus knee orthosis in repeated postures.

Our first hypothesis was that the contact point locations in OA subjects would be shifted medially on both medial and lateral compartment as a result of changes in joint morphology and alignment.

Our second hypothesis was that the valgus knee orthosis influences the contact point locations of the OA subjects and pushes the contact point location laterally on both medial and lateral compartments.

Chapters 3 and 4 address this first problematic of the thesis.

2.2 Problematic 2:

The external moments on the knee joint are counterbalanced by the musculo-tendon forces as well as the medial and lateral contact forces. Dynamics of the joint requires that a change in the contact point locations -by changing the lever arms of the contact forces- affects the medial and lateral contact forces. Based on the classical models of the tibiofemoral joint (i.e., parallel mechanisms, sliding hinge), the current musculoskeletal models of the lower limb do not allow the direct integration of personalized contact point trajectories in the contact force calculations.

The second aim of this thesis was to implement a musculoskeletal model of the lower limb which enables integration of personalized contact point trajectories.

Objective 1: Introduce a knee joint constraint using tibial and femoral contact point trajectories as input parameters and estimate the corresponding contact forces on the medial and lateral compartments.

Objective 2: Compare the medial and lateral contact forces using personalized contact point trajectory model with classical models of the tibiofemoral.

Objective 3: Validate semi-quantitatively the musculo-tendon forces with EMG signals to check if the results are realistic.

Chapters 5 addresses this second problematic of the thesis.

2.3 Problematic 3:

While the systematic risk factors of OA such as age, sex, or genetics affect both medial and lateral compartments equally, the cartilage on the medial compartment is almost always much more affected by the disease compared to the lateral compartment. Higher contact forces on the medial compartment are related to the severity of the OA on the medial side. Few studies have reported the medial and lateral contact forces in OA subjects in comparison with healthy controls. Moreover, regardless of the considerable amount of work on the role of external moments on the contact force distribution, the contribution of contact point locations has not been investigated up to now.

The third aim of this thesis was to investigate the contribution of contact point locations on the knee contact force distribution compared to the other mechanical and functional parameters.

Objective 1: Estimate and compare the medial, lateral, and total contact forces in OA and healthy subjects using the personalized contact point locations.

Objective 2: Identify the most important parameters affecting the medial-to-total contact force ratio (MR), and find the contribution of contact point locations to the MR with respect to the other parameters.

We hypothesized that the contact force point location is a significant parameter in the MR, and that the contribution of parameters to MR is different in OA and healthy groups.

Chapters 6 addresses this third problematic of the thesis

CHAPTER 3

TIBIO-FEMORAL JOINT CONTACT IN HEALTHY AND OSTEOARTHRITIC KNEES DURING QUASI- STATIC SQUAT: A BI-PLANAR X-RAY ANALYSIS

A. Zeighami[1*], R. Dumas[2], M. Kanhonou[1], N. Hagemeister[1], F. Lavoie[3], J.A. de Guise[1], R. Aissaoui[1]

1. Laboratoire de Recherche en Imagerie et Orthopédie (LIO), École de Technologie Supérieure (ÉTS), Centre de Recherche du CHUM, Montréal, Québec, Canada
2. Univ Lyon, Université Claude Bernard Lyon 1, IFSTTAR, UMR_T9406, LBMC, F69622, Lyon, France
3. Department of Orthopedic Surgery, Centre Hospitalier de l'Université de Montréal (CHUM), Montréal, Québec, Canada

The article has been published in Journal of Biomechanics 53 (2017): 178-184.

3.1 Preface

This chapter addresses the objectives 1,2,3 of the first aim of this thesis: assess the contact point kinematics in healthy and OA joints and quantify the location and direction of the contact point shift in pathological knees.

3.2 Abstract

The aim of this study was to quantify the tibio-femoral contact point (CP) locations in healthy and osteoarthritic (OA) subjects during a weight-bearing squat using stand-alone biplanar X-ray images.

Ten healthy and 9 severe OA subjects performed quasi-static squats. Bi-planar X-ray images were recorded at 0^o, 15^o, 30^o, 45^o, and 70^o of knee flexion. A reconstruction/registration process was used to create 3D models of tibia, fibula, and femur from bi-planar X-rays and to measure their positions at each posture. A weighted centroid of proximity algorithm was used to

calculate the tibio-femoral CP locations. The accuracy of the reconstruction/registration process in measuring the quasi-static kinematics and the contact parameters was evaluated in a validation study.

The quasi-static kinematics data revealed that in OA knees, adduction angles were greater ($p<0.01$), and the femur was located more medially relative to the tibia ($p<0.01$). Similarly, the average CP locations on the medial and lateral tibial plateaus of the OA patients were shifted (6.5±0.7 mm; $p<0.01$) and (9.6±3.1 mm; $p<0.01$) medially compared to the healthy group. From 0^o-70^o flexion, CPs moved 8.1±5.3 mm and 8.9±5.3 mm posteriorly on the medial and lateral plateaus of healthy knees; while in OA joints CPs moved 10.1±8.4 mm and 3.6±2.8 mm posteriorly. The average minimum tibio-femoral bone-to-bone distances of the OA joints were lower in both compartments ($p<0.01$). The CPs in the OA joints were located more medially and displayed a higher ratio of medial to lateral posterior translations compared to healthy joints.

Keywords: Osteoarthritis; *in vivo* tibio-femoral contact; Bi-planar X-ray; Squat; Knee quasi-static kinematics.

3.3 Introduction

An estimation of the *in vivo* 3D kinematics, the contact point (CP) locations, and the minimum distance between articular surfaces of knee joints can provide information that is useful in understanding osteoarthritis (OA) initiation and progression. Andriacchi et al., (2004) hypothesized that shifts in load-bearing CP locations towards less frequently loaded regions (i.e., far from the plateau center lines) initiate the cartilage degeneration process. However, the direction of the shift was not indicated in their proposed framework. A few literature studies have addressed CP locations in pathological knees. Experimental locations of CPs in anterior cruciate ligament (ACL)-reconstructed (Hoshino et al., 2012), ACL-deficient (Dennis et al., 2005), and OA knees (Fiacchi et al., 2014; Hamai et al., 2009; C. Li et al., 2015) have been investigated using 3D-to-2D registration techniques during different activities such as kneeling, squatting, stair climbing, chair rising, and lunge, but still little is known about the

quantitative differences in CP locations between OA and healthy subject during functional activities.

In 3D-to-2D registration techniques, bones are reconstructed from MRIs (Seungbum Koo et al., 2011; Qi et al., 2013) or CT-scans (Farrokhi et al., 2016; Fiacchi et al., 2014; Hamai et al., 2009) and are then rigidly transformed to match X-ray or fluoroscopic images captured during movements. In MRI-derived models, cartilage overlap was used to identify CP locations, whereas in the CT-scan-derived models, due to the absence the of cartilage layer in the reconstructions, the bone-to-bone closest point or a weighted center of tibio-femoral proximity has been used to determine the location of CPs.

Hamai et al. (2009) and Fiacchi et al. (2014) investigated the tibio-femoral anterior/posterior CP locations of OA subjects. However, they did not quantify the possible medial/lateral shifts in the CP locations. C. Li et al. (2015) reported that in OA knees the center of the medial and lateral CPs was located at the medial side of the tibia by 3.7% plateau width during a lunge activity. OA CPs were located medial to the both medial and lateral plateau centerlines throughout the lunge. After a posterior cruciate-retaining total knee arthroplasty, CPs had shifted laterally and had a reduced range of motion. In a recent study by Farrokhi et al. (2016), the excursion of CPs during a downhill gait task was found to be altered in the unstable OA group compared to healthy controls. The CP locations in the two groups during flexion were not reported in their study. Although previous works increase our knowledge of contact in OA, none of these studies compared the regions of contact in OA with healthy subjects, and a clear description of alterations in CP locations in OA is still lacking. Case-control studies comparing tibio-femoral CP locations between OA and healthy subjects are required before drawing any conclusion on altered tibio-femoral contact in OA.

The objective of the present study was to compare tibio-femoral CP locations of healthy and OA subjects during a load-bearing squat. We used a reconstruction/registration process based on stand-alone bi-planar X-ray images to quantify the contact parameters of OA and healthy

joints. We hypothesized that the CPs in OA subjects would shift medially on both tibial plateaus with respect to the healthy controls.

3.4 Methodology

3.4.1 Study subjects

Nineteen subjects volunteered to participate in this study. They included 10 healthy subjects (4 women, 6 men, 5 right sides, 5 left sides, age 55±17 years, weight 69±20 kg, height 1.67±0.17 m, body mass index (BMI) 24.67±5.33 kg/m^2) and 9 medial compartment OA subjects (2 men, 7 women, 7 right sides, 2 left sides, age 61±9 years, weight 89±15 kg, height 1.63±0.12 m, BMI 33.35±7.23 kg/m^2). The OA subjects were classified as grade 4 using the Kellgren-Lawrence grading scale. The subjects did not have any self-reported meniscus or ligament injuries. The following procedures were in accordance with the ethics committees of the Centre de recherche, centre hospitalier de l'Université de Montréal (CRCHUM) and École de technologie supérieure de Montréal (ÉTS) as well as the Helsinki Declaration of 1975, as revised in 2000.

3.4.2 Bi-planar X-ray images

The EOS® (EOS Imaging, Paris, France) bi-planar, low-radiation dose system recorded 5 pairs of orthogonal X-ray images of the lower limb at 0^o, 15^o, 30^o, 45^o, and 70^o of knee flexion. The subjects performed controlled quasi-static squats assisted by a positioning jig(Clément et al., 2014) (Figure 3-1(a)). Two digital X-ray images of the whole lower limb were captured simultaneously at each position.

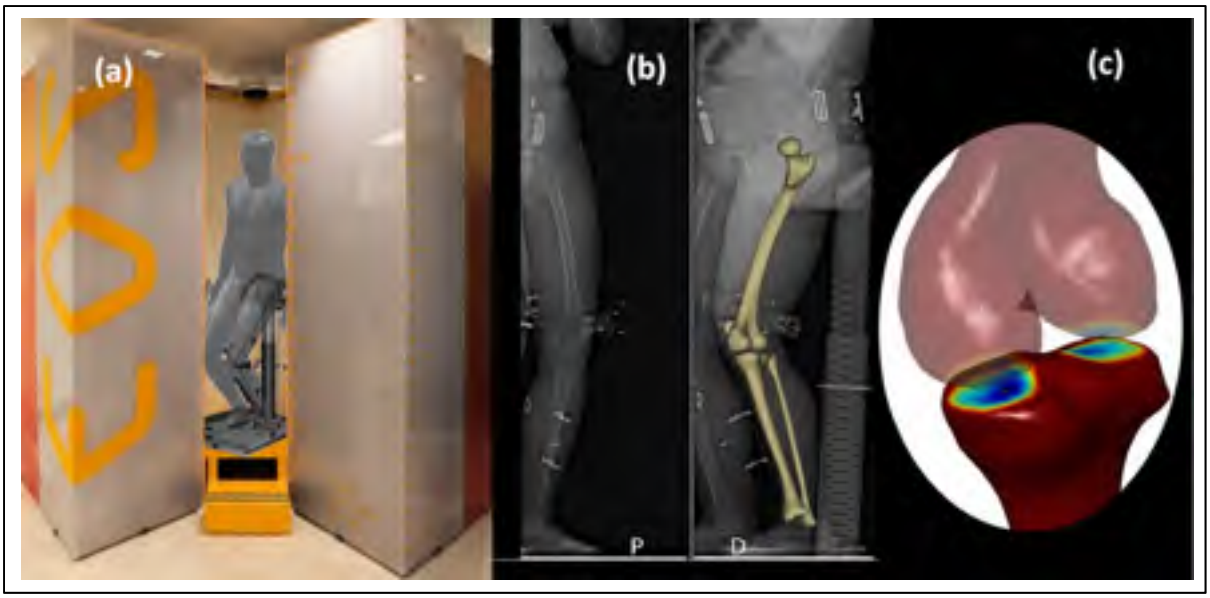

Figure 3-1 (a) Subjects performed a quasi-static squat assisted by a positioning jig standardized to put the knee in desired flexion angles. 5 pairs of orthogonal X-ray images of the lower limb at 0^o, 15^o, 30^o, 45^o, and 70^o of knee flexion were recorded. (b) Bones were reconstructed from bi-planar X-ray images and registered to each of the 5 squat positions the subjects adopt in the EOS® system cabinet. (c) 2 pairs of points on the medial and lateral sides of the tibia and femur represented CPs and minimum tibio-femoral bone-to-bone distances.

3.4.3 Reconstruction/registration

The first pair of X-ray images in a standing posture was processed using IdefX software (LIO, Montreal, Quebec, Canada) to reconstruct the 3D personalized models of the tibia, femur, and fibula. This was performed starting with a generic 3D model of each segment. Each generic 3D model was then deformed and reconstructed via an as-rigid-as-possible approach based on the moving least squares optimization method until its projected contours on 2 radiographic planes matched the boundaries of the bones on biplanar X-rays (T Cresson et al., 2010). The average reconstruction error of the bones using this technique was found to be 1 mm (STD=0.9 mm) (T Cresson et al., 2010).

To find the configuration in the other squat positions, the reconstructed bones were transformed rigidly until their silhouettes superimposed the acquired bi-planar X-ray images

of each position (Figure 3-1 (b)). Translations and rotations were calculated based on an iterative closest point algorithm (M. Kanhonou et al., 2014).

Through a fine-tuning process in each of the 5 squat positions, the reconstructions and registrations were further modified to take into account the features in the X-ray images that are not visible in other views. The final fit was decided by the operator based on the best possible visual matching of segmentations with background X-ray images in all 5 positions. The whole process took up to 90 minutes for each subject.

3.4.4 Quasi-static kinematic measurements

Orthogonal local coordinate systems were constructed on tibia/fibula and femur according to the anatomical definitions given in previous studies (Südhoff et al., 2007) (Figure 3-2). Flexion/extension, adduction/abduction, and internal/external rotations were measured according to the coordinate system proposed by Grood et al. (1983). Linear displacements were represented by the movement of the origin of the femoral coordinate system with respect to the origin of the tibial coordinate system as previously proposed in the literature (Asano et al., 2001; Yue et al., 2011).

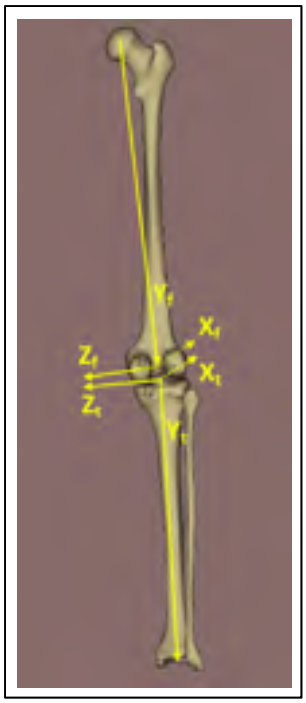

Figure 3-2 Origin of femur (Of): midpoint of 2 spheres fitted on the posterior femoral condyles. Proximal/distal axis of femur (Yf): Of - center of the femoral head. Zc: axis connecting centers of the posterior condyles. Anterior/posterior axis of femur (Xf): cross product of Yf and Zc, oriented anteriorly. Medial/lateral axis of femur (Zf): cross product Xf × Yf. Origin of tibia (Ot): center of intercondylar eminence. Proximal/distal axis of tibia (Yt): midpoint of the medial and lateral malleoli – Ot. Zp: axis passing through the posterior extremes of the tibial plateaus. Anterior/posterior axis of tibia (Xt): cross product of Yt and Zp, oriented anteriorly. Medial/lateral axis of tibia (Zt): cross product Xt × Yt (Südhoff, 2007).

3.4.5 Contact parameters

For each point on the tibial plateau, the minimal point-to-point distances to the opposing medial or lateral condyles were calculated at the 5 squat positions. A weighted center of proximity algorithm was performed to find a point on each plateau that most likely represented the CP (Anderst et al., 2003; Hoshino et al., 2012). A weight factor of 16 was considered for the points closer than the minimal point-to-point distance + 0.5 mm. Similarly, weight factors of 4, 1, and 0 were considered for the points in the distance ranges of [0.5-1] mm, [1-2] mm, and greater than 2 mm more than the minimal point-to-point distance, respectively. The corresponding points on the opposing femoral condyles represented CPs of the femur and the calculated

distances were assumed to represent minimum tibio-femoral bone-to-bone distances (Figure 3-1 (c)).

Since in the proposed reconstruction technique, the personalized bones were deformed versions of generic bones, a unique correspondence existed between each point on the generic bone and its deformed versions, such that vertices located on any anatomical landmarks (e.g., lateral intercondylar tubercle) correspond to the same landmark after deformation. These correspondences allowed a feature-based normalization to represent the calculated CPs of all subjects, on a right tibial plateau with 74 mm medial/lateral width.

A new validation study was designed to evaluate the accuracy of the whole reconstruction/registration technique used to calculate the contact parameters (see complementary methodology).

3.4.6 Statistical Analysis

Two-way analysis of variance (ANOVA) was performed to detect statistically significant differences in quasi-static kinematic parameters (i.e., rotations and linear displacements), CP locations in the anterior/posterior and medial/lateral directions, and the minimum bone-to-bone distances. Independent variables were the flexion angle and the OA status. Bonferroni test was performed to detect pair-wise different means and to compare the means in various levels of flexion angle. The level of significance was set at $p<0.05$.

3.5 Results

3.5.1 Contact Parameters

Figure 3-3 illustrates the average CP trajectories for all the OA and healthy subjects normalized on a right tibial plateau, and are presented in 5 positions of squat from 0^{o}-70^{o} flexion.

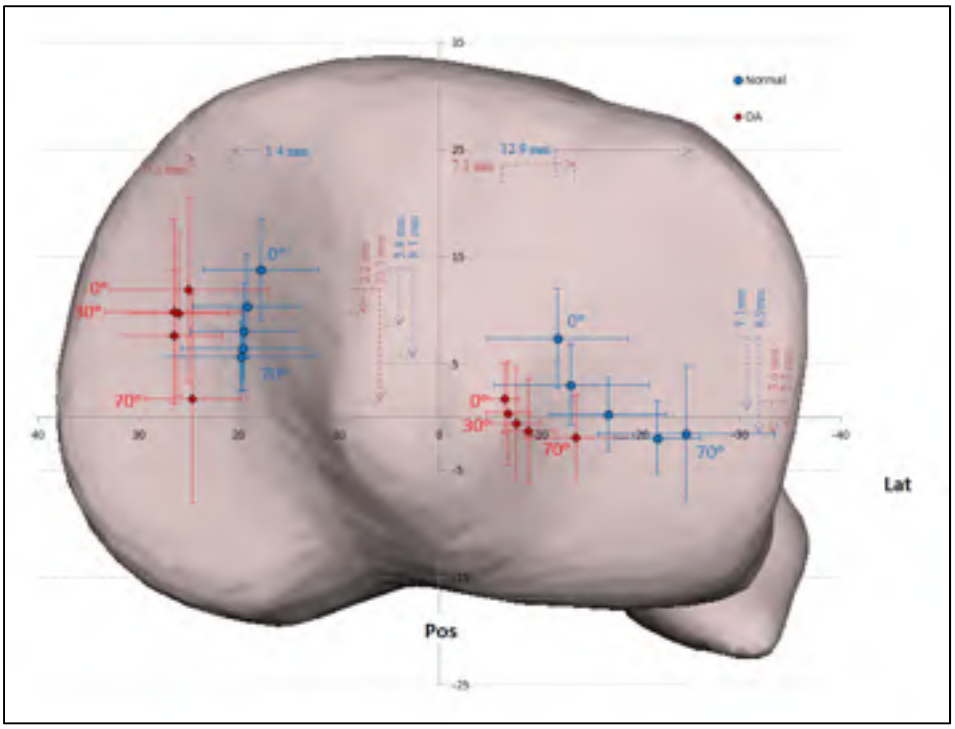

Figure 3-4 Average CP trajectories in 10 healthy (blue) and 9 OA (red) subjects during squat, normalized over a tibial plateau. CP locations are plotted at 0°, 15°, 30°, 45° and 70° flexion. Error bars stand for standard deviations (±1 SD). Dashed arrows represent CP movements from 0° to 30° or 70° flexion, in medial/lateral or anterior/posterior direction of healthy (blue) or OA (red) subjects.

As a general trend, the average CPs moved posteriorly during squat in both the OA and the healthy subjects, in both the medial and lateral compartments. Table 1 summarizes the CP locations over the tibial plateau, for the whole range of motion.

Table 3-1 CP locations of OA and healthy subjects on medial and lateral tibial plateaus in Anterior/posterior and medial/lateral directions at 5 flexion levels from 0°-70°. Tibial plateau width=74 mm, stretched from -35.5 mm to 38.5 mm. * denotes significant differences between OA and Healthy ($p<0.05$). † denotes significant differences between 0° flexion and the corresponding flexion level ($p<0.05$).

	Ant(+)/Pos(-) on Medial plateau		***Ant(+)/Pos(-) on Lateral plateau***		***Med(+)/lat(-) on Medial plateau***		***Med(+)/lat(-) on Lateral plateau***	
Flexion (degree)	OA	Healthy	OA	Healthy	OA	Healthy	OA	Healthy
0	11.9±8.6	13.8±4.6	1.7±3.2	7.3±4.6	25.0±8.0	17.8±5.7	-6.5±1.5	-11.7±7.0
15	9.8±8.6	10.4±4.8	0.4±5.1	3.0±3.8	26.5±6.7	19.2±5.4	-6.8±2.19	-13.1±7.7
30	9.7±7.7	8.0±4.5	-0.6±5.2	0.2±3.4†	26.0±4.8	19.6±5.2	-7.6±2.3*	-16.8±5.8
45	7.5±6.2	6.4±3.9	-1.3±4.8	-1.9±3.4†	26.5±4.9	19.6±6.0	-8.8±2.5*	-21.8±4.2†
70	1.7±9.7†	5.7±3.2	-1.8±3.9	-1.5±6.3†	24.7±4.8	19.9±7.2	-13.6±5.1*†	-24.6±8.8†
Average	8.1±3.9	8.9±3.2	-0.5±1.3	1.4±3.8	25.7±0.8*	19.2±0.8	-8.5±3.6*	-17.6±5.5

In the healthy subjects, the CPs on the lateral plateau moved 8.9±5.3 mm and 7.1±4.9 mm posteriorly during full (0°-70°) and low (0°-30°) flexion ranges, respectively. On the medial plateau, CPs moved 8.1±5.3 mm and 5.8±3.7 mm posteriorly during full and low flexion ranges. CP posterior movements were much larger on the medial plateau (10.1±8.4 mm) with respect to the lateral plateau (3.6±2.8 mm) among OA subjects through the full flexion range and were almost equal on the medial (2.2±8.1) and lateral (2.3±2.6) plateaus during low flexion range (Figure 3-4).

No significant difference was noted in the average anterior/posterior CP locations between the two groups on the medial ($p=0.28$) or lateral ($p=0.06$) sides.

In the medial/lateral direction and from 0°-70° flexion, the CPs moved laterally on the lateral plateaus for both OA (7.1±4.3 mm; $p=0.014$) and healthy (12.9±9.9; $p<0.01$) subjects. On the medial plateau, the medial/lateral locations of the CPs were not significantly different between 0° and 70° flexion in either group ($p>0.05$) (Figure 3-4, Table 3-1).

Distinct deviation occurred in the medial/lateral locations of the CPs in the OA compared to the healthy subjects. In the healthy subjects, the average of the medial/lateral CP locations was

around the middle of each compartment, whereas in the OA subjects the CPs on both sides deviated medially. The OA status was found to have a statistically significant effect on the medial/lateral location of the CPs on both sides ($p<0.01$). The average CPs across the flexion angles in the medial compartment were located 6.5±0.7 mm more medially ($p<0.01$) for the OA (25.7±0.8 mm) than for the healthy subjects (19.2±0.8 mm). Similarly, the average CPs on the lateral plateau were located 9.0±3.1 mm more medially ($p<0.01$) for the OA (-8.5±3.6 mm) than for the healthy (-17.6±5.5) subjects, with significant pair-wise differences from 30^o-70^o flexion ($p<0.05$).

The average minimum tibio-femoral bone-to-bone distances for all positions in the medial compartment was 1.2±0.7 mm in OA and 2.6±1.2 mm in the healthy subjects ($p<0.01$) with significantly different values at 0^o and 15^o flexion ($p<0.05$). In the lateral compartments, these values were 2.4±1.1 mm and 3.6±1.2 mm for the OA and the healthy subjects, respectively ($p<0.01$). These results indicate an average of 54% and 27% less medial and lateral minimum bone-to-bone distances in the OA joints.

3.5.2 Quasi-static kinematics

Quasi-static kinematic parameters were averaged in each of the 5 squat positions in both groups. The average femur location was 2.4±1.2 mm more medial in the OA group compared to the healthy group ($p<0.01$) with pair-wise significant differences at full extension ($p=0.38$) (Figure 3-5 (a)). The OA femur moved 3.3±2.3 mm laterally from 0^o-70^o flexion, while in the healthy joints it was displaced medially 1.7±2.5 mm until 15^o of flexion and then moved 2.3±1.4 mm laterally. Femur moved 9.8±3.6 mm and 9.6±4.8 mm anteriorly with respect to the tibia in the OA and healthy subjects, respectively (Figure 3-5 (b)).

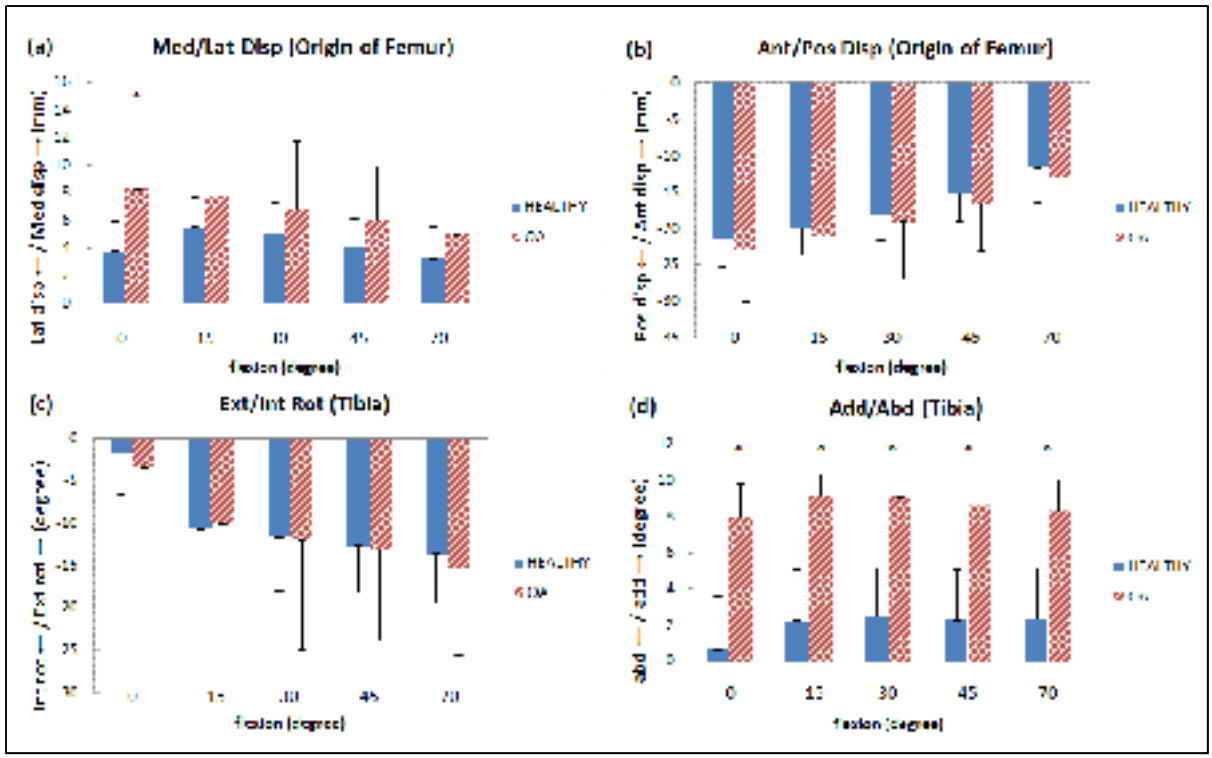

Figure 3-5 Quasi-static kinematics of OA and healthy joints during the controlled squat. Medial/lateral (a) and anterior/posterior (b) displacement of femur with respect to tibia, and internal/external rotation (c) as well as adduction/abduction (d) of tibia are illustrated as a function of 5 squat positions designed to reproduce 0◦, 15◦, 30◦, 45◦, and 70◦ of flexion respectively. * denotes a pair-wise significant difference between OA and healthy groups.

The OA and healthy tibio-femoral joints exhibited similar patterns of internal rotation ($p=0.68$). Tibia rotated $12.0^{o}\pm5.2^{o}$ in OA and $11.8^{o}\pm5.5^{o}$ in healthy joints during squat. The majority of rotation occurred in the first 30^{o} of flexion: 6.5^{o} in OA and 9.9^{o} in the healthy knees (Figure 3-5 (c)). The OA joints maintained significantly greater adduction angles throughout flexion ($p<0.01$) with pair-wise significant differences at all flexion levels ($p<0.05$). Adduction angles varied from $7.9^{o}\pm1.9^{o}$ to $8.3^{o}\pm1.7^{o}$ in OA, and from $0.6^{o}\pm3.0^{o}$ to $2.4^{o}\pm2.8^{o}$ in healthy joints (Figure 3-5 (d)).

3.6 Discussion

The tibio-femoral CP trajectories in healthy knee squats or lunges in the literature are generally described with posterior movements, with the lateral CPs located more posteriorly. However, inter-subject variabilities produced some dissimilarities in CP trajectories measured using similar protocols during the same activities (Guoan Li et al., 2005; Qi et al., 2013). The average values from previous studies for anterior/posterior CP trajectories of healthy subjects from 0◦-70◦ flexion suggest posterior movements of 6.7±2 mm (8.1±5.3 mm in our study) on the medial and 8.6±5.5 mm (8.8±5.3 mm) on the lateral plateaus. (Bingham et al., 2008; Dennis et al., 2005; Guoan Li et al., 2005; Moro-oka et al., 2008; Qi et al., 2013).

The medial/lateral location of the CPs was reported in the studies that used biplanar fluoroscopy for registration (Bingham et al., 2008; Dennis et al., 2005; Qi et al., 2013). The 0◦-70◦ medial/lateral movement of the CPs averaged among those studies was 1.7±0.5, which is close to 2.1±4.6 mm in our study, both in the medial direction. On the lateral plateau, we observed a larger lateral movement (12.9±9.9 mm) in the 0◦-70◦ CP locations of healthy subjects, compared to their 3.6±1.57 mm average lateral movement. The lateral shift of CPs in the lateral compartment occurs mainly between 0^o and 45^o of flexion, despite the fact that femur is slightly moving medially. This paradox highlights the importance of joint geometry in the estimation of CP locations. The average 0◦-70◦ CP locations for healthy subjects in the medial/lateral direction are located within a distance of 5 mm from the centers of the medial and lateral plateaus, which is consistent with our findings (Bingham et al., 2008; Dennis et al., 2005; Qi et al., 2013).

There is little consensus about the CP locations of OA tibio-femoral joints in previous studies. Hamai et al. (2009) reported medial and lateral posterior translations of 1 mm and 3 mm during 0◦-70◦ squats of OA subjects, while Fiacchi et al. (2014) reported 4.5 mm anterior translation on the medial and 15 mm posterior translation on the lateral plateaus during 0◦-70◦ flexion in chair rising activity with the average lateral CPs being more posterior in both studies (similar to our study). We observed a greater posterior translation on the medial side with respect to

the lateral side. An increased translation of the medial condyle in the ACL-deficient and ACL-reconstructed knees (Dennis et al., 2005; Hoshino et al., 2012) has been identified previously in the kinematics of pathological knees; but it has not yet been reported in CP locations of OA subjects.

The mean medial/lateral CP locations were not located close to the center of each compartment in the OA subjects. The average medial shifts in the CP location of the OA subjects with respect to healthy subjects in the medial (6.5 mm) and lateral (9.0 mm) compartments exceeded twice the uncertainty of the reconstruction/registration process in the medial/lateral direction (3 mm), found in our validation study (supplementary material 1). This corroborates the hypothesis of different contact kinematics of the tibio-femoral joints in OA made by Andriacchi et al. (2004). Medially located CPs in OA were observed in a previous study. (C. Li et al., 2015) reported that the 0◦-70◦ flexion CP locations in OA joints were located at approximately 4% of the tibial plateau width medial to the centerlines of both tibial plateaus. CPs were significantly shifted laterally after a total knee arthroplasty, but the results were not compared against healthy controls.

The quasi-static kinematics results demonstrated that OA and healthy subjects displayed similar internal/external rotation patterns, which was also suggested by Yue et al. (2011). The average 0◦-70◦ internal rotations of tibia for healthy and OA subjects, which was averaged among previous studies, were 11.25±5.6◦ and 9.6±1.37◦ (Dennis et al., 2005; Fiacchi et al., 2014; Hamai et al., 2009; Moro-oka et al., 2008; Qi et al., 2013; Yue et al., 2011), which compared to 12.0±5.2◦ and 11.8±5.5◦ in our study. Yue et al. (2011) reported OA joints to have 1◦ (6.6◦ in our study) greater adduction angles, and the adduction angles were maintained almost constant throughout 0◦-70◦ flexion in both groups (similar to our study). These authors reported that the femur was located 2.62±0.6 mm (2.4±1.2 mm) more medial with respect to the tibia in OA joints compared to healthy joints. It should be noted that the choice of coordinate systems may result in different kinematic patterns.

An altered adduction angle of joints might be associated with the medial shift of CP locations in OA subjects. A substantial medial joint space (bone-to-bone distance in the present study) reduction changes the alignment of the articular surface, and accordingly, increases the knee adduction. The altered alignment appears to change the joint structure, placing the femoral lateral condyle closer to the tibial eminence and the femoral medial condyle closer to the medial edge of the medial tibial plateau, shifting the CP locations medially. Changes in the geometry of the subchondral bone surfaces could also have an impact on the final location of CPs in OA and must be addressed in a future study.

The employed reconstruction/registration process was executed on a set of bi-planar X-ray images alone. Skin radiation dose with EOS® imaging is 6 to 9 times lower compared to regular digital radiography (Deschênes et al., 2010). Incorporation of model-creation and kinematic observations into a single low-dose process minimizes radiation exposure compared to 3D-to-2D registration techniques based on CT-derived bone models of the femur and tibia. Moreover, the use of a generic model for bone reconstruction allows feature-based normalizations and enables automatic definition of anatomical landmarks eliminating errors in the femur and tibia coordinate system definitions among individuals. The main drawback of the technique is its quasi-static nature which restricts the number of images (e.g., 5 pairs). In addition, as in CT-derived bone models, the menisci and the cartilage cannot be reconstructed.

In the absence of cartilage layers in images, CPs are estimated from the bone-to-bone proximity. Estimating CP locations using the closest point method (Asano et al., 2001; Guoan Li et al., 2004) may result in an abrupt oscillation of CPs (Beveridge et al., 2014). DeFrate et al. (2004) compared the location of CPs estimated using the closest point method and the cartilage-overlap method and found a significant difference in the location of CPs in low flexion despite a good agreement in higher flexions. To overcome the problems of the closest point method, a weighted center of proximity algorithm was suggested by Anderst et al. (2003) to incorporate the information of a close proximity region rather than a single point in which higher weights were assigned to closer points. Tuning the selected weights was reported to make very small changes in the location of CPs (Beveridge et al., 2014; Marouane et al., 2016).

Moro-oka et al. (2008) compared CPs calculated using the center of proximity with those calculated from the cartilage-overlap method and observed no significant difference between the femoral external rotations based on the contact locations with either method. In an FE model of the knee during a simulated stance, Marouane et al. (2016) compared the estimated CPs from various techniques and compared them with reference contact points at the center of pressure. Estimated CPs using the weighted center of proximity algorithm resulted in lower accuracy but higher precision (estimated by Bland and Altman bias and confidence interval). In this study, we used a weighted center of proximity algorithm to calculate CP locations. Although this algorithm does not take into account the menisci and cartilage thickness variations, it has been proven to be able to identify the contact kinematic changes and abnormalities in human and animal articular joint models (Beveridge et al., 2014; C. Li et al., 2015).

The limited number of subjects and unbalanced composition of males and females in the 2 study groups may have had a potential impact on the results and should be considered as the main limitation of the current work. The subjects were also not matched for body weight or BMI, which could have potentially affected the results. Nevertheless, obesity is typical in OA (Blagojevic et al., 2010) and matching subjects for BMI is difficult. Although the effect of BMI on CP locations should be more specifically addressed in a future study, an inter-subject analysis of the present data (see complementary methodology) does not provide any clue that obesity can shift CPs medially or laterally. Finally, tasks considered were weight-bearing but quasi-static. The validation study was also limited by the fact that only one set of CT bone-scans were available and tested.

The main finding of this study was that, in severe OA, CPs were located more medially and had a higher ratio of medial to lateral posterior movement compared to healthy subjects. The kinematics of tibio-femoral joint and bone-to-bone distances were also changed in OA. The results could provide insight into the mechanisms of OA progression. However, due to the small group size and the unmatched case-control parameters, the results of this work should be viewed with caution. Further research on low and moderate OA could better describe how these alterations occur during OA progression.

3.7 Conflicts of interest

There are no conflicts of interest to report.

3.8 Acknowledgments

This work was supported by the Fonds de Recherche du Québec en Santé (FRQ-S), the Fonds de Recherche du Québec en Nature et Technologie (FRQ-NT), as well as by the Natural Science and Research Council of Canada (NSERC). This work was performed within the framework of the LABEX PRIMES (ANR-11-LABX-0063) of Université de Lyon, within the program "Investissements d'Avenir" (ANR-11-IDEX-0007) operated by the French National Research Agency (ANR).

3.9 Complementary methodology

The original article includes a list of supplementary materials that are not reproduced *in extenso*. Conversely, in this section, we selected some of the important methodological aspects that are not extensively explained in the chapter due to the limited word count of the original article.

3.9.1 Multiple view reconstruction/registration

In the previous studies using EOS® X-ray images, the reconstruction was performed using one pair of X-ray images in the standing posture. A rigid transformation was then applied through a manual or automated process to register the bones onto the X-ray images captured at other postures. Using only one pair of X-ray images for the reconstruction usually results in the best match at the first (typically standing) posture, whereas greater errors exist in other positions. Given the availability of multiple EOS® images in 3D kinematics tracking studies, the

reconstructions could be improved using the features that are not necessarily visible in the first pair of images. For instance, in Figure 3-6 (right), tibia is imaged from a different angle, where the tibial plateau is visible and provides a good distinction of anterior and posterior edges of the plateau whereas in Figure 3-6 (left) the anterior and posterior edges of the plateau have almost overlapped in the X-ray images because they are viewed from a tight angle.

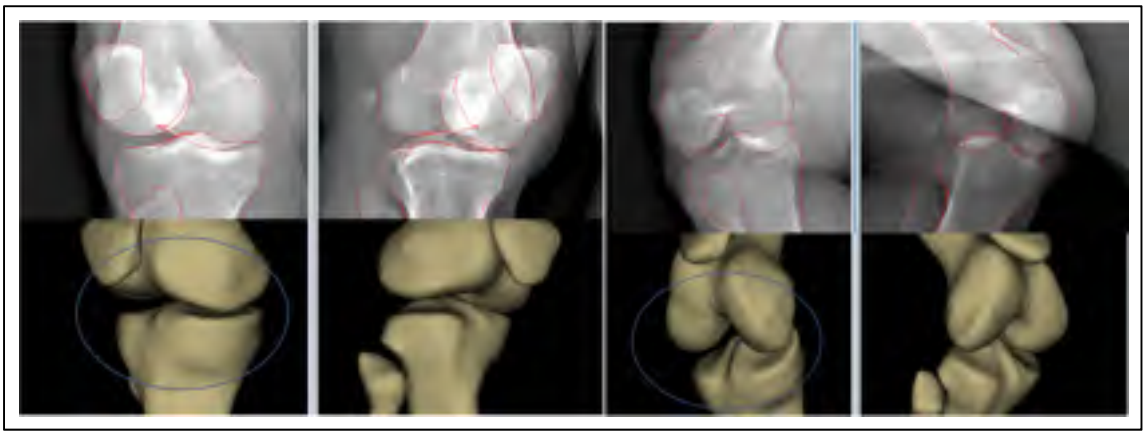

Figure 3-6 Tibiofemoral joint imaged from 2 different angles using EOS® biplane images. The tibial plateau in the left pair of images is viewed from a tight angle where the anterior and posterior edges in the X-rays are superimposed. The right pair of images is the joint images at a different posture where the edges are not superimposed.

In this thesis, we additionally fine-tuned the 3D reconstruction of the bones at the level of the articular surfaces using all available pairs of images. After any change in the 3D reconstruction, the registrations have been readjusted in all views. This process was repeated until the visual reconstruction/registration error i.e., the visual mismatch between the X-ray images and the reconstructed/registratered bone segment was uniformly distributed in all postures (Figure 3-7).

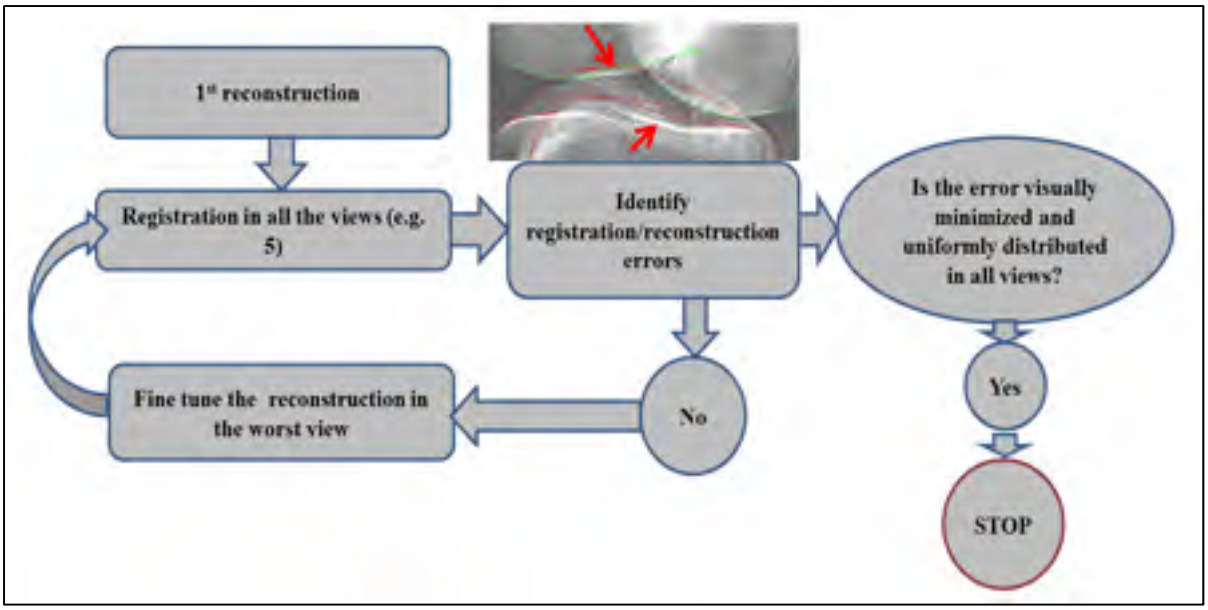

Figure 3-7 Manual multi-view reconstruction/registration using EOS® biplaneX-ray images

3.9.2 Contact point estimation using the weighted center of proximity

Following the reconstruction/registration of the bones, the proximity of the articulating surfaces could provide an approximation of the center of pressure. In the absence of cartilage layer, we assumed that the contact occurs where the two bony surfaces are closest. Therefore, a weighted center of bone-to-bone proximity algorithm was performed to find the contact points (Anderst et al., 2003; Hoshino et al., 2012). Higher weights are assigned to the closets regions as shown in Figure 1-1 A weight factor of 16 is assigned to the regions where the bone-to-bone distance is at its minimum plus 0.5 millimeters. Smaller weights are assigned to the farther regions accordingly.

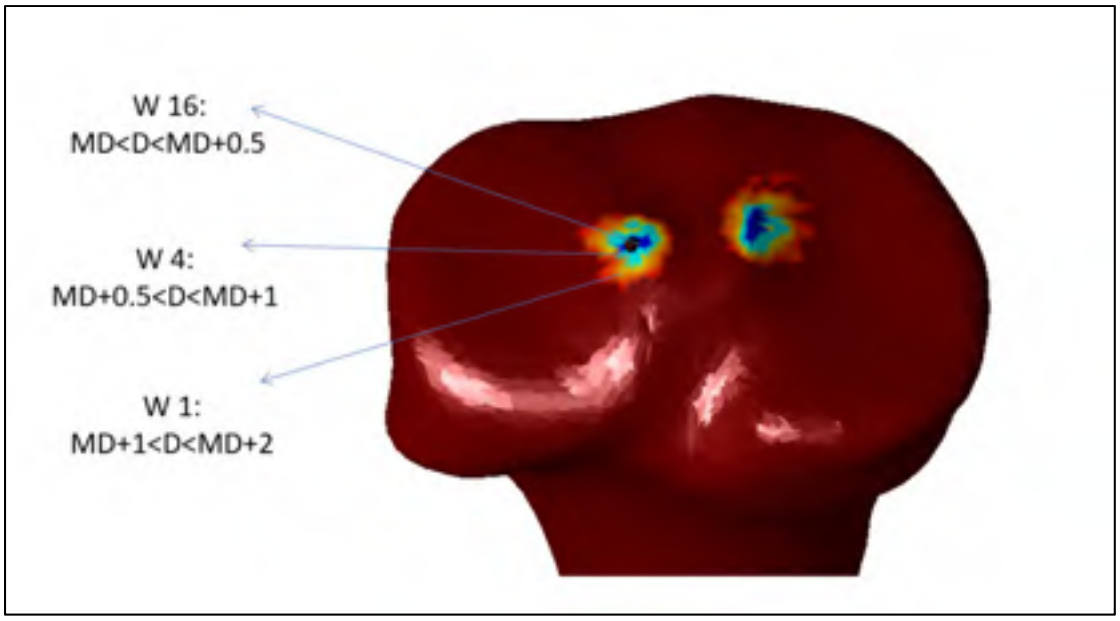

Figure 3-8 weighted center of proximity algorithm for calculation of contact points. Higher weights are assigned to the closest regions

The mesh size had an impact on the minimum bone-to-bone distance calculations. As shown in Figure 3-9, reducing the mesh size changed the estimated bone-to-bone distance from 0.52 mm (right) to 0.45 mm (left). Thereafter, reducing the mesh size had a negligible effect on the estimations. Therefore, the surface mesh in IdefX software was subdivided so that the maximum mesh dimensions be less than 0.2 mm.

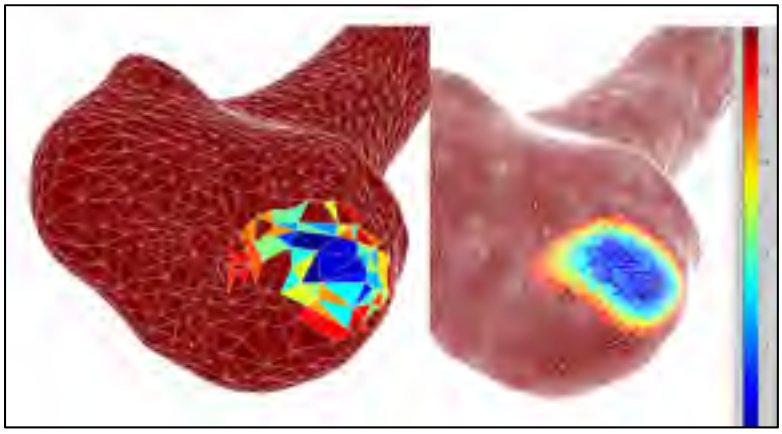

Figure 3-9 The minimum bone-to-bone distance is 0.52mm using a coarse mesh (left), and 0.45mm using a fine mesh.

3.9.3 Validation of contact point estimation

The accuracy of the contact parameters relies on both the accuracies of the reconstruction (T Cresson et al., 2010) and the registration (M. Kanhonou et al., 2014) steps. Thus, a new validation study was designed to evaluate the accuracy of the whole reconstruction/registration technique used to calculate the contact parameters.

One set of tibia, fibula, and femur that were reconstructed from a CT-scan of a healthy subject were positioned manually in 5 configurations to simulate a knee movement and to create a ground truth. This set forms control configurations where the geometry and position of bones are known (Figure 3-10 (right)). Five pairs of digitally generated bi-planar X-ray images were created through the back projection of the bones in each configuration (Moro-oka et al., 2007)(Figure 3-10 (left)).

The proposed reconstruction/registration process was implemented to reconstruct and register bones from the digitally generated bi-planar X-ray images (Figure 3-10 (left)). The root mean square errors (RMSE) between the contact parameters calculated after the simulated reconstruction/registration process and directly from the control configuration were calculated.

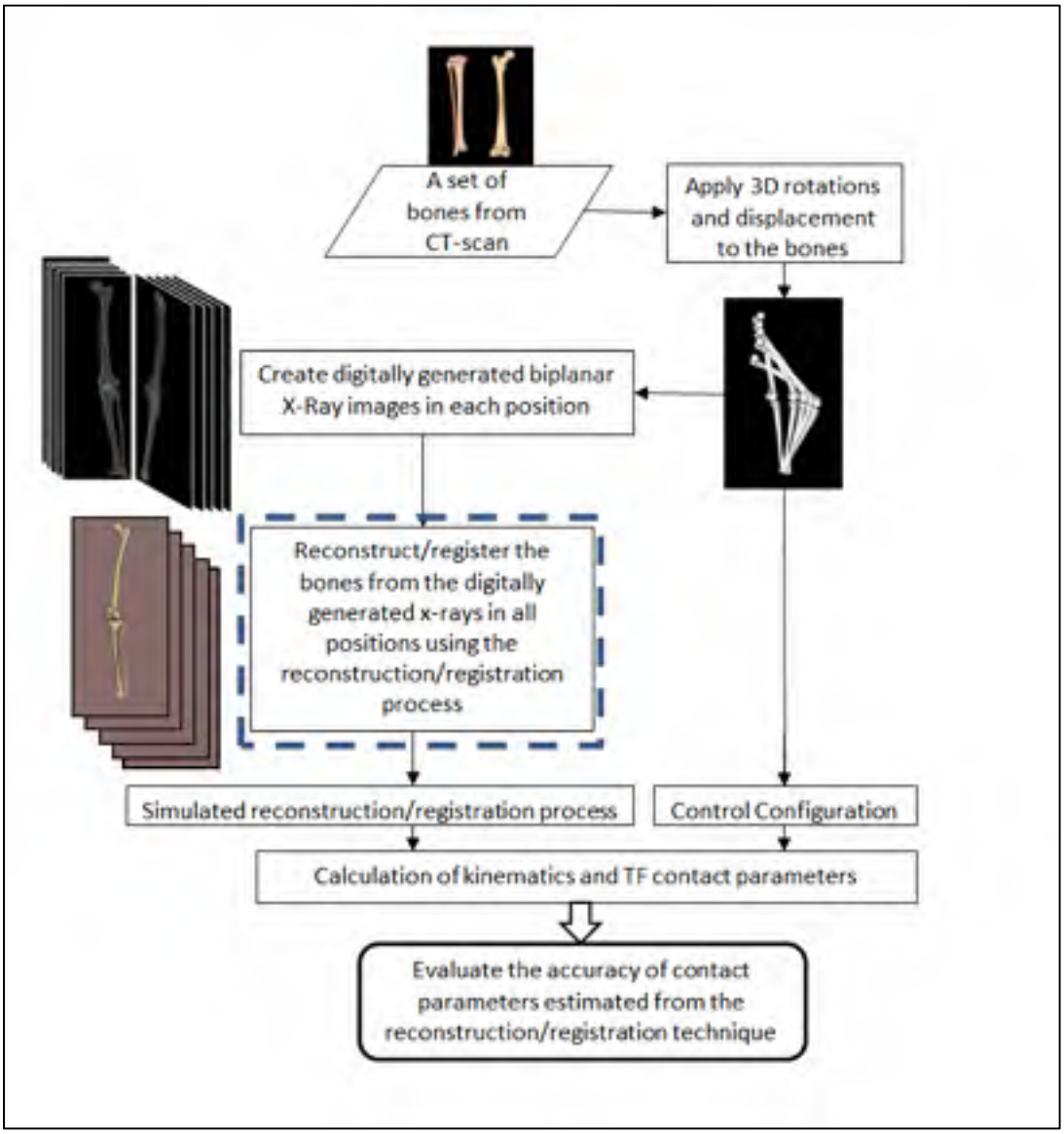

Figure 3-10 Algorithm of validation of the contact parameters estimated by a reconstruction/registration process using stand-alone bi-planar X-ray images, versus a set of controlled movements applied to a set of bones reconstructed from a CT-scan.

The results showed that RMS errors averaged 0.63° for all rotations and 0.8 mm for all displacements. CP locations on the tibial plateau showed RMSEs of 2.0 mm and 3.0 mm (2.5% and 3.8% of the control plateau medial/lateral width) in the anterior/posterior and

medial/lateral directions. The RMSE for the minimum tibiofemoral bone-to-bone distances averaged 0.8 mm in both the medial and lateral compartments (Table 3-2).

Table 3-2 RMSE of quasi-static kinematic parameters, and CP locations estimated by simulated reconstruction/registration process in the validation study.

Parameter	**RMSE**
Tibia flexion/extension	0.2°
Tibia abduction/adduction	1.1°
Tibia internal/external rotation	0.6°
Femur anterior/posterior displacement	1.2 mm
Femur medial/lateral displacement	0.7 mm
Femur proximal/distal displacement	0.6 mm
Anterior/posterior location of CPs on the tibial plateau	2.0 mm
Medial/lateral location of CPs on the tibial plateau	3.0 mm

The validation study assessed the contact parameter accuracies, which represented the cumulative errors of the entire reconstruction/registration process in estimating the CP locations and minimum tibiofemoral bone-to-bone distances. In many 3D/2D registration studies, the reported accuracies were limited to errors in the measured kinematics (Dennis et al., 2005; Guoan Li et al., 2004). Guoan Li et al. (2004) reported accuracies of 0.1 mm and 0.1◦ in measuring the position and orientation of a sphere and a cylinder using dual fluoroscopy. Moro-oka et al. (2007) found that CT-derived bone models offered better kinematics predictions compared to MRI-derived models with RMSE of 1.1 mm and 0.6◦ for all knee joint displacements and rotations, which compares to 0.8 mm and 0.6◦ for the corresponding pseudo-kinematic values in our study.

3.9.4 Medial and lateral contact point location vs. BMI

Since the OA and healthy groups are not matched for BMI, we tested if the medial shift of the contact point could be the result of different BMI rather than the pathology.

Figure 3-11) shows the mean medial and lateral CP locations for all 19 healthy and OA subjects averaged at the 5 squat positions, on the medial and lateral plateaus versus BMI. The goal is to find out if BMI has a correlation with the medial lateral CP locations in each of the 2 groups and on each plateau.

1- The Pearson's correlation coefficients in each of the 4 data series showed a weak correlation between the mean medial lateral CP locations and BMI. These results suggest that BMI alone can barely result in a trend in medial lateral CP locations.

Medial OA and BMI: r=0.15, p=0.68
Lateral OA and BMI: =0.47, p=0.19
Medial healthy and BMI: r=-0.30, p=0.39
Lateral healthy and BMI: r =0.29, p=0.40

2- For the few OA and healthy subjects with similar BMIs (see ellipses in Figure 3-11), CP location of OA subjects tended to be more medial compared to similar healthy controls, which is consistent with the general findings of the present study about a medial shift in OA.

Although the effect of BMI on CP locations needs to be more specifically addressed in a future study, the inter-subject data does not provide clear clues that obesity can shift CPs medially or laterally. However, a confounding parameter such as BMI could have affected the results and further study on this issue is important.

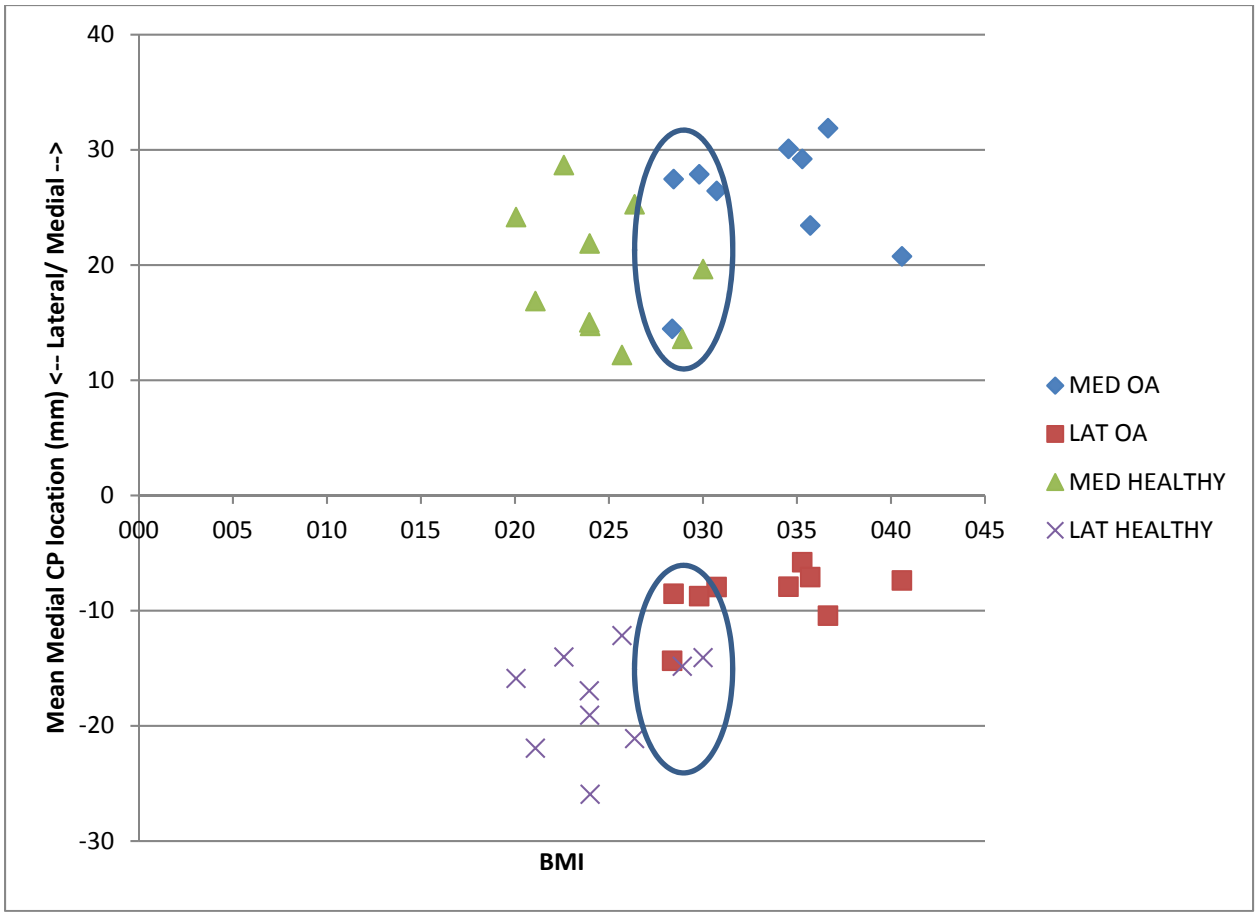

Figure 3-11 Average medial and lateral CP locations for healthy and OA, on the medial and lateral plateaus versus BMI

CHAPTER 4

QUANTITATIVE EVALUATION OF EVOKE™ KNEE ORTHOSIS USING EOS® BIPLANE X-RAY IMAGES DURING SQUAT MOVEMENT

4.1 Preface

This project was performed in the framework of an industrial collaboration with the company Medicus during May 2015 – November 2017. The aim of the project was to compare the contact point locations of OA subjects during a quasi-static task with and without wearing a valgus knee orthosis. The contact points measurement was similar to chapter 3 methods. Our hypothesis was that the valgus knee orthosis shifts the contact point location laterally on both the medial and lateral compartments of OA joints. This chapter addresses the fourth objective of the first problematic of the thesis. In this thesis, the methodology and the preliminary results for one subject are presented. This could be seen as a proof of concept for the use of contact point locations as a parameter for evaluating the effectiveness of knee orthoses.

4.2 Introduction

Knee orthoses are medical devices intended to stabilize or limit the movement of the knee. The considerable increase in the supply of these devices has not been followed by an evaluation of the real effectiveness of these orthoses, both in terms of the postulated physiological effects or the therapeutic effects in the short or long term. Knee orthoses are classified into four categories: knee sleeves, functional knee braces, rehabilitative or post-operative knee braces, or prophylactic knee braces (Martin et al., 2001; Thoumie et al., 2001). In this project, we will focus on functional orthoses, particularly, in case of medial compartment knee OA. Previous works attempted to test the concept of reducing the stresses on the medial compartment of the knee during walking with the use of a valgus orthosis and Matsuno et al. (1997) showed a

reduction in pain as well as a 16% improvement in isokinetic quadriceps strength in 20 subjects with internal compartment knee osteoarthritis over a period of 12 months. Komistek et al. (1999) showed, with dynamic fluoroscopy, a 2-mm increase in joint space in the tibiofemoral joint and a reduction in pain in 80% of subjects. A more recent meta-analysis conducted by (Moyer et al., 2015) on valgus orthoses approved a significant reduction in the external KAM during walking. Furthermore, this meta-analysis revealed that the biomechanical parameters most often used in the measurement of the results are: the KAM during the stance phase (17 studies), followed by the alignment in the frontal plane (11 studies), external KFM (4 studies), joint space (4 studies), measured forces on the orthosis (3 studies), computed contact forces as well as muscle activations (2 studies). Most of these studies were performed with fixed-axis and fixed valgus orthoses. In addition, 3D joint kinematics and tibiofemoral contact point locations have never been measured. The company Médicus has developed a new orthosis (Evoke™) with a light yet strong material which is adjusted to the morphology of the subject through 3D printing of the brace. The orthosis has a hinge with a polycentric axis capable of generating an articular coupling between the flexion/extension and the internal/external rotation close to the joint kinematics of the normal knee measured on cadaver (Walker et al., 1985). Our hypothesis is that this orthosis while limiting unwanted movements of the knee, gives it a dynamic and kinematics close to the healthy knee. The goal of this project is to accurately assess the immediate effect of wearing Evoke™ knee orthosis on 3D kinematics, tibiofemoral contact points, as well as the ground reaction forces and moments during a controlled squat movement.

4.3 Methodology

4.3.1 Subjects

Six subjects (n = 6) with severe medial knee osteoarthritis participated in the project with a Kellegren-Lawrence grade 4. Due to the ongoing status of the project and confidentiality of the results at this time, only the results of one participant (68 yrs., female, 1.70 m, 89 kg, left knee) are presented in this thesis.

A personalized Evoke™ orthosis was fabricated for each participant at Médicus laboratory. A 4-week adaptation period is required for wearing the orthosis before doing the test. The subject performed the test 12 weeks after receiving the orthosis. Two Knee injury and Osteoarthritis Outcome Score (KOOS) questionnaires were filled by the subject at the time of first clinical evaluation and again after the adaptation period upon arrival for doing the experiments. The subject completed the consent form approved by the CRCHUM and ETS ethics Committees.

4.3.2 Experimental protocol

The subject adopted 5 weight-bearing squat postures from the standing to a maximum flexion of 70^{o} i.e. at 0^{o}, 15^{o}, 30^{o}, 45^{o}, and 70^{o} knee flexion. The subject then performed the same 5 postures while wearing the orthosis. A positioning support with adjustable height helped the participant to keep the posture. For each of the 10 postures, a pair of EOS® biplane images were acquired. To ensure that the posture is the same with and without the orthosis, 3 inertial APDM sensors were placed on the shank, thigh, and sternum to control the knee flexion/extension angle and trunk inclination in real-time and adjust the position if necessary.

An AMTI force platform (ORS-6) was fixed inside the EOS® cabinet to measure the forces and moments under the studied foot. A platform was designed to isolate the reaction forces under the contralateral foot while both feet are maintained at the same level (Figure 4-1). The spacing between the feet was defined so that the distance between the external malleoli corresponds to the inter-acromion gap at the shoulder.

Figure 4-1: Force platform in the EOS® cabinet measures the forces under the studied foot in the middle while the contralateral foot is isolated from the force platform.

4.3.3 Analysis of biomechanical parameters

Following the two sets of squat positions with and without wearing the orthosis, the following parameters were be calculated accordingly: the 6 DOF kinematics of the knee joint from the internal landmarks using the biplane images; the flexion / extension of the knee and the trunk inclination using the inertial sensors; the medial and lateral contact point locations; the medial/lateral vector connecting the contact points; ground reaction forces; minimum bone-to-

bone distance; location of medial/lateral femoral epicondyle; and the 3D geometry of the bone to check the joint configuration and identifying the orthosis hinge screw location with respect to the joint. The details of the experimental protocol, the 3D/2D registration technique, and the estimation of the contact point location are detailed in Chapter 3 or in A Zeighami et al. (2017).

4.4 Results

4.4.1 KOOS questionnaire

The global KOOS score was improved ~23 points after 12 weeks of wearing the orthosis (Table 4-1), showing a remarkable improvement in the subject's opinion about the symptoms and relevant problems to OA.

Table 4-1 The KOOS results before and after wearing the orthosis: KOOS Pain, KOOS Symptoms, KOOS Disability on the level of daily activities (ADL), KOOS Sport/Rec, KOOS QOL: Quality of life (QOL)

KOOS outcome	***Without orthosis***	***With orthosis***
KOOS Pain:	47.22	36.11
KOOS Symptoms:	57.14	32.14
KOOS ADL:	51.47	23.53
KOOS Sport/Rec:	80.00	60.00
KOOS QOL:	81.25	50.00
Global score:	63.42	40.36

4.4.2 Posture control using inertial sensors and kinematics

The squat postures were controlled and repeated with and without wearing the orthosis using the inertial sensors. The knee flexions were maintained in ± 5° range from the 5 targeted squat positions i.e. (0°, 15°, 30°, 45°, and 70° knee flexion) (Table 4-2). Between the two sets of

experiments with and without the orthosis, the postures were repeated with an average difference of 2.8° ± 2.3° (maximum error = 5.1°) for the knee flexion and 0.35° ± 3.63° (maximum error = 5.8°) for the trunk inclination.

The kinematics calculated from the internal landmarks (bone-imbedded landmarks) resulted in 10.3±4.1 higher flexion angles compared to those calculated from the inertial sensors.

Table 4-2 (1) kinematics: The knee flexion and trunk inclination from the inertial sensors and from the knee flexion/extension (Flx(+)/Ext(-)), adduction abduction (Add(-)/Abd(+)), and internal/external rotation (Ext(-)/Int(+) rot) measured from internal landmarks on the reconstructed bones and the femur origin: the origin of femur (middle of condyles) on the tibia coordinate system. (2) Force platform: vertical ground reaction force (Fz). (3) Contact point location: medial and lateral contact point locations in anterior/posterior (AP (x)), medial/lateral (ML (z)), and proximal/distal directions (PD (y)). (4) Minimum distance: minimum bone-to-bone distance on the medial and lateral sides

			without orthosis					with orthosis				
			0°	15°	30°	45°	70°	0°	15°	30°	45°	70°
Kinematics	APDM inertial sensor	knee flexion	0°	15°	30°	45°	70°	0°	15°	30°	45°	70°
		trunk inclination	1.7	18.8	39.4	50.0	69.1	2.5	15.4	35.6	44.8	66.6
	internal landmarks	Flx(+)/Ext(-)	7.3	11.3	22.1	28.2	27.8	9.5	14.9	21.9	22.3	26.4
		Add(-)/Abd(+)	8.9	25.9	47.7	57.6	84.0	3.8	20.4	40.8	53.8	80.6
		Ext(-)/Int(+) rot	-1.8	-0.1	-2.0	-0.2	-1.1	-1.4	-2.1	0.3	0.9	0.4
	femur origin	Ant(+)/Pos(-)	4.1	15.5	13.2	19.4	19.6	7.8	9.4	17.7	18.0	19.2
		Prox(+)/dist(-)	-8.4	-8.8	-7.0	-6.5	-5.0	-5.0	-10.4	-7.6	-8.4	-5.6
		Med(-)/lat(+)	-12.7	-10.9	-10.4	-10.8	-10.0	-15.2	-11.5	-11.2	-9.7	-10.4
Force platform		Fz (N)	433.16	-9.6	-8.8	-7.6	-7.7	-7.6	-5.7	-9.4	-7.9	-8.1
Contact points	CP location medial	AP (x)	433.16	433.2	490.7	462.6	368.4	320.3	489.0	508.6	502.3	455.9
		PD (y)	1.4	2.9	-1.9	0.8	3.0	13.0	-2.8	5.0	-3.1	2.4
		ML (z)	10.1	10.1	10.0	10.1	10.0	6.6	10.3	9.7	10.0	10.0
	CP location lateral	AP (x)	-31.3	-31.7	-30.8	-30.9	-30.4	-20.6	-32.5	-30.2	-30.9	-29.3
		PD (y)	-1.1	-4.7	-3.5	-5.3	-8.7	1.5	-3.1	-5.3	-6.8	-9.0
		ML (z)	0.2	1.4	1.6	2.0	3.6	0.9	0.6	2.1	3.0	4.4
Minimum distance		Medial	2.30	5.4	5.7	7.1	6.6	7.6	7.9	4.9	7.1	8.0
		Lateral	0.35	2.30	2.3	1.4	1.5	2.1	0.1	3.3	1.0	2.7

4.4.3 Tibiofemoral contact

The effect of wearing the orthosis on the location of contact points is mainly noticeable on the medial tibial plateau. In the first squat position, the medial contact point is shifted 11.52 mm laterally and 10.75 mm anteriorly after wearing the orthosis. Other noticeable shifts of the contact points occurred on the medial plateau in anterior/posterior direction with the contact points at 15°, 30°, and 45° knee flexion were accordingly shifted 5.63 mm posteriorly, 6.8 mm anteriorly, and 3.86 mm posteriorly (Table 4-2). Other shifts of the contact point locations in the medial/lateral or anterior/posterior directions fell below 3 mm which is the accuracy of the contact point location estimation as described in chapter 3.

The center of the femur with respect to the tibia demonstrated small displacements in medial/lateral or anterior/posterior directions except at 0° with 3.4 mm anterior and 3.9 mm lateral shift.

The minimum bone-to-bone distance on the medial side increased by 0.52±0.82 mm after wearing the orthosis.

Table 4-3 Location of the medial and lateral contact points (* marks) before (blue) and after (red) wearing the orthosis, the origin of femur (middle of condyles) on the tibia coordinate system (x mark), and the epicondyles projected on the tibial plateau (o marks).

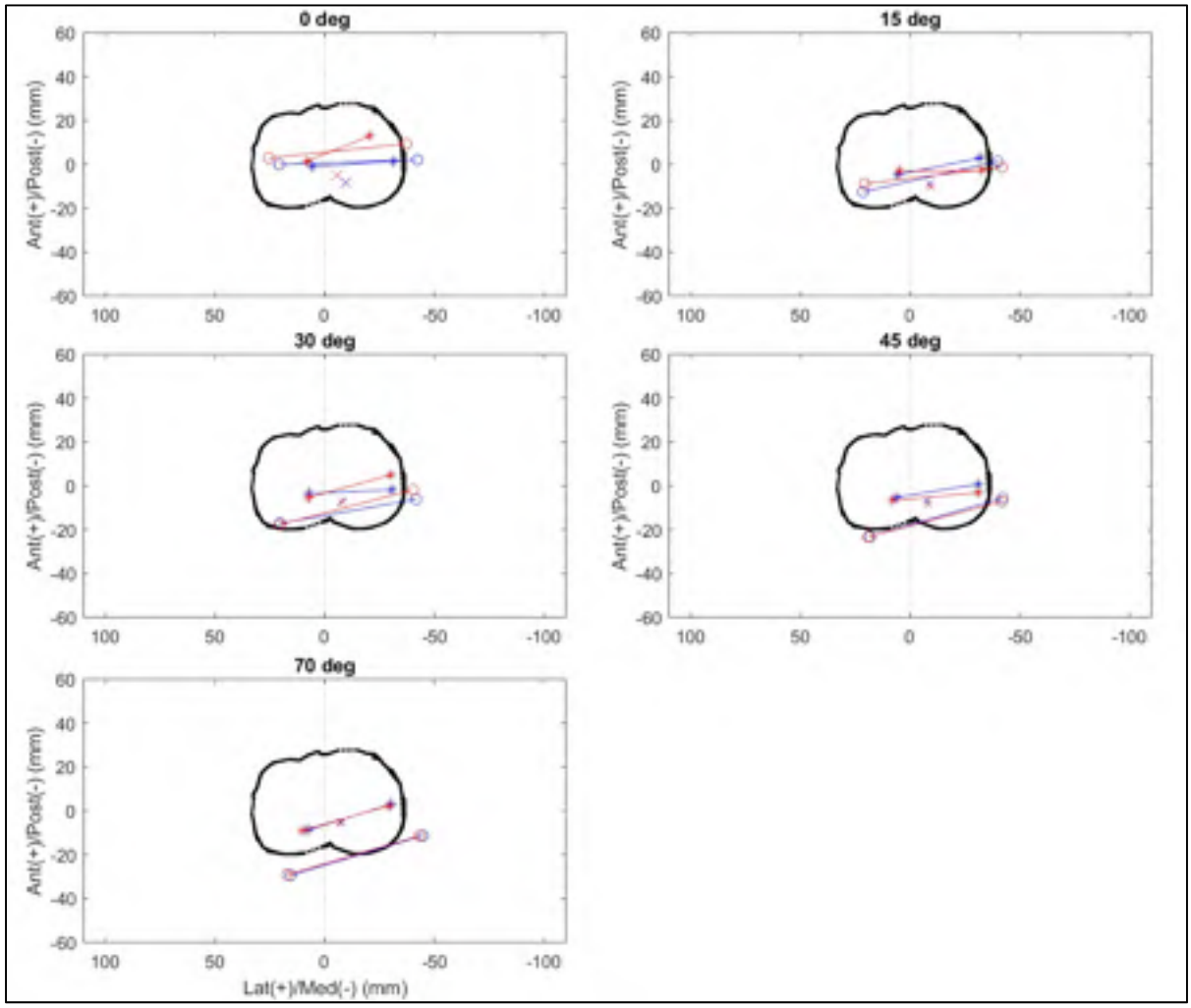

4.5 Conclusion:

This project was a proof of concept for the use of 3D/2D registration techniques to investigate the effect of a valgus knee orthosis on the knee kinematics and contact points locations. The contact point locations of the subject in this study did not demonstrate big shifts after wearing the orthosis expect for the standing posture on the medial side.

Comparing the contact point location with and without the orthosis requires accurately repeating the posture in the two set of experiments to minimize the effect of posture differences on the contact point locations. Inertial sensors provided a repeatable means of controlling and adjusting the posture in real-time, however, knee flexion measured by these sensors always showed smaller values with respect to the flexion calculated using internal landmarks on the bones. The sensors attached to the skin are not necessarily aligned with the bone causing a bias in the flexion/extension estimations. This bias can be amplified by the soft tissue artefact.

Each orthosis is designed according to the anatomical landmarks which are estimated from the digitized skin surface of the subject. The extent to which these estimated points correspond to the real anatomical landmarks requires knowledge of the skeleton configuration with respect to the orthosis. Using the 3D/2D imaging techniques for the analysis of the orthoses allows accurate localization of the orthosis with respect to the skeleton and the joint (Figure 4-2). Having the orthosis and the skeleton in one frame during movement is of high interest and importance in the design of the orthoses. This could also help to verify if the orthosis is placed as expected with respect to the joint and if desired design kinematics (e.g., that of (Walker et al., 1985)) is reproduced.

This study showed the feasibility of testing the impact of a knee orthosis on the kinematics, ground reaction forces (not presented here), contact points, and joint configurations using 3D/2D registration techniques. However, it is not clear if the observed changes exist in the other subjects and if wearing the orthosis affects them in the same direction/manner. More

subjects are required to draw a conclusion about the effectiveness of the orthosis. Moreover, given the availability of the ground reaction forces in this experiments, it is possible to use inverse dynamics to compare the external loads at the knee level or use the musculoskeletal models (as presented in Chapter 5) to estimate the contact forces and evaluate the impact of the knee orthosis on them.

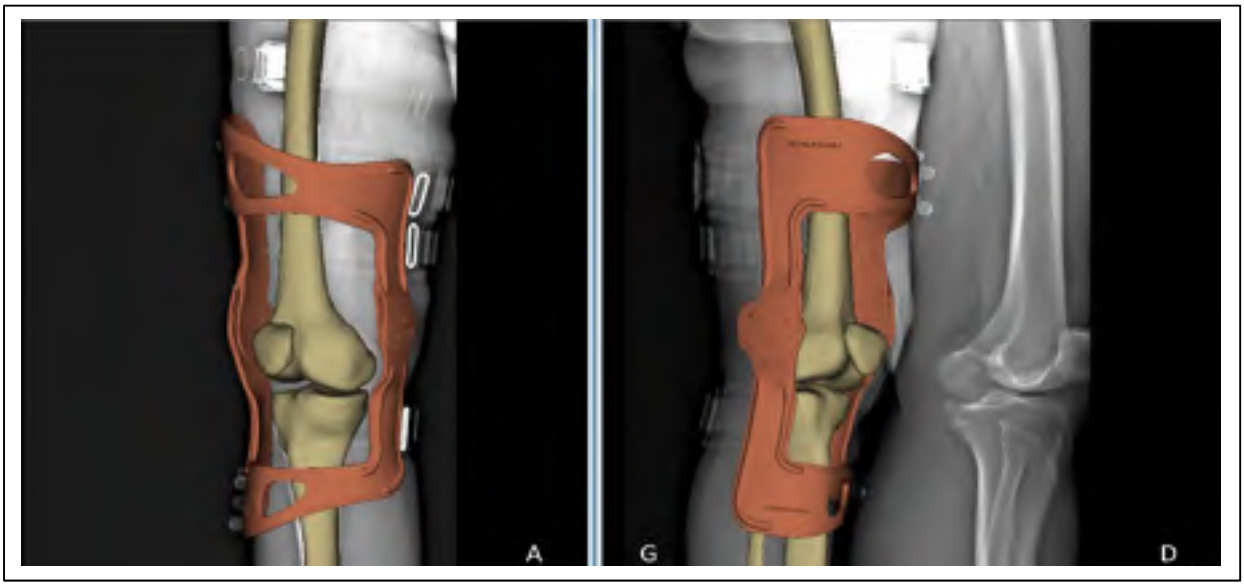

Figure 4-2 Illustration of the placement of the orthosis with respect to the joint.

CHAPTER 5

KNEE MEDIAL AND LATERAL CONTACT FORCES IN A MUSCULOSKELETAL MODEL WITH SUBJECT-SPECIFIC CONTACT POINT TRAJECTORIES

A. Zeighami[1*], R. Aissaoui[1], R. Dumas[2]

1. Laboratoire de Recherche en Imagerie et Orthopédie (LIO), École de Technologie Supérieure (ÉTS), Centre de Recherche du CHUM, Montréal, Québec, Canada
2. Université Lyon, Université Claude Bernard Lyon 1, IFSTTAR, UMR_T9406, LBMC, F69622, Lyon, France

This article has been published in Journal of Biomechanics 69 (2018): 138-145.

5.1 Preface

This chapter addresses the second aim of this thesis: Providing a musculoskeletal model of the lower limb which enables integration of personalized contact points.

5.2 Abstract

Contact point (CP) trajectory is a crucial parameter in estimating medial/lateral tibio-femoral contact forces from the musculoskeletal (MSK) models. The objective of the present study was to develop a method to incorporate the subject-specific CP trajectories into the MSK model. Ten healthy subjects performed 45-second treadmill gait trials. The subject-specific CP trajectories were constructed on the tibia and femur as a function of extension/flexion using low-dose bi-plane x-ray images during a quasi-static squat. At each extension/flexion position, the tibia and femur CPs were superimposed in the three directions on the medial side, and in the anterior/posterior and proximal/distal directions on the lateral side to form the five kinematic constraints of the knee joint. The Lagrange multipliers associated to these constraints directly yielded the medial/lateral contact forces. The results from the personalized CP trajectory model were compared against the linear CP trajectory and sphere-on-plane CP trajectory models which were adapted from the commonly used MSK models. Changing the

CP trajectory had a remarkable impact on the knee kinematics and changed the medial and lateral contact forces by 1.03 BW and 0.65 BW respectively, in certain subjects. The direction and magnitude of the medial/lateral contact force were highly variable among the subjects and the medial/lateral shift of the CPs alone could not determine the increase/decrease pattern of the contact forces. The suggested kinematic constraints are adaptable to the CP trajectories derived from a variety of joint models and those experimentally measured from the 3D imaging techniques.

Keywords: knee contact force, musculoskeletal model, subject-specific, contact point trajectory, gait.

5.3 Introduction

Current musculoskeletal (MSK) models of the lower limb demonstrated good accuracy in the estimation of the contact forces between femoral and tibial instrumented prosthetic components (Gerus et al., 2013; Jung et al., 2016; Kia et al., 2014; Marra et al., 2015). However, the accuracy of the medial/lateral contact force estimation considerably improved by customizing the point of contact force application (Lerner et al., 2015). The estimation of the intact knee joint contact forces still remains a challenge, because the medial and lateral contact forces cannot be well calculated without a good estimate of the subject's contact point (CP) trajectories (Saliba et al., 2017a). Such information is very difficult to obtain *in vivo* because it relies on both joint kinematics and articular surface geometries. However, recent methods could estimate knee contact parameters in weight-bearing conditions using either bi-plane fluoroscopy (Farrokhi et al., 2016; Farrokhi et al., 2014), or bi-plane low-dose radiography (A Zeighami et al., 2017). Biplane imaging allows for a relatively small registration error and yields an estimation of CPs based on the concept of minimal bone-to-bone distance (A Zeighami et al., 2017). The CP trajectory predictions were similar to *in vitro* measurements of the center of pressure (Draganich et al., 1987). Each of these studies showed

that the trajectory of the center of bone-to-bone proximity reveals inter-subject differences as well as distinctions between healthy and osteoarthritic knees.

Within inverse dynamics computational frameworks, subject-specific joint kinematics has been introduced in MSK models at the step of inverse kinematics (Gerus et al., 2013; Scheys et al., 2011; Valente et al., 2015; L. Zheng et al., 2014). Nevertheless, the definition of CP trajectories, at the step of joint contact force computation, remains most of the time very basic, i.e. at a fixed distance from the tibial plateau centreline. This fixed distance is typically set at 25% of tibial plateau width (Johnson et al., 1981) in a range from 20 mm (Gerus et al., 2013; Schipplein et al., 1991) to 25 mm (Crowninshield, 1978; D. Lloyd et al., 1996; Morrison, 1970) in various studies or, eventually, a customized distance determined using a standing radiograph (Lerner et al., 2015).

In an earlier study, (Nissan, 1980) performed a sensitivity analysis by moving the CP 5 mm in the anterior/posterior direction and found that the posterior and anterior displacements would respectively increase the contact force by about 500N and decrease it by about 350N. More recently, Lerner et al. (2015) and Saliba et al. (2017a) moved the CP locations only in the medial/lateral direction. They found that reducing the lever arm by moving the CP close to the knee joint fulcrum increased the contact forces in the corresponding compartment by a gradient up to 0.06 BW/mm. Therefore, it is crucial to take into account the CP trajectories. Nevertheless, these authors computed the contact forces in a two-step procedure by considering the equilibrium of the contact forces, the musculo-tendon forces and the joint moment in the frontal plane. Therefore, they could not consider anterior/posterior shifting of the CP. Moreover, the modification of the CP trajectories was totally independent of the knee kinematics. In the light of articular surface geometrical complexity, recent experimental studies have demonstrated that each subject has a unique CP trajectory which showed medial/lateral and anterior/posterior excursions (Farrokhi et al., 2016; C. Li et al., 2015; Qi et al., 2013; A Zeighami et al., 2017). The anterior/posterior and medial/lateral excursion of CPs in healthy subjects could reach 7.1 mm and 5.1 mm in 0^{o}-30^{o} flexion range (A Zeighami et al., 2017). This excursion should be taken into account in contact force calculation.

To our knowledge, no study has yet estimated the contact forces along the subject-specific CP trajectories. The objective of the present study is to propose a new method to introduce subject-specific CP trajectories directly at the step of inverse kinematics, through relevant kinematic constraints. Moreover, similar to the anatomical constraints standing for the articular surfaces and ligaments (Florent Moissenet et al., 2012, 2014), the Lagrange multipliers associated to these kinematic constraints stand straightforwardly for the contact forces at the medial and lateral CPs. This allows for a one-step procedure to compute simultaneously musculo-tendon forces and contact forces.

5.4 Material and Methods

5.4.1 Musculoskeletal Model

The musculoskeletal model of the lower limb used in the present study is the same as (Florent Moissenet et al., 2014) except for the tibiofemoral joint constraints. The model is parameterized with natural coordinates $\mathbf{Q}_i$ where each segment is defined by two unitary directional vectors and two position vectors (De Jalon et al., 2012; R. Dumas et al., 2007). It consists of five segments, i.e. foot, shank, patella, thigh, and pelvis (i = 1, …, 5). The hip joint is spherical and the patellofemoral and ankle joints are parallel mechanisms. Muscular lever arms were computed using the muscular geometry of Delp et al. (1990).

In the present study, the tibiofemoral joint (T) is modeled with five kinematics constraints:

$$\mathbf{\Phi}_T^k = \begin{pmatrix} \left(\mathbf{N}_4^{V_4^1}(\theta)\mathbf{Q}_4 - \mathbf{N}_2^{V_2^1}(\theta)\mathbf{Q}_2\right) \bullet \mathbf{N}_2^{\mathbf{X}_2}\mathbf{Q}_2 \\ \left(\mathbf{N}_4^{V_4^1}(\theta)\mathbf{Q}_4 - \mathbf{N}_2^{V_2^1}(\theta)\mathbf{Q}_2\right) \bullet \mathbf{N}_2^{\mathbf{Y}_2}\mathbf{Q}_2 \\ \left(\mathbf{N}_4^{V_4^1}(\theta)\mathbf{Q}_4 - \mathbf{N}_2^{V_2^1}(\theta)\mathbf{Q}_2\right) \bullet \mathbf{N}_2^{\mathbf{Z}_2}\mathbf{Q}_2 \\ \left(\mathbf{N}_4^{V_4^2}(\theta)\mathbf{Q}_4 - \mathbf{N}_2^{V_2^2}(\theta)\mathbf{Q}_2\right) \bullet \mathbf{N}_2^{\mathbf{X}_2}\mathbf{Q}_2 \\ \left(\mathbf{N}_4^{V_4^2}(\theta)\mathbf{Q}_4 - \mathbf{N}_2^{V_2^2}(\theta)\mathbf{Q}_2\right) \bullet \mathbf{N}_2^{\mathbf{Y}_2}\mathbf{Q}_2 \end{pmatrix} \tag{5.1}$$

with $\mathbf{N}_i^{V_i^j}(\theta)$ the interpolation matrix for the j^{th} virtual marker of the i^{th} segment depending on the tibiofemoral extension/flexion angle θ and with $\mathbf{N}_2^{\mathbf{X}_2}$, $\mathbf{N}_2^{\mathbf{Y}_2}$, $\mathbf{N}_2^{\mathbf{Z}_2}$ the interpolation matrices for the axes of the tibia segment coordinate system. The interpolation matrices, $\mathbf{N}$, allow determining the position of any point (or the orientation of any direction) embedded in the relevant segment knowing its natural coordinates $\mathbf{Q}_i$.

Specifically, these virtual markers (i.e., V_2^1, V_2^2, V_4^1, and V_4^2) correspond to the medial and lateral CPs embedded in the shank and thigh segment, respectively. The position of these CPs is prescribed as a function of the tibiofemoral extension/flexion angle in the same way as the ligament lengths in (Gasparutto et al., 2015; Sancisi et al., 2017). The CP locations are provided in annex 1. Just like the coupling curves between the degrees of freedom introduced in many MSK models (Arnold et al., 2010; Delp et al., 1990; DeMers et al., 2014; Liu et al., 2008), there are five kinematic constraints at each position in extension/flexion of the joint. The medial CPs of tibia and femur were superimposed in the three directions of space while the lateral CPs of tibia and femur were superimposed only in the **X** (anterior/posterior) and **Y** (proximal/distal) directions of the shank.

The inverse kinematics step is formulated as:

$$\min_{\mathbf{Q}} f = \frac{1}{2}\left(\mathbf{\Phi}^m\right)^T \mathbf{\Phi}^m \qquad (5.2)$$
$$\text{subject to } \begin{pmatrix} \mathbf{\Phi}^k \\ \mathbf{\Phi}^r \end{pmatrix} = \mathbf{0}$$

with the complete definitions of the objective function f, driving constraints $\mathbf{\Phi}^m$, kinematic constraints $\mathbf{\Phi}^k$, and rigid body constraints $\mathbf{\Phi}^r$ detailed in (Duprey et al., 2010; El Habachi et al., 2015).

The kinematic constraints $\mathbf{\Phi}^k$ include all the constraints for ankle (A), patellofemoral (P), tibiofemoral (T) (i.e., $\mathbf{\Phi}_T^k$) and hip (H) joints.

The inverse dynamics step is then formulated as:

$$\begin{bmatrix} \mathbf{L} & -\mathbf{K}^T \end{bmatrix} \begin{pmatrix} \mathbf{f} \\ \boldsymbol{\lambda} \end{pmatrix} = \mathbf{G}\ddot{\mathbf{Q}} - \mathbf{R} - \mathbf{P} \qquad (5.3)$$

solved by the following optimization procedure:

$$\min_{\begin{pmatrix} \mathbf{f} \\ \boldsymbol{\lambda}_1 \end{pmatrix}} J = \frac{1}{2}\begin{pmatrix} \mathbf{f} \\ \boldsymbol{\lambda}_1 \end{pmatrix}^T \mathbf{W} \begin{pmatrix} \mathbf{f} \\ \boldsymbol{\lambda}_1 \end{pmatrix} \qquad (5.4)$$
$$\text{subject to } \begin{cases} \mathbf{Z}_{\mathbf{K}_2{}^T} \begin{bmatrix} \mathbf{L} & -\mathbf{K}_1{}^T \end{bmatrix} \begin{pmatrix} \mathbf{f} \\ \boldsymbol{\lambda}_1 \end{pmatrix} = \mathbf{Z}_{\mathbf{K}_2{}^T} \left(\mathbf{G}\ddot{\mathbf{Q}} - \mathbf{P} - \mathbf{R}\right) \\ \begin{pmatrix} \mathbf{f} \\ \boldsymbol{\lambda}_1 \end{pmatrix} \geq \mathbf{0} \end{cases}$$

with the complete definitions of the objective function *J*, the vector of musculo-tendon forces **f**, the Lagrange multipliers $\boldsymbol{\lambda}$, the sub-vector of Lagrange multipliers $\boldsymbol{\lambda}_l$ in the objective function, the optimisation weights matrix **W**, the projection matrix $\mathbf{Z}_{\mathbf{K}_2{}^T}$, the matrix of generalised muscular lever arms **L**, the Jacobian sub-matrix $\mathbf{K}_1$, the matrix of generalised masses **G**, the vector of generalised accelerations $\ddot{\mathbf{Q}}$, the vector of generalised weights **P**, and the vector of generalised ground reaction **R** detailed in Florent Moissenet et al. (2014).

The two sub-matrices $\mathbf{K}_1$ and $\mathbf{K}_2$ of the Jacobian matrix $\mathbf{K} = \frac{\partial \begin{pmatrix} \mathbf{\Phi}^k \\ \mathbf{\Phi}^r \end{pmatrix}}{\partial \mathbf{Q}}$ are introduced to select the Lagrange multipliers to be included in the optimization and cancel the others with the projection matrix $\mathbf{Z}_{\mathbf{K}_2{}^T}$. As such, the Jacobian sub-matrix $\mathbf{K}_1$ includes, among others, the derivatives $\frac{\partial \mathbf{\Phi}_T^k}{\partial \mathbf{Q}}$ and the corresponding Lagrange multipliers stand straightforwardly for the contact forces at the medial and lateral CPs and about the axes of the shank segment coordinate system.

The MSK modeling package runs on Matlab™. The simulation time of the MSK model for a single gait cycle was around 90 seconds.

5.4.2 Experimental protocol

Ten healthy (6 men, 4 women, 55.4 ± 9.5 yrs., 1.67 ± 0.10 m, 71.5 ± 13.3 kg) subjects walked with their comfortable speed on an instrumented split-belt treadmill (AMTI, Watertown, MA, USA) for 45 seconds. A 12-camera VICON system (Oxford Metrics, UK) recorded the 3D motion of the reflective markers mounted on the KneeKG™ (Emovi Inc., Laval, QC, Canada) system. Markers and force platform data were filtered using a 2nd order zero-lag Butterworth filter with automatic estimation of cut-off frequencies

(Aissaoui et al., 2006). The joint angular displacements at the hip, knee, and ankle levels were assessed using a functional calibration method (Hagemeister et al., 2005). The joint kinematics and contact forces were normalized to 100% of the stance phase of gait. EMG signals of 8 muscles were collected to find the active/inactive concordance with the estimated musculo-tendon forces (see complementary methodology). The experimental protocol was approved by the ethics committees of the Centre de recherche (CRCHUM) and the École de technologie supérieure de Montréal (ÉTS).

5.4.3 CP trajectories

Three CP trajectory models were used in the MSK model. The corresponding polynomial equations are presented in the annex I.

1) Linear CP trajectory (LCP): This model represents the general assumptions made in many MSK models (Johnson et al., 1981; Lerner et al., 2015; D. Lloyd et al., 1996; Morrison, 1970; Saliba et al., 2017a; Winby et al., 2009). The contact forces, musculo-tendon forces and joint moment are only balanced in the frontal plane of the tibia at a given distance from the tibial plateau centreline. To build the complying version of the model to the Eq. (5-1), the tibial CPs were represented by two straight lines in the sagittal plane as in Lemieux et al. (2016). The medial/lateral CP locations were fixed at 20 mm from the centreline and the anterior/posterior location of the CPs was driven by a regression equation as a function of flexion angle (Delp et al., 1990; Nisell et al., 1986).

2) Sphere-on-plane trajectory (SPP): The CP trajectories represent the femur/tibia sphere-on-plane contact mechanism guided by three isometric ligaments. (Duprey et al., 2010; Feikes et al., 2003). The mechanism geometry is based on *in vitro* measurements (Parenti-Castelli et al., 2013), and was not personalized.

3) Personalized CP trajectory (PCP): The CP trajectories were interpolated from the weighted center of bone-to-bone proximity measured during a quasi-static squatting task.

Bi-plane X-ray images of the lower limb were recorded at 0^o, 15^o, 30^o, 45^o, and 70^o of knee flexion using the EOS® low-dose imaging system (EOS® Imaging, Paris, France). The accuracy of estimating the weighted center of bone-to-bone proximity was reported 2 mm in the anterior/posterior and 3 mm in the medial/lateral directions in a simulation test (A Zeighami et al., 2017).

Once the CP trajectories are found in thigh and shank segment coordinate system (as a function of θ), the terms of Eq. (5-1) are obtained (Annex II) using the matrix **B** relating the natural coordinates $\mathbf{Q}_i$ with the segment axes (R. Dumas et al., 2007).

5.4.4 Statistical Analysis:

One-way repeated measures analysis of variance (ANOVA) was performed to detect statistically significant differences in contact forces estimated using the three CP trajectory methods ($p<0.05$). Bonferroni post-hoc test detected the pair-wise differences. In the PCP model, a linear correlation test was performed to find the possible correlation between the medial peak forces and the anterior/posterior and medial/lateral locations of the medial CPs, and between the lateral peak forces and the anterior/posterior and medial/lateral locations of the lateral CPs.

5.5 Results

The trajectories of PCP and SPP models showed a distinct deviation from the LCP model on the medial and lateral compartments both in medial/lateral and anterior/posterior directions as shown for a sample subject in Figure 5-1). The CP trajectories had a remarkable impact on the knee joint kinematics as well as the contact forces (Figure 5-2). However, this impact varied widely among the subjects. For instance, the first peak of the medial contact forces estimated from the PCP model with respect to the LCP model,

increased from 1.43 BW to 2.46 BW in subject N4, whereas it decreased from 1.45 BW to 1.32 BW in subject N2 (Table 5-1).

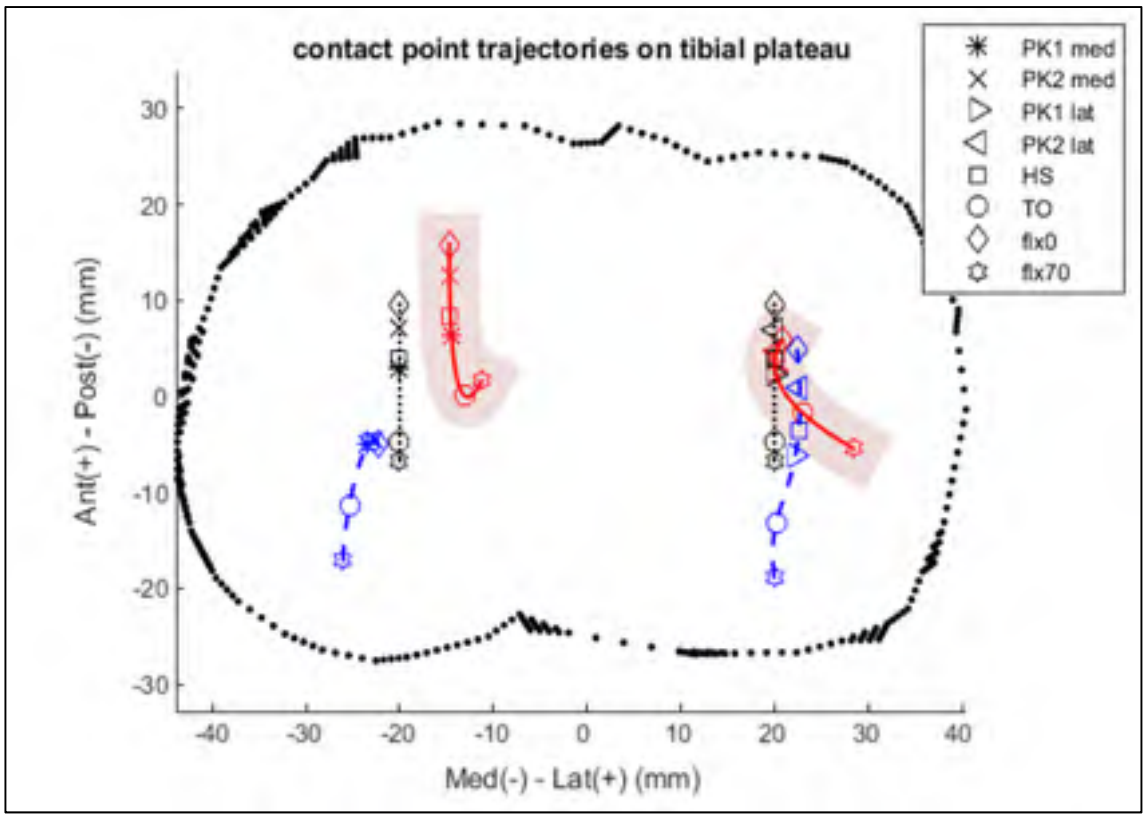

Figure 5-1 Contact point trajectories of subject N10 from the three contact point trajectory models over the tibial plateau: linear contact point (LCP) trajectory (: black), sphere-on-plane (SPP) trajectory (-- blue), and personalized contact point (PCP) trajectory (- red) models. The sequence of stance phase events is illustrated on each contact point trajectory: first and second peaks of medial (pk1 Med, pk2 Med), first and second peaks of lateral (pk1 Lat, pk2 Lat) contact force, heel strike (HS), toe off (TO), 0° (flx0) and 70° (flx70) knee flexion. The shaded region around the PCP model represents the uncertainty of estimating the weighted center of bone-to-bone proximity (±3 mm) in the medial/lateral direction (Zeighami et al. 2016).

The maximum difference in estimating the first medial peak between the PCP and LCP models was 1.03 BW in subject N4, between the PCP and SPP models was 0.65 BW in subject N5, and between the LCP and SPP models was 0.89 BW in subject N1. The

maximum difference in estimating the first lateral peak between the PCP and LCP models was 0.64 BW in subject N5, between the PCP and SPP models was 0.25 BW in subject N5, and between the LCP and SPP models was 0.50 BW in subject N8 (Table 5-1).

Table 5-1 (a) characteristics of the ten subjects in this study. (b) First and second peaks of the medial and lateral (pk1Med, pk2Med, pk1Lat, pk2Lat) contact forces from the linear CP trajectory (LCP), sphere-on-plane (SPP) trajectory, and personalized CP (PCP) trajectory models, and location of the CPs in medial (M) – lateral (L) and anterior (A) – posterior (P) directions of the tibial plateau at the corresponding events.

(a)

subject		N1	N2	N3	N4	N5	N6	N7	N8	N9	N10
subject characteristics	Gendre	M	M	M	F	M	F	M	F	M	F
	Age (yrs)	39	66	38	57	61	60	61	60	59	58
	Weight(kg)	76.9	54	84.5	58.1	81.9	60.8	89.8	58.8	80.7	60.6
	Height(m)	1.73	1.5	1.71	1.66	1.81	1.64	1.73	1.56	1.75	1.59

(b)

LCP(pk1 Med)	Medial Contact force (BW)		1.9	1.45	1.13	1.43	1.3	1.01	1.69	1.49	0.71	1.59
	Medial CP (mm)	M(+)-L(-)	-20	-20	-20	-20	-20	-20	-20	-20	-20	-20
		A(+)-P(-)	2.64	0.9	2.5	2.27	1.77	1.56	5.61	4.17	4.81	2.88
LCP(pk1Lat)	Lateral contact force (BW)		1.13	0.92	1.31	1.67	0.76	1.86	0.26	0.99	1.1	0.72
	Lateral CP (mm)	M(+)-L(-)	20	20	20	20	20	20	20	20	20	20
		A(+)-P(-)	1.8	-0.85	1.11	0.88	1.71	0.91	5.61	3.19	3.55	2.33
SPP(pk1Med)	Medial Contact force (BW)		2.79	1.36	1.35	2.09	1.45	1.41	2.08	1.51	0.66	1.94
	Medial CP (mm)	M(+)-L(-)	-23.3	-23.8	-23.4	-23.2	-23.5	-23.1	-22.8	-23	-23	-23
		A(+)-P(-)	-4.92	-5.79	-5.07	-4.78	-5.13	-5.09	-4.42	-4.56	-4.5	-5
SPP(pk1Lat)	Lateral contact force (BW)		1.81	1.32	1.81	1.79	1.15	2.32	0.27	1.49	1.37	1.12
	Lateral CP (mm)	M(+)-L(-)	22.2	21.5	22.1	22.2	22.3	22	22.7	22.4	22.5	22.2
		A(+)-P(-)	5.89	6.85	6.42	6.25	5.7	6.82	0.01	4.58	3.7	6.2
PCP(pk1Med)	Medial Contact force (BW)		2.32	1.32	1.15	2.46	2.1	0.99	1.78	1.45	1.02	1.67
	Medial CP (mm)	M(+)-L(-)	8.9	14.4	10.4	12.6	12.7	17.9	15.2	12.6	15	14
		A(+)-P(-)	0.41	1.86	13.44	9.97	13.66	6.38	13.2	10.7	12.6	6.4
PCP(pk1Lat)	Lateral contact force (BW)		1.09	0.97	1.8	1.6	1.4	2.14	0.22	1.2	0.88	0.92
	Lateral CP (mm)	M(+)-L(-)	18.5	18.9	16.4	22.5	20.6	18.4	17.4	20.8	24.8	20
		A(+)-P(-)	2.22	11.62	5.25	0.9	0.57	3	4.3	4.36	0.2	2.64

The average second peak of the medial contact force was significantly higher in the SPP model (2.88 BW) compared to the LCP (2.07 BW) and PCP (1.87 BW) models ($p<0.05$). The second peak of the total contact force was also greater in the SPP model, however,

the difference was not significant (p=0.10). In general, the LCP and PCP models demonstrated closer estimations compared to the SPP model (Figure 5-3).

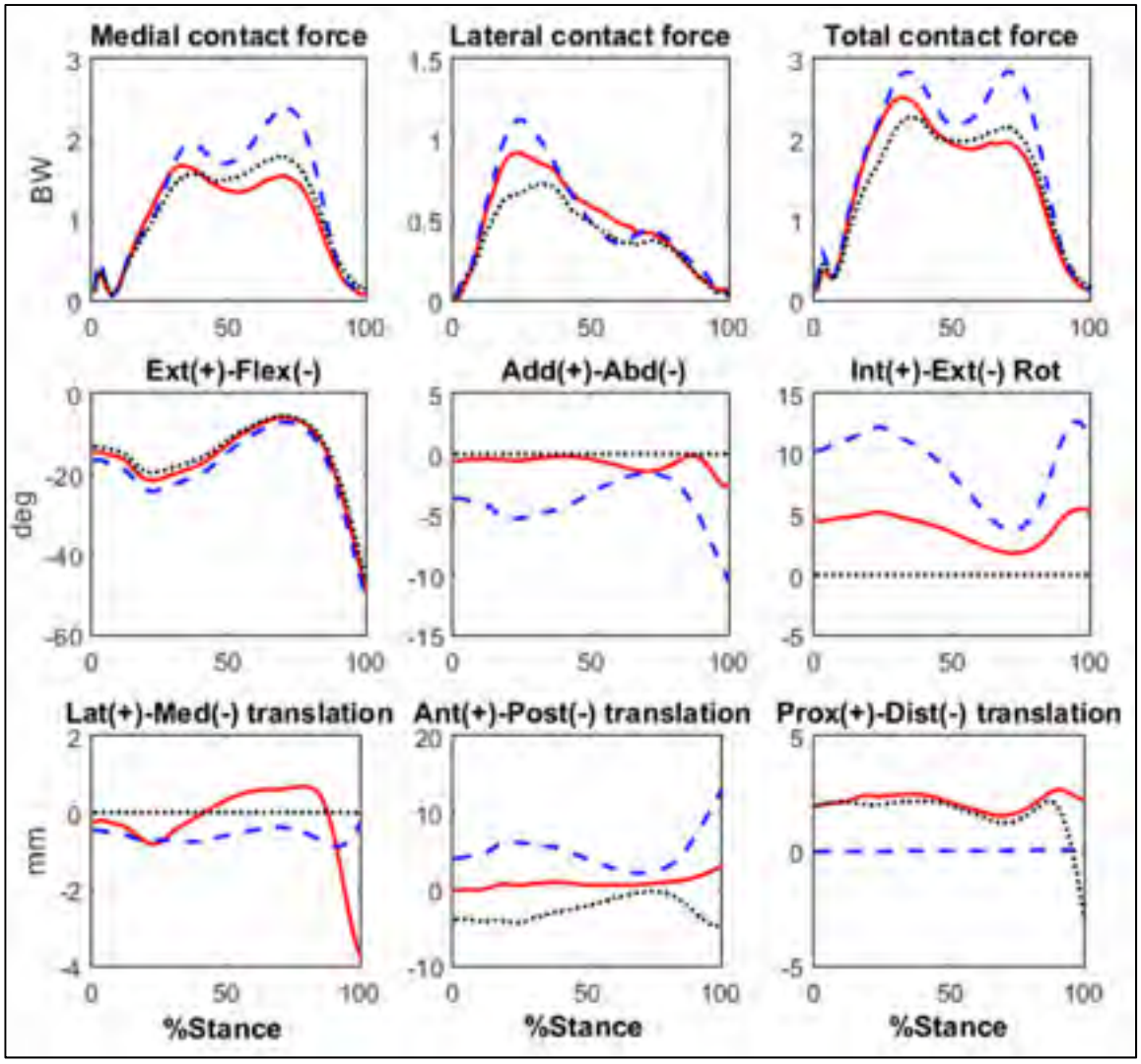

Figure 5-2 Medial, lateral, and total contact forces as well as the knee extension/flexion (Ext-Flex), adduction/abduction (Add-Abd), Internal/external (Int-Ext) rotations, lateral-medial (Lat-Med), anterior/posterior (Ant-Post), and proximal/distal (Prox-Dist) translations of subject N10 using the linear contact point (LCP) trajectory (:black), sphere-on-plane (SPP) trajectory (--blue), and personalized contact point (PCP) trajectory (-red) models. The corresponding contact point trajectories are presented in Figure (5-1).

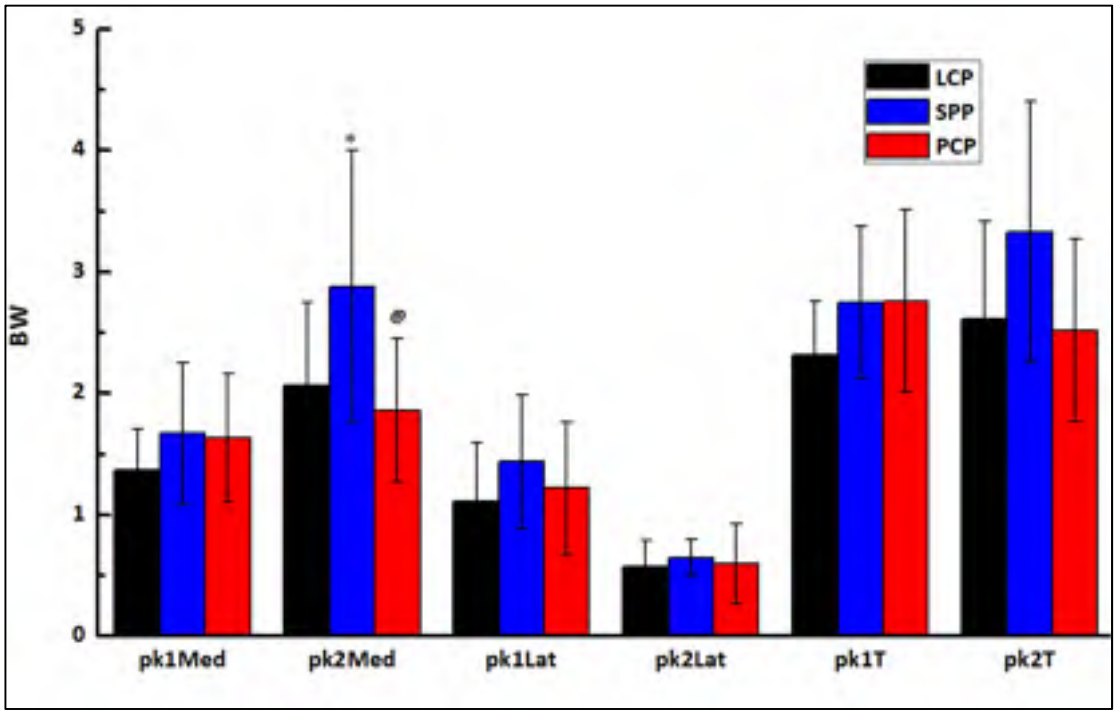

Figure 5-3 The average (10 subjects) first and second peaks of medial (pk1 Med, pk2 Med) , first and second peaks of lateral (pk1 Lat, pk2 Lat) , first and second peaks of total (pk1 T, pk2 T) contact forces using the linear contact point (LCP) trajectory, sphere-on-plane (SPP) trajectory, and personalized contact point (PCP) trajectory models. * and @ denote statistically significant differences between the SPP and LCP models and between the SPP and PCP models respectively.

All the medial compartment CPs in the PCP model were located lateral to the LCP model CPs. The first peak medial contact forces in PCP increased in six subjects and slightly decreased in four subjects with respect to the LCP model (See complementary methodology) (Table 5-1). Similarly, on the lateral side, the direction of the CP shift could not predict the direction of the change in the lateral contact forces with respect to the LCP model.

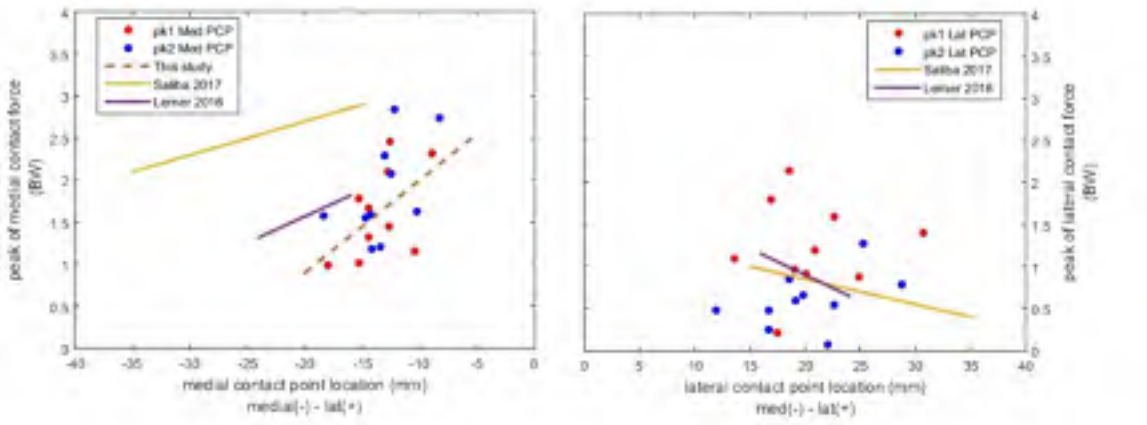

Figure 5-4 First (red marks) and second (blue marks) peaks of the medial and lateral contact forces (pk1 Med, pk2 Med, pk1 Lat, pk2 Lat) from the personalized contact point trajectory (PCP) model and the location of the personalized contact points at the corresponding events. Coordinates of the points are presented in Table 1 for all 10 subjects. The dashed line represents the regression line on the medial side ($r=0.53$, $p<0.001$). No correlation existed on the lateral side ($r=0.18$, $p=0.43$). Results adapted from two previous sensitivity analysis studies are also presented. The range of contact point perturbations were ±25±10 mm in Saliba et al. (2017), and ±20±4 mm in Lerner et al. (2016).

The PCP model generally suggested lower medial contact forces when the CPs were more medially located (Figure 5-4). A moderate positive correlation existed between the peaks of medial contact forces and the medial/lateral location of the medial CPs ($r=0.53$, $p<0.001$). Conversely, no correlation was observed in the lateral compartment (Figure 5-4). No correlation was found between the peaks of medial ($r=0.14$, $p=0.54$) and lateral ($r=0.1$, $p=0.6$) contact forces and anterior/posterior location of the CPs.

5.6 Discussion

The present study focuses on inverse dynamics computational frameworks where the personalization of the joints relies on the kinematic constraints and/or model geometrical parameters. In the literature, the joint kinematics and the position of the CPs appear to be treated independently (Gerus et al., 2013; Lerner et al., 2015; Saliba et al., 2017a). In our

formulation, it appears clearly that the subject-specific kinematics constraints $\mathbf{\Phi}_T^k$ and contact forces (i.e., the Lagrange multipliers associated to $\frac{\partial \mathbf{\Phi}_T^k}{\partial \mathbf{Q}}$) are directly related. Therefore, the joint kinematics were correspondingly adapted to the subject-specific CP trajectories and contributed to the contact force. Certain knee joint constraints such as sphere-on-plane mechanism could be personalized based on the anatomical measures from bi-plane radiography (Clément et al., 2015, 2017) or MRI (da Luz et al., 2017). However, the kinematics constraints proposed in Eq. (3-1) are certainly the most versatile ones as they can be deduced from any joint model and geometry. As such, they have been used in the present study to compare two tibiofemoral joints of the literature (Delp et al., 1990; Florent Moissenet et al., 2014) as well as to integrate personalized CP measurements obtained by quasi-static squat (Ali Zeighami et al., 2016). Future works could integrate the personalized CP trajectories obtained from methods such as bi-plane fluoroscopy within the same activity i.e., treadmill walking.

Within the simulated finite element computational frameworks, subject-specific joint models can also be built including detailed deformable geometry. The CP trajectories are therefore not inputs but rather outputs of the model together with the contact forces (Rachel L. Lenhart et al., 2015; Marouane et al., 2016). It allows these models to simulate relationships between joint structure and mechanics. Nevertheless, the computed CPs could vary from the experimentally measured CPs since several parameters including the stiffness of the ligament with a high impact on the CPs (Rachel L Lenhart et al., 2015) cannot be personalized. To our knowledge, the present study is the first to implement the experimentally measured CP trajectories into the inverse kinematics and contact force calculation steps.

Our study showed that using the PCP model in certain subjects increased the estimated peak contact forces up to 1.03 BW (subject N4) and 0.65 BW (subject N5) on the medial and lateral sides compared to the LCP model (Table 5-1). For these two specific subjects, a remarkable increase in the vastus medialis and vastus lateralis muscle forces were

observed in the PCP model, which is not the case in the other subjects (See complementary methodology). According to the Lerner et al. (2015) gradient, the medial contact force in subject N4 would have increased by 0.44 BW due to 7.4 mm lateral shift of the CP, and the lateral contact force in subject N4 would have decreased by 0.64 BW due to the 10.7 mm lateral shift of the CP. The estimated contact forces could vary largely when different CP trajectory models were used. However, the difference between the average contact forces from the three models was significant only in the second peak of medial contact force (Figure 5-3). The contact force variations were generally larger on the medial side. The sphere-on-plane model tended to show larger differences with respect to the other two models (Figure 5-3).

Our results showed that the medial/lateral shift of the CPs alone could not determine the increase/decrease pattern of the contact forces. Lerner et al. (2015) and Saliba et al. (2017a) reported that if the CPs were shifted medially the medial contact force would decrease and the lateral contact force would increase by 1-6% BW/mm. Our results showed that there is no correlation between the lateral contact, yet a moderate relationship existed for the medial contact (Figure 5-4). Lack of a strong relationship between the contact location shifts and the medial/lateral force was not unexpected in our multifactorial study. In Lerner et al. (2015) and Saliba et al. (2017a), the musculotendon forces are first calculated and the joint equilibrium in the frontal plane determines the contact forces. In this study, the musculotendon forces and the contact forces were calculated in one step and the equilibrium was attained in all planes. In addition, the kinematics of the joints was affected by the alteration of the CP trajectories. It has been long known that the contact locations are non-straight subject-specific paths (Ahmed et al., 1983) and that the CP locations alter the contact force estimation (Nissan, 1980). Therefore, the change in the CP distance from the tibial plateau centreline was not adequate in estimating the medial/lateral contact force.

Moreover, the CP trajectories are significantly altered in knee pathologies such as osteoarthritis (Farrokhi et al., 2016; C. Li et al., 2015; A Zeighami et al., 2017); yet still

most of the MSK models use the LCP-like models to estimate the medial/lateral contact forces both for osteoarthritic subjects and healthy controls (Kumar et al., 2013). Our method may serve to further personalize tibiofemoral joints in the MSK models and to develop a more realistic estimation of contact forces in osteoarthritic population.

The MSK model used in this study was previously validated using knee instrumented implant data (Florent Moissenet et al., 2014, 2016b; F Moissenet et al., 2015). With the SPP model, it could predict the medial and lateral contact forces with a mean RMSE difference of 0.39 BW and 0.28 BW (Florent Moissenet et al., 2014). Unfortunately, there is no means to validate the PCP model. To check if the results were realistic or not a pseudo-validation using EMG data was used (Complementary methodology). EMG results revealed no remarkable difference between the three CP trajectory models yet, the PCP model demonstrated a slightly better concordance with EMG data for rectus femoris and vasti muscle that are two main contributors to the first peak contact force (Florent Moissenet et al., 2017).

The main limitation of this study is the application of CP trajectories extracted from a quasi-static squat into the gait. Indeed, a mismatch between the kinematics of the tibiofemoral joint would result in different CP trajectories. Nevertheless, Gasparutto et al. (2017) synthesized the kinematics of the normal knee during various weight-bearing activities measured by intra-cortical pins and bi-plane fluoroscopy and concluded that the impact of the dynamic activity on the couplings between the joint degrees of freedom was limited. Treadmill walking also creates some differences in the kinematics of the gait (Alton et al., 1998; Murray et al., 1964; Strathy et al., 1983; Warabi et al., 2005). However, this latter applies to all the 3 models used in this study and is not likely to affect the conclusion regarding the difference between the models. The other limitation of this work is the accuracy of the measured CPs. The accuracy of the bone-to-bone proximity estimation was reported <3mm (A Zeighami et al., 2017). The CPs at the five flexion angles were interpolated to find the trajectory as a function of knee extension/flexion that may add further errors. Moreover, cartilage thickness is not uniformly distributed over the

joint regions (Favre et al., 2017). Therefore our method relying solely on bone proximity and neglecting cartilage thickness could be biased to predict CPs in regions with minimal cartilage (DeFrate et al., 2004; Marouane et al., 2016). Finally, the definition of the CP has to be clarified. Since there is no practical way to measure the center of pressure in the menisci and cartilage, a weighted center of bone-to-bone proximity was considered as the CP location.

This study introduced a new method to incorporate personalized CP trajectories in the MSK model contact force estimations. Currently, the CP trajectories are based on biplane radiography during squat which is subjected to limitations. But, more precise dynamic CP trajectories by considering layers of cartilage and menisci tissues could be introduced the same way in the proposed model. The impact of changing the CP trajectories on the medial/lateral contact forces was substantially large and was variable between the medial/lateral compartments and among the subjects. Due to the multifactorial nature of contact force calculations, the medial/lateral shift of the CP distance from the tibial plateau centreline alone could not predict the direction of compartmental contact force changes.

5.7 Conflicts of interest

There are no conflicts of interest to report.

5.7.1 Acknowledgements

The present work was supported by the Fonds de Recherche du Québec en Santé (FRQ-S), the Fonds de Recheche du Québec en Nature et Technologie (FRQ-NT) and the Natural Science and Research Council of Canada (NSERC). This work was performed within the framework of the LABEX PRIMES (ANR-11-LABX-0063) of Université de Lyon, within the program "Investissements d'Avenir" (ANR-11-IDEX-0007) operated by the French National Research Agency (ANR).

5.8 Complementary methodology

The original article includes a list of supplementary materials that are not reproduced *in extenso*. Conversely, in this section, we selected some of the important methodological aspects that are not extensively explained in the chapter due to the limited word count of the original article.

5.8.1 Medial and lateral contact forces over the stance phase

The mean contact forces of the 10 healthy 12 OA subjects are presented in Figure 5-5). The contact forces in healthy subjects are slightly higher but the difference is not significant.

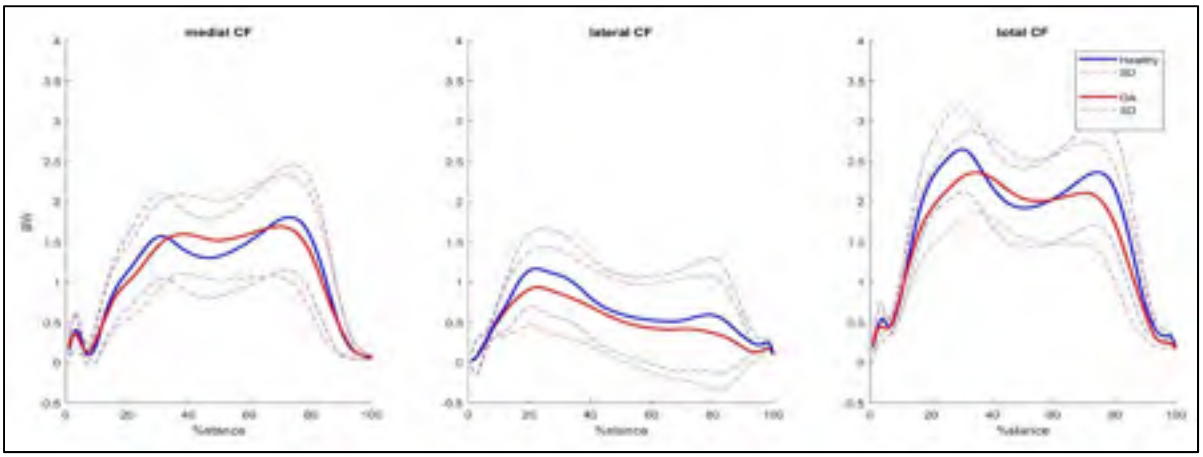

Figure 5-5 Medial, lateral, and total contact forces of the healthy and OA subjects during the stance phase

5.8.2 Marker labeling in biomechanical trials

The motion data in our study were recorded using A 12-camera VICON system (Oxford Metrics, UK). The reflective markers were placed on the lower limb as illustrated in (Figure 5-6). Three reflective markers were placed on the femoral part of KneeKG™ (FemurG/D 1,2,3)

and three on the tibial part of KneeKG^{TM} (TibiaG/D 1,2,3). Three markers were mounted on a belt fixed around the waist (Bassin 1,2,3). Six markers were placed on the foot on the navicular bone (NacG/D), 1st and 5th metatarsal bones (Meta1G/D, Meta5G/D), Internal and external malleoli (MalIG/D, MalEG/D), and the calcaneus bone (TalonG/D).

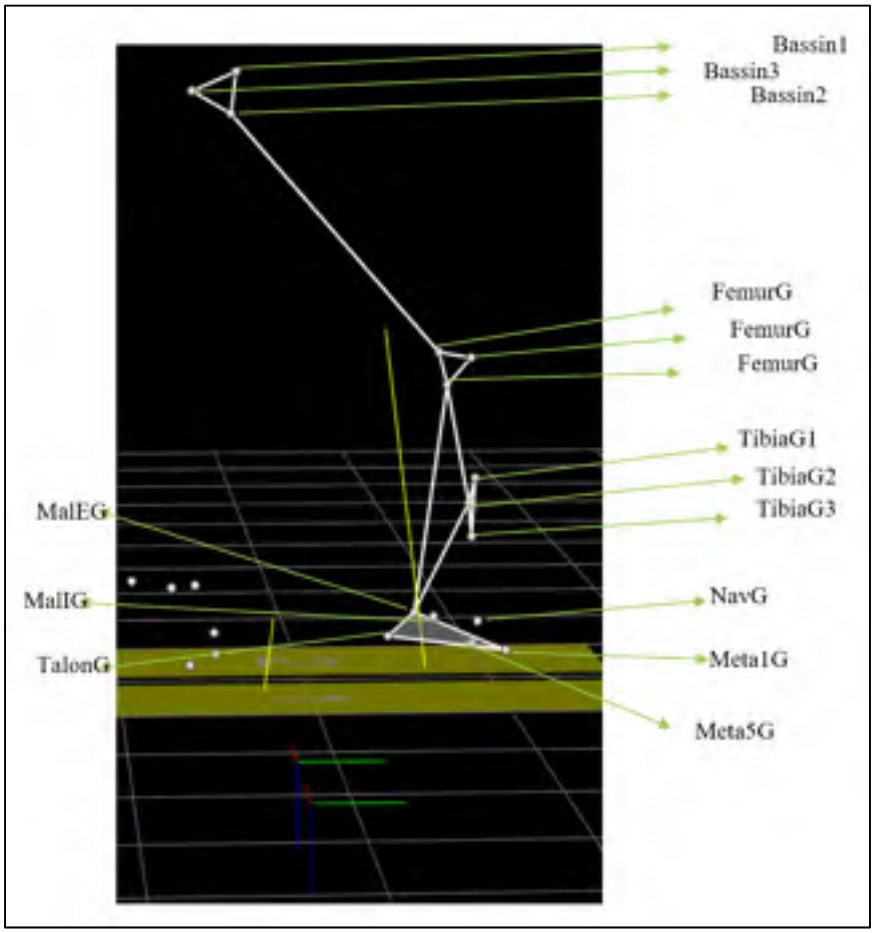

Figure 5-6 Placement of reflective markers on the lower limb to track the 3D motion of the limbs.

5.8.3 Contact forces in personalized and linear contact point models

The contact forces and contact point locations of PCP and LCP models are compared for the 10 healthy subjects in the following figure. All the medial compartment CPs in the PCP model were located lateral to the LCP model CPs. The first peak medial contact forces in PCP

increased in six subjects and slightly decreased in four subjects with respect to the LCP model. It shows that the direction of the CP shift could not predict the direction of the change in the lateral contact forces with respect to the LCP model.

Figure 5-7 shows the difference in contact force estimations at the 1st and 2nd medial and lateral peaks between the personalized contact point (PCP) and linear contact point (LCP) models. The horizontal axis is the personalized medial/lateral contact point location at the corresponding events: pk1 med (first peak of medial force), pk1 lat (first peak of lateral force), pk2 med (second peak of medial force), and pk2 lat (second peak of lateral force). The medial and lateral contact points in the LCP model were always located at -20 mm and +20 mm from the plateau centreline.

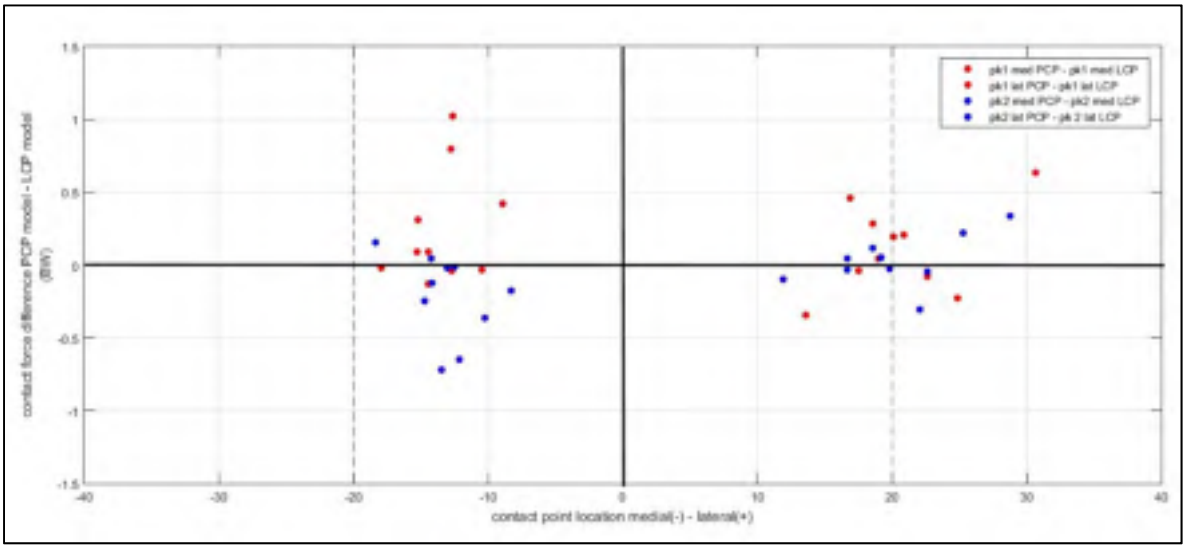

Figure 5-8 difference between the contact force estimated using personalized contact point and linear contact point models on the vertical axis and the corresponding contact point locations on the horizontal axis

5.8.4 Muscle forces in personalized and linear contact point trajectory models

Our study showed that using the PCP model in subject N4 and N5 the estimated peak contact forces increased up to 1.03 BW and 0.65 BW on the medial and lateral sides compared to the

LCP model which is bigger than the difference in the other subjects (Table 5-1). The main contributor muscles to the first peak contact force in our model are the vasti and rectus femoris (Florent Moissenet et al., 2017). The muscle force estimations using PCP and LCP models are compared for all 10 healthy subjects (Table 5-2). We observed that for these two subjects, we have a remarkable increase in the vasti muscles whereas the rectus femoris force has been reduced or stayed unchanged. This table was added to the supplementary.

Table 5-2 Rectus femoris (RF), vastus lateralis (VL), and vastus medialis (VM) musculo-tendon force estimations from the musculoskeletal model using personalized contact point (PCP) model (a), linear contact point (LCP) model (b), and the difference (c) between the two models at the first and second peaks of medial (pk1 med, pk2 med), and first and second peaks of lateral (pk1 lat, pk2 lat) contact forces.

a)	**PCP model muscle / BW**			**RF**	**VL**	**VM**
subjects	N1	pk1	med	0.71	0.5	0.89
		pk1	lat	0.58	0.58	1
	N2	pk1	med	0.07	0.06	0.09
		pk1	lat	0.17	0.14	0.23
	N3	pk1	med	0.26	0.5	0.8
		pk1	lat	0.04	0.6	0.99
	N4	pk1	med	0.63	0.68	1.14
		pk1	lat	0.36	0.84	1.35
	N5	pk1	med	0.06	0.89	1.43
		pk1	lat	0.1	0.88	1.42
	N6	pk1	med	0.61	0.52	0.9
		pk1	lat	0.29	0.58	0.95
	N7	pk1	med	0.06	0.23	0.37
		pk1	lat	0.08	0.21	0.33
	N8	pk1	med	0.06	0.23	0.37
		pk1	lat	0.08	0.21	0.33
	N9	pk1	med	0	0.14	0.21
		pk1	lat	0	0.19	0.28
	N10	pk1	med	0.53	0.34	0.62
		pk1	lat	0.18	0.43	0.7

b)	**LCP model muscle / BW**			**RF**	**VL**	**VM**
subjects	N1	pk1	med	0.83	0.38	0.74
		pk1	lat	0.58	0.52	0.92
	N2	pk1	med	0.01	0.14	0.22
		pk1	lat	0.26	0.18	0.33

b)	LCP model muscle / BW			RF	VL	VM
subjects	N3	pk1	med	0.26	0.27	0.48
		pk1	lat	0.1	0.43	0.7
	N4	pk1	med	0.89	0.28	0.59
		pk1	lat	0.52	0.51	0.88
	N5	pk1	med	0.02	0.41	0.65
		pk1	lat	0.07	0.4	0.64
	N6	pk1	med	0.63	0.44	0.8
		pk1	lat	0.27	0.53	0.88
	N7	pk1	med	0.05	0.14	0.22
		pk1	lat	0.05	0.14	0.22
	N8	pk1	med	0.02	0.12	0.19
		pk1	lat	0.03	0.28	0.44
	N9	pk1	med	0	0.12	0.19
		pk1	lat	0	0.18	0.28
	N10	pk1	med	0.18	0.25	0.43
		pk1	lat	0.2	0.29	0.49

c)	difference PCP -LCP			RF	VL	VM
subjects	N1	pk1	med	-0.1	0.1	0.2
		pk1	lat	0	0.1	0.1
	N2	pk1	med	0.1	-0.1	-0.1
		pk1	lat	-0.1	0	-0.1
	N3	pk1	med	0	0.2	0.3
		pk1	lat	-0.1	0.2	0.3
	N4	pk1	med	-0.3	0.4	0.6
		pk1	lat	-0.2	0.3	0.5
	N5	pk1	med	0	0.5	0.8
		pk1	lat	0	0.5	0.8
	N6	pk1	med	0	0.1	0.1
		pk1	lat	0	0.1	0.1
	N7	pk1	med	0	0.1	0.2
		pk1	lat	0	0.1	0.1
	N8	pk1	med	0	0.1	0.2
		pk1	lat	0.1	-0.1	-0.1
	N9	pk1	med	-0.1	0.1	0.2
		pk1	lat	0	0.1	0.1
	N10	pk1	med	0.1	-0.1	-0.1
		pk1	lat	-0.1	0	-0.1

5.8.5 Musculo-tendon forces pseudo-validation using EMG data

Surface electromyography (EMG) signals of the rectus femoris (RF), vastus lateralis (VL), vastus medialis (VM), tibialis anterior (TA), gastrocnemius medialis (GM), gastrocnemius lateralis (GL), semitendinosus (ST), and biceps femoris (BF) muscles were collected at 2 kHz during the gait trials using a Delsys Myomonitor system (Delsys, Inc., Boston, MA). A semi-quantitative pseudo-validation of estimated musculo-tendon forces from the MSK model was performed to find the active/inactive concordance with the EMG signals (Giroux et al., 2013). The stance phase was divided into 4 sub-phases (i.e., loading response, mid-stance, terminal stance, pre-swing) during which the EMG envelope and the musculo-tendon force states could take active or inactive state. Muscles were defined active when the mean value during a phase was above 20% of the maximum of the estimated musculo-tendon force and of the EMG envelope reached during the whole movement, respectively (Florent Moissenet et al., 2014). The concordance coefficient represents the ratio of phases that indicate concordance (i.e., simultaneously active or inactive) during the gait trial.

The average EMG coefficient of concordance showed no remarkable difference between the three contact point trajectory models. Five out of eight muscles indicated slightly better concordances using the PCP model whereas the remaining three had slightly higher values using the SPP model (Table 5-3).

Table 5-3 Coefficient of concordance (%) for the rectus femoris (RF), vastus lateralis (VL), vastus medialis (VM), tibialis anterior (TA), gastrocnemius medialis (GM), gastrocnemius lateralis (GL), semitendinosus (ST), and biceps femoris (BF) muscles using the three contact point trajectory models: linear contact point (LCP), sphere-on-plane (SPP), and personalized contact point (PCP) models.

Muscle	LCP	SPP	PCP
RF	0.56±0.05	0.52±0.07	**0.60±0.06**
VL	0.69±0.05	0.68±0.07	**0.75±0.08**
VM	0.70±0.12	0.66±0.14	**0.72±0.09**

Muscle	LCP	SPP	PCP
TA	0.63±0.09	0.60±0.09	**0.65±0.11**
GM	0.56±0.13	**0.66±0.12**	0.54±0.13
GL	0.48±0.08	**0.49±0.14**	0.44±0.12
ST	0.75±0.13	0.74±0.14	**0.78±0.13**
BF	0.57±0.13	**0.60±0.18**	0.59±0.13
Average	**0.62±0.09**	**0.62±0.08**	**0.63±0.11**

CHAPTER 6

FLEXION AND ADDUCTION MOMENTS AND CONTACT POINT LOCATIONS PREDICT THE MEDIAL TO TOTAL RATIO OF THE KNEE LOADS IN OA SUBJECTS

A. Zeighami[1*], R. Dumas[2], R. Aissaoui[1]

4. Laboratoire de Recherche en Imagerie et Orthopédie (LIO), École de Technologie Supérieure (ÉTS), Centre de Recherche du CHUM, Montréal, Québec, Canada
5. Université Lyon, Université Claude Bernard Lyon 1, IFSTTAR, UMR_T9406, LBMC, F69622, Lyon, France

This article has been submitted to the Journal of Orthopaedic Research.

6.1 Preface

This chapter addresses the third aim of this thesis: investigate the contribution of contact point locations on the knee contact force distribution compared to the other mechanical and functional parameters.

6.2 Abstract

High prevalence of knee osteoarthritis on the medial compartment is attributed to elevated medial-to-total contact force ratio (MR) in the joint. This study aimed to estimate the knee medial and lateral contact forces in OA and healthy subjects, and to evaluate the role of contact point locations in the MR. A musculoskeletal model of the lower limb with personalized tibiofemoral contact point trajectories was used to estimate the contact forces in ten healthy and twelve OA subjects during treadmill gait. Regression analyses were performed to evaluate the contribution of the contact point locations along with the knee adduction moment (KAM), knee flexion moment (KFM), frontal plane alignment, and gait speed to MR in OA and healthy subjects. Medial contact points location in medial/lateral direction had a significant but small contribution (R^2=0.05) to the MR in OA subjects. Contact point location was not among the

significant predictors of MR in healthy subjects ($p>0.05$). KAM and KFM remained the best predictors of MR, together accounting for $R^2 = 0.85$ and $R^2 = 0.79$ of variation in healthy and OA groups, respectively. Entering the medial contact point locations to the regression model increased the value of R^2 by 6% in OA group. Our results suggest different mechanisms of contact force distribution in OA joint and can help to understand the part of the variation in the MR of OA subjects which is not explained by the KFM and KAM.

Keywords: Tibiofemoral contact force, knee load distribution, osteoarthritis, contact point, knee moments

6.3 Introduction

Excessive loading is believed to play a crucial role in the pathogenesis of knee osteoarthritis (OA) (Miyazaki et al., 2002). Knee OA is mostly developed on the medial compartment where a major percentage of the total contact load is transferred (Johnson et al., 1981; Miyazaki et al., 2002; C. C. Prodromos et al., 1985). Reducing the knee medial contact force (F_{med}) has been the focus of many studies using osteotomy surgery (Briem et al., 2007), or noninvasive techniques such as using cane or shoe soles, gait modifications, and valgus braces (Erhart et al., 2010; Fregly et al., 2009; Kemp et al., 2008; Kutzner et al., 2011) through the variation of frontal plane alignment or knee adduction moment (KAM). Estimating the F_{med} in OA and healthy knees could help clarifying the loading role in OA. Therefore, characterizing the parameters that contribute to the F_{med} can help to find more effective therapeutic interventions to potentially slow down the OA progression.

Due to the complexity and the limited feasibility of estimating the contact forces using either musculoskeletal models or instrumented implants, the KAM has been widely used as a surrogate for the F_{med} or the medial-to-total contact force ratio (MR) (Astephen et al., 2005; Butler et al., 2007; Kinney et al., 2013; Schipplein et al., 1991; Zhao et al., 2007). MR is particularly much better predicted by the KAM compared to the F_{med} (Kutzner et al., 2013; Meyer et al., 2013). Despite the considerable evidence on the relationship between the KAM

with both F_{med} and MR (Trepczynski et al., 2014), and the medial compartment OA progression (Bennell et al., 2011; Miyazaki et al., 2002; L. E. Thorp et al., 2006), the weight of KAM contribution to F_{med} and MR is debated (Adouni et al., 2014). In fact, the coefficient of determination (R^2) between KAM and F_{med} from the linear regression models in previous studies falls in a wide range from 19% - 76% (Esculier et al., 2017; Kutzner et al., 2013; Meyer et al., 2013; Walter et al., 2010; Walter et al., 2015). The values of R^2 were also considerably variable across the subjects suggesting that the KAM alone could not be generalized as the sole indicator of the F_{med} and/or MR (Kutzner et al., 2013). Several other parameters were suggested to improve the F_{med} and MR predictions. Among those, the knee flexion moment (KFM) (Esculier et al., 2017; Kumar et al., 2013), frontal plane alignment (Adouni et al., 2014), and gait speed (Kutzner et al., 2013) were found to have substantial contributions to the F_{med} and MR. Moreover, sensitivity analysis studies showed that anterior/posterior and medial/-lateral locations of the tibiofemoral contact points had also a high impact on the contact forces and the forces distribution between the medial and lateral compartments (Lerner et al., 2015; Nissan, 1980; Saliba et al., 2017b; A Zeighami et al., 2018). For instance, Lerner et al. (2015) demonstrated a 6% increase in the MR per each millimeter of the contact point medial shift ($R^2 = 0.99$). Since there has been no means to integrate the personalized contact point trajectories in the contact force estimations; no study could have tested the contribution of the contact point locations with respect to the other parameters. Recently, Zeighami et al. (A Zeighami et al., 2018) integrated personalized contact point trajectories obtained from 3D/2D registration techniques in the medial and lateral knee contact force estimations. This technique currently allows evaluating the importance of the contact point locations along with the other parameters to predict the MR.

In addition, most of the studies on the F_{med} of the knee are performed in knee arthroplasty subjects, and the data on the healthy and OA knees are scarce. The few available OA-control studies estimated the medial and lateral contact forces using a generic model of the contact point trajectories (Kumar et al., 2013; Sritharan et al., 2017), and therefore, did not factor in the inter-subject variations and the distinct patterns of the anterior/posterior and medial/lateral

contact point locations in healthy and OA subjects (Farrokhi et al., 2016; A Zeighami et al., 2017).

The objective of this study is (1) to estimate the medial and lateral knee contact forces in both healthy and OA subjects using the personalized contact point trajectories obtained from 3D/2D registration techniques, and (2) to analyze the impact of the medial/lateral and anterior/posterior contact point locations along with KAM, KFM, gait speed, and frontal plane alignment on the MR.

6.4 Materials and methods

6.4.1 Musculoskeletal model with personalized contact point trajectories:

The medial and lateral knee contact forces were estimated using a musculoskeletal model of the lower limb with the integration of the personalized contact point trajectories (A Zeighami et al., 2018). The model consists of 5 segments and 5 joint degrees of freedom (DOF), with the hip joint modeled as a ball and socket joint (3 DOF) and the ankle modeled as a ball and socket joint plus two isometric ligaments (1 DOF). The tibiofemoral joint (1 DOF) is defined by 5 kinematic constraints derived from the personalized tibiofemoral contact point trajectories: at each flexion angle, the femoral and tibial contact points are superimposed in the 3 spatial directions on the medial compartment, and in both anterior/posterior and proximal/distal directions on the lateral compartment. The proximal/distal constraints on each compartment allow for a straightforward computation of medial and lateral contact forces (A Zeighami et al., 2018). The musculo-tendon lever arms were adopted from Delp et al. (1990).

A full description of the musculoskeletal model of the lower limb (except for the tibiofemoral joint) is detailed in (Florent Moissenet et al., 2014). The model estimations were previously validated (Florent Moissenet et al., 2014, 2016b; F Moissenet et al., 2015) compared to instrumented implants data. For a semi-quantitative validation of the model with the personalized tibiofemoral contact points, the active/inactive state of 8 muscles was compared

(i.e. concordance coefficients (Giroux et al., 2013)) to the EMG signals to if check the model predictions are realistic for 10 healthy subjects (A Zeighami et al., 2018).
The contact forces were calculated in a one-step procedure simultaneously minimizing the contact and musculo-tendon forces. Internal joint moments are derived from the inter-segmental action of muscles, ligaments, and contacts forces, and represent the action of the proximal onto the distal segment expressed in the joint coordinate system. The external knee adduction (KAM) and knee flexion moments (KFM) were obtained by reversing the corresponding internal moment signs.

The knee contact forces were normalized to body weight (BW) and the KAM and KFM were normalized to BW*height.

6.4.2 Experimental protocol:

Ten healthy (6 men, 4 women, 55 yrs., 1.68m, 71 kg) and 12 severe OA (2 men, 10 women, 59 yrs.1.61m, 85.53kg, K-L grade 4) subjects were asked to walk with their comfortable speed on an instrumented split-belt treadmill for 45 seconds (Table 6-1). Data from force platforms and reflective markers mounted on the kneeKG^{TM} system (Hagemeister et al., 2005) were filtered using a zero-lag 2nd order Butterworth filter with cut-off frequencies automatically calculated using a power spectrum analysis (PSA) algorithm (Aissaoui et al., 2006).

The personalized contact point trajectories introduced into the musculoskeletal model were approximated using a weighted center of bone-to-bone proximity algorithm during a quasi-static squat task. The 3D models of the tibia and femur were reconstructed and registered using EOS® low-dose biplane X-ray images of the subjects at 0^{o}, 15^{o}, 30^{o}, 45^{o}, and 70^{o} of knee flexion. The personalized tibiofemoral contact point trajectories were built as a function of the knee flexion angle as described earlier (A Zeighami et al., 2018). The frontal plane alignment was measured from the reconstructed tibia and femur of the subjects at 0^{o}.

All subjects signed an informed consent form and the experimental protocol was approved by the ethics committees of the Centre de Recherche, Centre Hospitalier de l'Université de Montréal (CRCHUM) and École de Technologie Supérieure de Montréal (ÉTS).

6.4.3 Statistical analysis:

A non-parametric Mann-Whitney U-test was used to compare the gait speed, frontal plane alignment as well as the magnitude and ratio of the medial, lateral and total contact forces between OA and healthy subjects ($p < 0.05$). Two sets of linear regression tests, one for healthy and one for OA, were performed to evaluate the extent to which the independent variables were predictive of the MR in OA and healthy subjects, respectively. The dependant variable was MR at 4 peak instances being the 1st and 2nd medial and lateral peaks. The independent variables were the KAM, KFM, frontal plane alignment, gait speed, and positions of the medial and lateral contact points in the anterior/posterior (CPxmed, CPxlat), and medial/lateral (CPzmed, CPzlat) directions at the corresponding timing. The rationale for considering 4 peaks was different timings of the medial and lateral contact force peaks. The coefficients of determination (R^2) were compared to identify the set of parameters that explains the greatest proportion of the variance of the dependent variable. The correlation was considered poor, moderate, or good if $R^2 \leq 0.05$, $0.5 < R^2 < 0.75$, and $R^2 > 0.75$, respectively. The regression model was rated as significant for $p < 0.05$. The correlation with each variable was first independently tested and the variables with significant effects were selected for multiple regression.

6.5 Results

The contact forces in healthy subjects averaged slightly higher than the OA subjects at the 2nd peak medial (OA = 1.7 BW, healthy = 1.9 BW), 1st peak lateral (OA = 1.1 BW, healthy = 1.2 BW), 2nd peak lateral (OA = 0.5 BW, healthy = 0.6 BW), 1st peak total (OA = 2.5 BW, healthy = 2.7 BW), and 2nd peak total (OA = 2.1 BW, healthy = 2.4 BW) contact forces, and were similar at the 1st medial peak (OA = healthy = 1.6 BW). However, the differences at 1st and 2nd

peak medial, lateral, and total contact forces were not significant ($p>0.05$) (Figure 6-1). Similarly, the mean medial and lateral contact forces over the stance phase were not significantly different between the 2 groups, even though the mean lateral contact force was 0.2 BW greater in the healthy group. The average MRs at the 1st and 2nd peaks of medial and lateral contact forces represented no significant difference between the 2 groups ($p>0.05$) (Table 6-1).

The frontal plane alignment in OA subjects (6.26°) revealed significantly greater varus than in the healthy subjects (0.57°, $p<0.01$). The groups were not matched for height, BMI ($p<0.05$), and gender (Table 6-1). Gait speed did not significantly differ between the two groups ($p=0.11$).

The linear regression tests revealed that each independent variable alone was not a good predictor of the MR. The best-achieved coefficient of determination with a single predictor was $R^2 = 0.58$ for KFM in OA subjects. None of the other parameters taken alone accounted for more than 50% of the variability in MR in either group (Table 6-2). The contribution of frontal plane alignment, gait speed, CPxmed, CPxlat and CPzlat to MR was not significant neither in OA nor in healthy subjects ($p > 0.05$). In OA subjects, the MR was significantly correlated with the KAM ($R^2 = 0.46$, $p<0.001$), KFM ($R^2 = 0.57$, $p<0.001$), and CPzmed ($R^2 = 0.18$, $p<0.01$). In healthy subjects, the MR was significantly correlated with the KAM ($R^2 = 0.44$, $p<0.0001$) and KFM ($R^2 = 0.40$, $p<0.001$). This makes the KFM and KAM the best single predictors for OA and healthy subjects, respectively. CPzmed failed to have a significant contribution to MR in healthy subjects ($R^2 = 0.06$, $p=0.13$).

The best multiple regression models consist of KAM, KFM, and CPzmed ($R^2 = 0.84$) for OA subjects; and KAM and KFM ($R^2 = 0.85$) for healthy subjects, respectively. A regression model with KFM and KAM as predictors yielded R^2 value of 0.78 for OA group. Adding the CPzmed to this regression model increased R^2 by 6% in OA but had no effect in the healthy group.

Table 6-1 The anthropometrics, frontal plane alignment and gait speed of 12 healthy (H) and 12 OA subjects. The medial to total contact force ratio (MR) represents the ratio of the medial contact force to the total contact force at 4 instants of gait being the 1st and 2nd peaks of the medial contact force (pk1 Med, pk2 Med), and 1st and 2nd peaks of the lateral contact force (pk1 Lat, pk2 Lat). Average data ± SD are provided; * denotes a statistically significant difference from the healthy group.

Healthy subjects								**MR**			
subject	**Height (m)**	**gender**	**Weight (kg)**	**Age (yrs)**	**BMI**	**frontal plane alignment (deg)**	**gait speed (m/s)**	**timing of pk1 Med**	**timing of pk2 Med**	**timing of pk1 Lat**	**timing of pk2 Lat**
H01	1.73	M	76.9	39	25.69	1.91	0.96	0.69	0.85	0.66	0.85
H02	1.5	M	54	66	24	-2	0.46	0.67	0.73	0.34	0.73
H03	1.71	M	84.5	38	28.9	0.98	0.67	0.43	0.82	0.33	0.45
H04	1.66	F	58.1	57	21.08	3.63	0.9	0.69	0.70	0.57	0.69
H05	1.81	M	81.9	61	25	-1.59	0.82	0.60	0.63	0.60	0.56
H06	1.64	F	60.8	60	22.61	-1.76	0.79	0.33	0.74	0.25	0.44
H07	1.73	M	89.8	61	30	1.67	0.57	0.91	0.91	0.89	0.86
H08	1.56	F	58.3	60	23.96	-0.96	0.45	0.57	0.81	0.54	0.59
H09	1.75	M	80.7	59	26.35	6.75	0.42	0.66	0.70	0.31	0.66
H10	1.75	F	60.6	53	19.79	-2.97	0.48	0.67	0.79	0.59	0.78
Average (SD)	**1.68 ± 0.1**		**70.56 ± 13.38**	**55.40 ± 9.49**	**24.74 ± 3.20**	**0.57 ± 3.02**	**0.65 ± 0.20**	**0.62 ± 0.16**	**0.77 ± 0.08**	**0.51 ± 0.20**	**0.66 ± 0.15**
OA subjects								**MR**			
subject	**Height (m)**	**gender**	**Weight (kg)**	**Age (yrs)**	**BMI**	**frontal plane alignment (deg)**	**gait speed (m/s)**	**pk1 Med**	**pk2 Med**	**pk1 Lat**	**pk2 Lat**
OA01	1.64	F	99.34	56	36.93	0.5	0.54	0.68	0.79	0.61	0.76
OA02	1.63	F	85.8	61	32.29	3.6	0.77	0.51	0.81	0.38	0.79
OA03	1.75	M	87	66	28.41	6.8	0.71	0.84	0.90	0.79	0.89
OA04	1.61	F	95	56	36.65	9.8	0.5	0.47	0.60	0.29	0.61
OA05	1.5	F	74	53	32.89	7.8	0.51	0.56	0.84	0.32	0.80
OA06	1.63	F	81.6	52	30.71	6.95	0.49	0.93	0.94	0.79	0.55
OA07	1.72	M	84	69	28.39	7.75	0.49	0.92	0.99	0.63	0.85
OA08	1.63	F	91.8	58	34.55	10.03	0.34	0.44	0.49	0.44	0.46
OA09	1.67	F	98.4	57	35.28	10.98	0.4	0.79	0.85	0.49	0.85
OA10	1.55	F	72.57	62	30.21	-2.3	0.4	0.39	0.65	0.39	0.64
OA11	1.58	F	74.4	64	29.8	6.61	0.31	0.91	0.76	0.52	0.72
OA12	1.52	F	82.5	61	35.71	6.65	0.48	0.89	0.89	0.89	0.89
Average (SD)	**1.62 (0.1)**		**85.53 ± 9.2***	**59.58 ± 5.2**	**32.65 ± 3.1***	**6.26 ± 3.9 ***	**0.5 ± 0.1**	**0.69 ± 0.21**	**0.79 ± 0.15**	**0.54 ± 0.20**	**0.73 ± 0.14**

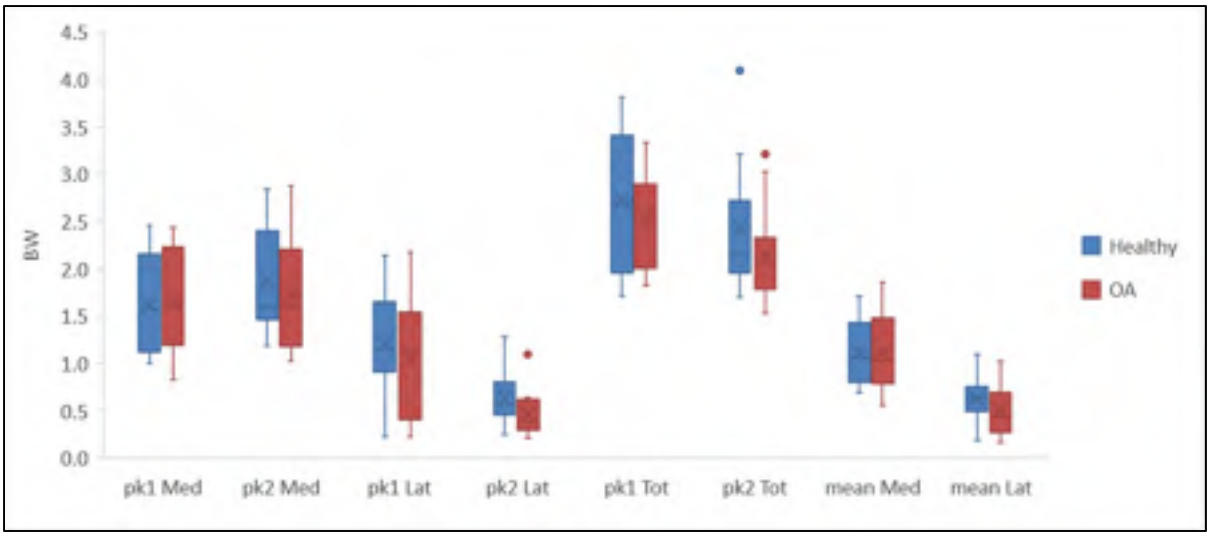

Figure 6-1 Box and whisker plot of contact forces of the healthy (blue) and OA (red) groups at the 1st and 2nd peaks of medial contact force (pk1 Med, pk2 Med), 1st and 2nd peaks of the lateral contact force (pk1 Lat, pk2 Lat), 1st and 2nd peaks of the total contact force (pk1 T, pk2 T), and the average medial (mean Med) and lateral (mean Lat) contact forces during the stance phase. The plot represents the minimum, maximum, lower and higher quartiles, and the median as well as the mean value (X mark), and the outliers (o mark).

6.6 Discussion

The objective of this study was to estimate the knee contact forces in both healthy and OA subjects and to analyze the impact of contact point locations along with other mechanical and functional parameters on the medial-to-total contact force ratio (MR). For that, we used a musculoskeletal model with personalized tibiofemoral joint contact point trajectories to investigate if the personalized contact point trajectories provide extra information about the knee contact forces distribution in OA and healthy subjects. The external moments on the knee joint are thought to be counterbalanced by the musculotendon and the tibiofemoral contact forces. Therefore, it is conceivable that the load taken by each compartment is proportional to the contact point distance from the joint center as postulated by previous sensitivity analyses (Lerner et al., 2015; Saliba et al., 2017a). Nevertheless, a recent multifactorial study suggested that there are other factors which confound a strong correlation between the contact point location and the F_{med} (A Zeighami et al., 2018). Nevertheless, the contributing parameters and their role in the F_{med} or MR was not investigated. In the present study, the personalized contact

point trajectories obtained from a 3D/2D imaging technique were integrated into the contact force estimations. Regression analysis was performed to assess the contribution of the contact point locations, among other parameters (KAM, KFM, frontal plane alignment, and gait speed), to the knee contact force distribution.

The contact point locations had no significant contribution to MR in the healthy group. The only significant correlation we found was between CPzmed (medial/lateral direction on the medial compartment) and MR in OA subjects. In a previous study on healthy subjects, we found that a weak correlation existed between the peaks of F_{med} and the CPzmed (A Zeighami et al., 2018). Here we tested the correlation with MR instead of F_{med} and observed that CPzmed-MR correlation was only significant in the OA group.

Table 6-2 Regression models in OA and healthy groups predicting MR and the corresponding independent variable (indep. Variable) combinations, (adjusted) coefficient of determination (adj.) R2, model significance p, the significance of the independent variables pn, and the regression coefficients corresponding to the independent variables and the y-intercept (y intcp.). Independent variables consist of the following parameters: Knee adduction moment (KAM), knee flexion moment (KFM), medial and lateral contact point locations in the anterior/posterior (CPxmed, CPxlat), and medial/lateral (CPzmed, CPzlat) directions, frontal plane alignment, and the gait speed (speed).

OA/Healthy	dep. variable	indep. variable	R^2	adj. R^2	p (model)	p1	p2	p3	c1 (y intcp.)	c2	c3	c4
OA	MR	KAM	0.46	0.45	0.000	0.000			0.590	0.126		
OA	MR	KFM	0.57	0.56	0.000	0.000			0.773	-0.076		
OA	MR	CPzmed	0.18	0.16	0.003	0.003			1.133	0.025		
OA	MR	CPxmed	0.07	0.05	0.070	0.070			0.488	0.020		
OA	MR	CPzlat	0.02	0.00	0.312	0.312			0.854	-0.010		
OA	MR	CPxlat	0.05	0.03	0.131	0.131			0.459	0.012		
OA	MR	frontal plane alignment	0.00	-0.02	0.925	0.925			0.696	-0.001		
OA	MR	speed	0.03	0.01	0.252	0.252			0.568	0.250		
OA	MR	KAM, KFM	0.79	0.78	0.000	0.000	0.000		0.683	0.092	-0.061	
OA	MR	KAM, CPzmed	0.54	0.52	0.000	0.000	0.006		0.912	0.115	0.018	
OA	MR	KFM, CPzmed	0.66	0.65	0.000	0.000	0.001		1.090	-0.071	0.018	
OA	MR	KAM, KFM, Cpzmed	0.84	0.83	0.000	0.000	0.000	0.000	0.935	0.085	-0.058	0.014
Healthy	MR	KAM	0.44	0.43	0.000	0.000			0.667	0.136		
Healthy	MR	KFM	0.40	0.39	0.000	0.000			0.720	-0.063		
Healthy	MR	CPzmed	0.06	0.04	0.125	0.125			0.867	0.017		
Healthy	MR	CPxmed	0.07	0.05	0.090	0.090			0.513	0.012		
Healthy	MR	CPzlat	0.05	0.03	0.156	0.156			0.812	-0.009		
Healthy	MR	CPxlat	0.08	0.06	0.068	0.068			0.605	7.402		
Healthy	MR	frontal plane alignment	0.00	-0.02	0.666	0.666			0.636	0.004		
Healthy	MR	speed	0.00	-0.03	0.913	0.913			0.650	-0.016		
Healthy	MR	KAM, KFM	0.85	0.85	0.000	0.000	0.000		0.748	0.137	-0.064	

The KFM and KAM accounted for a bigger proportion of the variability in MR compared to the CPzmed. In OA subjects, KAM and KFM taken alone accounted for 46% and 57% of the MR variability, respectively. If CPzmed is added as the second variable to the KAM or KFM, it accounts for an additional 9% of the variability in either case. In healthy subjects, the KAM and KFM accounted for 40% and 44% of the variability, respectively. The KAM-KFM combination was a good predictor of MR in both OA and healthy groups. Entering CPzmed to this combination as a third variable accounted for an additional 6% of the variance in OA (Table 6-2), and had no significant effect in the healthy group.

Regression coefficients revealed information about the magnitude and the direction of change in MR due to one-unit change in the predictor variable. In OA subjects, the coefficients of the KAM-KFM-CPzmed model were respectively 0.085, -0.058, and 0.014. Therefore, in our predictive model, an increase in the KAM and a decrease in the KFM (increase in knee extension moment) would result in greater MR values where changing KAM affects the MR by a higher rate. CPzmed coefficient implies that shifting the medial contact point laterally (+) i.e., closer to the joint center, would increase the MR by a rate of 0.014 per millimeter. In healthy subjects, the KAM-KFM was the best predictor model with the coefficients being 0.137 and -.064 for KAM and KFM respectively. Again, KAM can more quickly change MR by a rate almost twice as high as the KFM.

The KAM is sometimes considered as a surrogate of the knee medial loading (L. Thorp et al., 2010). We found that KAM was the primary contributor to the MR ($R^2 = 0.44$) followed by KFM ($R^2 = 0.40$) in healthy subjects. However, in the OA group, the KFM accounted for a bigger proportion of the variance in MR ($R^2 = 0.57$) with respect to the KAM ($R^2 = 0.46$) (Table 6-2). The importance of the KFM in estimating the magnitude or variation of F_{med} was highlighted in previous studies both in OA and healthy subjects (Creaby, 2015; Kumar et al., 2013). Moreover, Meireles et al. (2016) performed regression tests with KFM and KAM inputted independently. They found that in early OA subjects, the contribution of KFM to the 1st peak medial contact force ($R^2 = 62\%$) was close to that for KAM ($R^2 = 67\%$). They also reported that in healthy controls the contribution of KAM ($R^2 = 65\%$) was much greater than

the contribution of KFM (R^2 = 21%). This shows that the contribution of sagittal and frontal moments to the load sharing can be affected by the knee pathology with KFM having a more important impact on the F_{med} in OA group with respect to the healthy group. This is similar to the higher contribution of KFM to the MR in OA subjects in our study. Manal et al. (2015) reported that the KFM adds an additional 22% to the 63% of the variance in the F_{med} peak which is explained by the KAM. Both moments together accounted for ~85% of variation similar to what we found in this study for OA (R^2 = 79%) and healthy (R^2 = 85%) subjects. It should be noted that in our model the knee joint equilibrium was performed in 3D, balancing the joint moments in the 3 planes and along with the musculotendon and contact forces simultaneously (Florent Moissenet et al., 2014). This shall give a higher weight to the KFM compared to calculating the musculotendon forces in a first step and the contact forces in a second step considering the joint equilibrium in the frontal plane (Lerner et al., 2015; Saliba et al., 2017a). In an instrumented implant study, Trepczynski et al. (2014) observed that the KAM alone accounted for 87% of the F_{med} variation and R^2 value increased by ~4% when KFM is added to the regression. The smaller contribution of KFM in their study could be attributed to the prosthetic knee which has a different joint configuration and congruence compared to the native knees.

The contribution of CPxmed, CPxlat, CPzlat, frontal plane alignment, and gait speed to MR was not found significant ($p>0.05$). The correlation of frontal plane alignment with MR was addressed in other studies. In an FE simulation study with one subject, the frontal plane alignment was reported a much more effective factor in reducing MR compared to the KAM (Adouni et al., 2014). Nevertheless, Kumar et al. (Kumar et al., 2013) failed to find a significant correlation between frontal plane alignment and the F_{med} peak in neither healthy (n=12) or OA (n=16) groups. In our study, we did not find a significant correlation between the frontal plane alignment and MR in the regression ($p>0.05$).

A large body of the literature reported the contact forces using prosthetic measurements or musculoskeletal model estimations. Our contact force estimations (Table 6-3) falls within the literature range for the medial (2.1 ± 0.5 BW), lateral (0.9 ± 0.4 BW), and total (3.1 ± 0.8 BW) peaks of contact forces (Erhart et al., 2010; Fregly et al., 2009; Kim et al., 2009; Kutzner et al.,

2011; Lerner et al., 2015; Lin et al., 2010; Lundberg et al., 2009; Manal et al., 2013; Florent Moissenet et al., 2014, 2016a; Shelburne et al., 2005, 2006; Sritharan et al., 2017; Winby et al., 2009; Zhao et al., 2007). However, the number of studies comparing the medial and lateral natural knee contact forces of OA and healthy subjects are limited. Sritharan et al. (2017) and Kumar et al. (2013) used musculoskeletal models with generic contact point trajectories to estimate the contact forces. They reported that despite the differences between the absolute values of the contact forces in the two groups (Table 6-3), the differences were not significant which is in accordance with our results. Peak of medial contact forces in both studies were greater than the peak of lateral contact forces (Table 6-3). Kumar et al. (Kumar et al., 2013) reported a lateral compartment unloading (MR ~ 100%) at the late stance phase in half of the OA subjects. The MRs in our study tend to achieve higher values in OA subjects at the 2nd peak of medial contact force; however, the near-zero lateral loading (MR = 99%) is observed only in one subject. Marouane et al. (2016) used an FE model of the lower limb with the simulated biomechanics of OA to estimate the contact forces at the actual tibiofemoral center of pressure. They found that the maximum MR values at the peak contact force were between 0.76 and 0.81 for healthy and OA models which is very close to 0.77 to 0.79 for maximum MR in our study. primarily due to the absence of cartilage layer and menisci in the X-ray images and the errors in the reconstruction and registration process (DeFrate et al., 2004; Marouane et al., 2016; A Zeighami et al., 2017). Finally, the number of subjects is not enough to generalize the conclusions made in this study.

The current study has several limitations. The personalized contact point trajectories were measured during a quasi-static squat and may vary in different weight-bearing tasks. In addition, the estimation of the contact point trajectories is based on a weighted center of bone-to-bone proximity (A Zeighami et al., 2018) and is subject to inaccuracies in approximating the center of pressure. This is primarily due to the absence of cartilage layer and menisci in the X-ray images and the errors in the reconstruction and registration process (DeFrate et al., 2004; Marouane et al., 2016; A Zeighami et al., 2017). Finally, the number of subjects is not enough to generalize the conclusions made in this study.

Table 6-3 The 1st and 2nd peaks of medial contact force (pk1-pk2 Med), 1st and 2nd peaks of the lateral contact force (pk1- pk2 Lat), and 1st and 2nd peaks of the total contact force (pk1-pk2 Tot) in the case-control studies with OA and healthy subjects. The contact force (CF) estimations (BW) were obtained using musculoskeletal (MSK) or finite element (FE) models.

Study	**No of subjects**	**CF estimation**	**OA status**	**pk1-pk2 Med**	**pk1-pk2 Lat**	**pk1-pk2 Tot**
Strithan 2017	19	MSK model	Healthy	2.0-3.0	0.3-0.52	2.3-3.5
Strithan 2017	39	MSK model	OA	2.1-3.3	0.3-0.59	2.3-3.8
Marouane 2016	1	FE model	Healthy	3.2-3.0	2.6-0.8	4.1-3.7
Marouane 2016	1	FE model	Simulated OA	2.7-3.0	1.8-0.7	3.3-3.5
Kumar 2013	16	MSK model	Healthy	2.4-1.8	1.3-0.5	3.7-2.2
Kumar 2013	12	MSK model	OA	2.6-2.1	0.9-0.1	3.5-2.2
This study	10	MSK model	Healthy	1.6-1.9	1.2-0.6	2.7-2.4
This study	12	MSK model	OA	1.6-1.7	1.1-0.5	2.5-2.1

As a conclusion, in the current work, we assessed the contribution of the contact point locations to the knee contact forces distribution. CPzmed had a significant but limited role in dictating the MR in OA subjects and had an inferior weight compared to the KAM and KFM. The combined use of the 3 parameters together provided the most accurate predictions of the MR. In healthy subjects, the contact point locations had no significant contribution to MR and KFM and KAM remained the best predictors of the contact forces distribution. KAM and KFM can be easily estimated from classical inverse dynamics while obtaining personalized contact points require more complex procedures. Therefore, the external moments represent a good surrogate for the MR estimation. However, the extra information provided by the shifting in the medial contact point closer to the joint center helps to understand partially the 15% - 20% of the variation that is not explained by the KAM and KFM in OA subjects. Knowledge of the contribution of various parameters to the knee contact forces distribution could eventually lead to better understand the OA progression mechanism and help better planning the most effective interventions to slow the disease process.

6.7 Acknowledgement

This work was supported by the Fonds de Recherche du Québec en Santé (FRQ-S), the Fonds de Recheche du Québec en Nature et Technologie (FRQ-NT), as well as by the Natural Science and Research Council of Canada (NSERC). This work was performed within the framework of the LABEX PRIMES (ANR-11-LABX-0063) of Université de Lyon, within the program "Investissements d'Avenir" (ANR-11-IDEX-0007) operated by the French National Research Agency (ANR). The funding sources were not involved in any part of the study design, collection, analysis, and interpretation of data; in the writing of the manuscript, nor in the decision to submit the manuscript for publication.

CHAPTER 7

GENERAL DISCUSSION

7.1 Preface

The general objective of this thesis was to quantify the contact zones, contact forces, and their correlation in OA subjects when compared to healthy subjects. This goal was divided into four specific objectives. A summary of the results of the four chapters related to these objectives is presented, followed by limitations and recommendations, and the conclusion of this work.

7.2 Synthesis of articles

The aim of **chapter 3 (article1)** was to quantify and compare the contact point locations in OA and healthy knee joints. Biplane radiographs of 10 healthy and 9 OA subjects were used to reconstruct/register the 3D models of the tibia and femur at 5 quasi-static squat positions i.e., at 0^o, 15^o, 30^o, 45^o, and 70^o knee flexion. The contact point locations and the quasi-static kinematics at each position were compared between the two groups and revealed an altered functional anatomy due to OA.

The contact points on the medial compartment demonstrated a posterior excursion of 8.1 mm and 10.1 mm in OA and healthy subjects, respectively. On the lateral compartment, the posterior excursion was accompanied by a lateral excursion in both OA and healthy groups. Contact points on the lateral compartment exhibited posterior and lateral excursions of 3.6 mm and 7.1 mm in OA subjects and of 7.1 mm and 12.9 mm in healthy subjects. A medial shift was observed in the contact point location of OA subjects at all squat positions and on both compartments. Across all squat positions, the contact points in OA subjects were shifted 6.5 ± 0.7 mm and 9.6 ± 3.1 mm medially with respect to those in healthy subjects on the medial and lateral compartments, respectively. The quasi-static kinematic analysis showed that the OA group had bigger adduction angles at all squat positions compared to the healthy group.

Therefore, while the knee joint is lateralized due to the varus (both static and dynamic) pathological alignment, the contact points are medialized.

In addition, it can be noted that this first article also has some technical contributions:
Use of stand-alone biplane images for contact point estimation: Biplane imaging has been already used in combination with CT-scan- or MRI-based reconstructions of the joint surfaces to study the contact point locations (Farrokhi et al., 2016; Fiacchi et al., 2014; Hamai et al., 2009; Seungbum Koo et al., 2011; Qi et al., 2013). In this study, we used stand-alone EOS® biplane images to estimate the contact point locations. To minimize the reconstruction errors, a manual multiple view reconstruction/registration technique was used to include the information from all available pairs of biplane images rather than 1 pair at the reconstruction step.
Pseudo-validation of estimated contact points: The accuracy of the contact points estimations is affected by the errors in both reconstruction and registration steps. The pseudo-validation in this study estimated the cumulative errors of the entire reconstruction/registration process in calculating the contact point locations.

The aim of **chapter** 4 was to compare the contact point locations of OA subjects during a quasi-static task with and without wearing a valgus knee orthosis. Knee orthosis is one of the non-invasive interventions aimed at enhancing the stability and reproducing the kinematics of a normal knee (Martin et al., 2001). This chapter examined the feasibility of using contact point locations as a measure of the effectiveness of the Evoke™ knee orthosis. The kinematics obtained from the inertial sensors placed on shank and thigh appeared considerably biased with respect to those obtained from the internal landmarks due to the soft tissue artefact. This showed that subtle impacts of wearing the orthosis on the kinematics and on the contact point locations could not be reliably evaluated from the external kinematic measurements. Therefore, imaging techniques are required to more accurately measure these impacts directly from the internal kinematics. The results of the studied subject showed that wearing the orthosis shifted the medial contact points in medial/lateral and anterior/posterior directions in smaller knee

flexion angles. However, conclusions on the effectiveness of the orthosis require observing meaningful patterns of the contact point shift in a cohort of OA subjects.

As for the chapter 4, this complementary study has a technical contribution:
Using biplane imaging to reconstruct the orthosis and the joint: The visibility of the orthosis in the biplane X-ray images allowed registering the CAD model of the orthosis on the reconstructed bone models. Beside the possibility to examine the correctness of the orthosis placement with respect to the joint, it enables comparing the kinematics generated by the orthosis hinges with respect to the joint kinematics.

The aim of **chapter 5 (article 2)** was to integrate the personalized contact point trajectories obtained from the 3D/2D reconstruction technique into the musculoskeletal model of the lower limb. The tibial and femoral contact points were superimposed in all directions on the medial compartment, and in proximal/distal and anterior/posterior directions on the lateral compartment to form the constraints of the knee. The contact force estimated using personalized contact point trajectory model was compared to the classical models of the knee joint. The impact of personalization of the contact point trajectory was very variable among the subjects. This work suggested that the medial and lateral contact forces are affected by multiple parameters, and the contact point trajectories alone could not explain their variation. On healthy subjects, no significant difference was observed between the personalized model and the sliding hinge model which is the most used in the literature. However, this sliding hinge model is more sensitive to the shift in the contact points (Lerner et al. 2015, Saliba et al. 2016) than the personalized model and this may have an impact when studying OA subjects. Still, when studying OA subjects, no sliding hinge model with customized contact points has been reported so far.

This second article has a technical contribution:
Introducing a versatile constraint for the knee joint: The knee joint constraint in the musculoskeletal model can be deduced from any knee model including personalized or classical joint models. This paves the way towards integration of the contact point locations

measured during gait using the dynamic stereo-radiography methods such as dual fluoroscopy or any other modality.

The aim of **chapter 6 (article 3)** was to use the musculoskeletal model with the personalized contact points to investigate the contribution of contact point locations to the knee contact force distribution alongside the other mechanical and functional parameters. The results showed that the KAM and KFM were the main contributors to the MR explaining 75% and 81% of its variation in OA and healthy subjects, respectively. CPzmed (the medial contact point location in medial/lateral direction) explained 18% of the variance of MR in OA subjects but had no significant contribution to the MR in healthy subjects. This study showed that the KFM and KEM together are good predictors of the load distribution in the OA and healthy joints. However, the mechanism of load distribution was different in OA joints where the CPzmed was a significant contributor to MR and where KFM had a higher contribution than KAM whereas in healthy subjects KAM was the most significant contributor to the MR.

7.3 Limitations and recommendations for future study:

This thesis work has some limitations some of which have already been discussed in the articles while others have not yet been fully addressed. The next paragraphs present the most important limitations, as well as the recommendations as a continuation to this work or for future studies.

7.3.1 Contact parameters not fully investigated

The contact point location is indeed an important parameter in the study of the biomechanics of the joint. However, the contact mechanism of the joint is not fully described by this parameter. Previous studies have explored other parameters of the tibiofemoral contact. The excursion of contact points was used as a measure of tibiofemoral joint instability in the downhill gait of OA and healthy subjects (Farrokhi et al., 2016; Farrokhi et al., 2014). They showed that the excursion of contact points increased in OA subjects which they considered an indication of mechanical instability. The other important parameter in the contact

kinematics of the joint is the proportion of the rolling and sliding in the overall relative movement of the tibia with respect to the femur. Hoshino et al. (2012) reported larger sliding on the medial compartment of ACL-reconstructed subjects compared to the lateral compartment. This can potentially induce more shear stress on the medial compartment. The velocity of the contact points was also considered a key parameter in the study of OA joints. Increased velocity of the contact points was observed in the human knee (Farrokhi et al., 2016) and canine stifle (Anderst et al., 2009) joints affected by OA. Large differences in the relative velocity of femur and tibia contact points imply a "plowing" mechanism that can create big tangential forces which may lead to the wear of the cartilage (Anderst et al., 2009). In the presence of the tangential contact force estimations from the musculoskeletal models, it is possible to compute the power of the personalized tangential contact forces. It should be noted that the above studies were performed using dynamic stereo radiography. However, it is possible to approximate the excursion, sliding and rolling, velocity and the power of the contact points from the quasi-static tasks using the interpolation functions similar to the ones used in chapter 5 to obtain the contact point trajectories as a function of knee flexion. Further research on the already existing data could be considered for future studies.

The contact point trajectories are very variable among the subjects and do not follow a similar pattern. Figure 7-1) illustrates the individual contact point trajectories of the subjects presented in chapter 3. Therefore, averaging the results of a group does not provide a typical contact point trajectory representing the individuals in OA or healthy group, but it can rather help distinguishing the regions of contact in the two groups. Therefore, it is important to identify the factors causing the individual patterns of contact points. Parametrization of the effect of the 6 DOF joint kinematics and the surface geometry (convexity/concavity if the tibial plateau, geometry of the femoral condyles, the relative alignment of the articulating bones, etc.) on the contact point trajectories could be considered for future research.

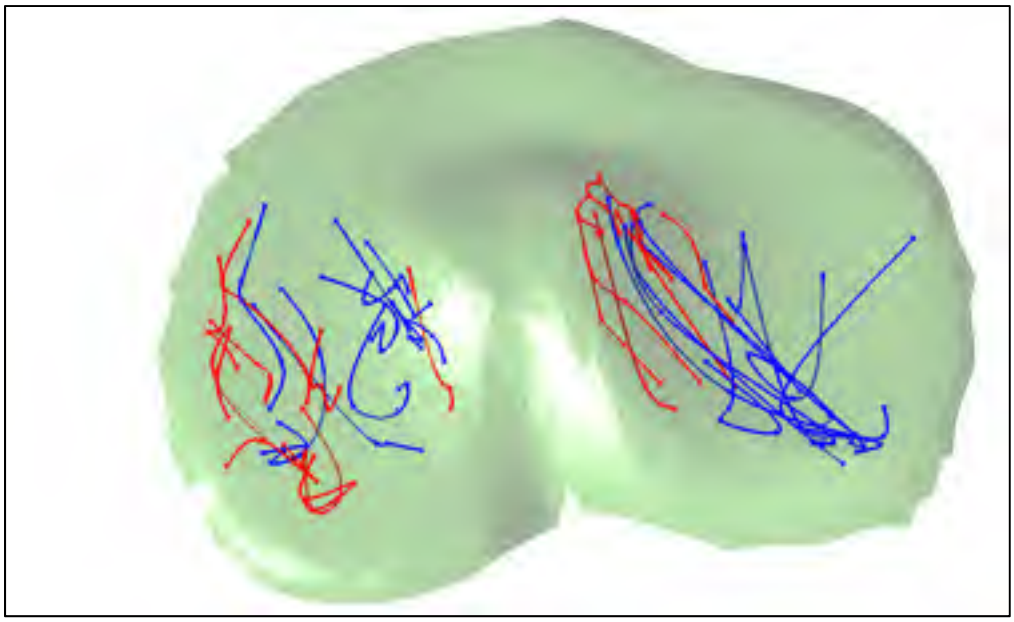

Figure 7-1 Individual contact point trajectories of 9 OA (red) and 10 healthy (blue) subjects described in chapter 3

7.3.2 Recommendations for further study on contact point locations

Other recommendations for future research in this topic are automatization of the multiple view reconstruction/registration technique to increase the repeatability and reduce processing time, integration of cartilage layer from MRI to take into account the non-uniformity of cartilage thickness in different regions of the joint, and include more subjects at different stages of OA to study the changes of contact parameters during the disease progression.

7.3.3 Further personalization of the musculoskeletal model using biplane EOS® images

In this study EOS® biplane images were used to personalize the tibiofemoral contact point trajectories in the musculoskeletal mode. However, more parameters could have been personalized using these images. Raphaël Dumas et al. (2005) calculated the body segment inertial parameters (BSIP) from the external envelope geometry of the subject and, extracted

the anatomical points and the joint lengths from EOS® biplane images. Südhoff (2007) used the same approach to integrate the BSIP and the hip joint center in the musculoskeletal model of the lower limb. A recent study showed that due to the soft tissue artefact, the kinematics obtained from the kneeKG™ system and the functional calibration of Hagemeister et al. (2005) could have errors up to 9.1 mm and up to 8.0° compared to those obtained from biplane EOS® images. Therefore, integration of anatomical points and the BSIPs from the biplane images to the musculoskeletal model would be beneficial. The principle of multiple calibrations of the KneeKG™ using a series of positions measured from EOS® biplane images could be also investigated (Lucchetti et al., 1998).

7.3.4 EMG integration in the musculoskeletal model

Inverse dynamic-based static optimization methods have been widely used to estimate the musculo-tendon and contact forces (Erdemir et al., 2007). Even though the surface EMG data are often collected as routine in many biomechanical experiments, they are mostly used as a pseudo-validation measure for the muscle activities (as done in this thesis), and they do not contribute to the estimation of the musculo-tendon force at the step of static optimization. On the other hand, the EMG-driven models also suffer from several limitations. Joint torque estimations require accurate estimation of all the muscle forces and it is difficult to translate the neural EMG commands to muscle forces for each of those muscles. Therefore, integration of EMG in the inverse dynamic-based models was suggested to improve the accuracy of the muscle force estimations during walking (Amarantini et al., 2004; Higginson et al., 2012; Sartori et al., 2014) and running (D. G. Lloyd et al., 2003). For the future studies, we recommend including the EMG data in the musculoskeletal model to have more accurate estimation of the musculo-tendon and contact forces. For instance, this can be done using a multi-objective optimisation (F Moissenet et al., 2014).

7.3.5 Alternative regression models for MR prediction

In Chapter (6) two linear regression models including KAM-KFM-CPzmed, and KAM-KFM was suggested to predict MR in OA and healthy subjects respectively. Previous studies on the predictive models for F_{med} or MR have used linear regression models with a variety of dependent variables (Table 1-4). Nevertheless, Trepczynski et al. (2014) suggested that a nonlinear regression with arctangent function provides better predictions for the MR compared to the linear regression models. In a preliminary exploratory analysis, we observed that other nonlinear combination of variables can appropriately follow the MR patterns in both healthy and OA subjects. (Figure 7-2) shows the MR and a nonlinear function of KAM and KFM, (i.e. $f(KAM, KFM) = \frac{KAM}{\max(KAM) \times (1 + \frac{KFM}{\max(KFM)})}$) for two random subjects from the OA and healthy groups over the stance phase. The rational for this function was the assumption that the MR is directly correlated to KAM and inversely to KFM. This implies that the nonlinear regression models may offer better predictions of the MR. Finding a function that better reflects the biomechanics of contact force distribution and comparing them with the current linear regression models could be done in a future study.

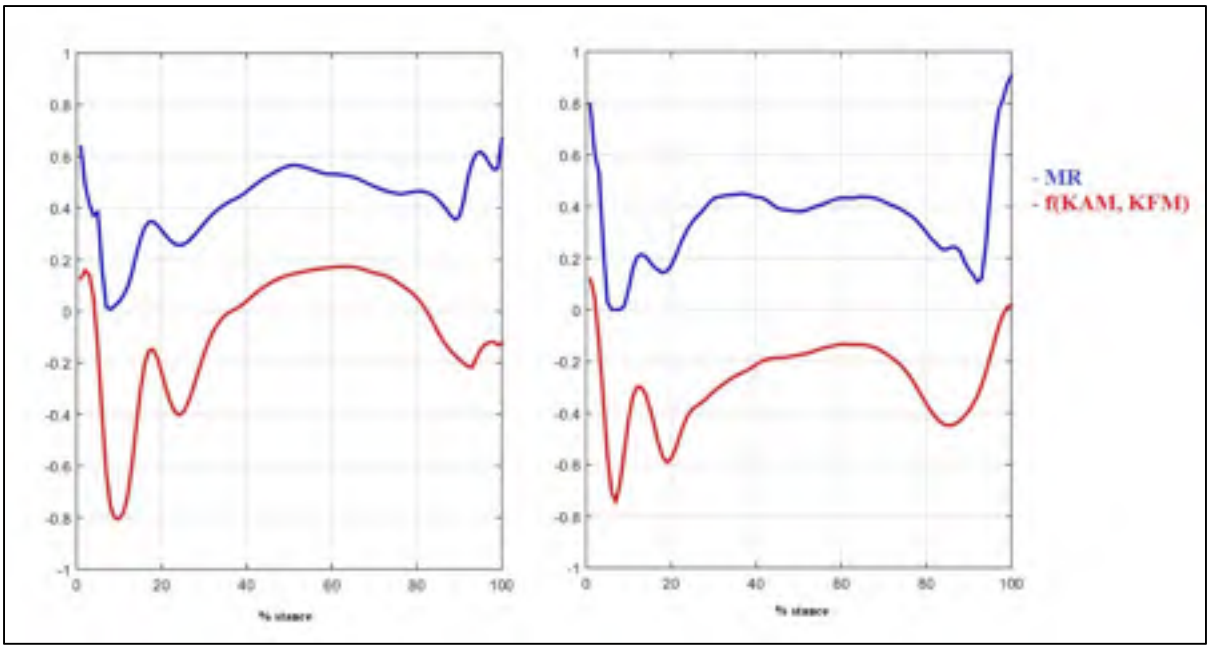

Figure 7-2 MR and $f(KAM, KFM) = \frac{KAM}{\max(KAM) \times (1 + \frac{KFM}{\max(KFM)})}$ demonstrating similar patterns in one healthy (left), and one OA (right) subject.

CONCLUSION

From a biomechanical point of view, the initiation and progression of OA are associated to changes in the contact regions of the joint and the excessive loading of the cartilage (Andriacchi et al., 2015; Clements et al., 2001; Vincent et al., 2012). In this project, we focused on the quantification of the contact point locations, contact forces, and the distribution of the contact forces in both OA and healthy joints.

This study revealed distinct patterns in the contact biomechanics of OA joints. The contact points are shifted medially in severe OA on both medial and lateral compartments. The contact forces are slightly lower in OA subjects but demonstrate higher media-to-total ratios. The media-to-total contact force ratio in OA joints is less influenced by adduction and flexion moments, and, contrary to healthy subjects, is influenced by the medial shift of the contact points in the medial condyle.

To achieve the objectives of this thesis, a method was developed for low-dose assessment of knee contact areas during weight-bearing squat which was also used for a clinical application to evaluate the effectiveness of a knee orthosis. In addition, a method was presented to introduce the subject-specific contact points into the musculoskeletal models with the potential of being used in EOS-based as well as MRI- or fluoroscopy-based kinematic tracking techniques.

The findings of this study add to our knowledge of the biomechanics of OA and introduced new approaches and techniques to study the biomechanical risk factors of OA and the mechanisms behind them.

ANNEX I

CONTACT POINT TRAJECTORY POLYNOMIALS

This appendix provides extra information regarding the polynomials of contact point trajectories as described in **chapter 5.**

This appendix provides information to construct the contact point trajectories of the linear contact point (LCP), sphere-on-plane (SPP), and personalized contact point (PCP) models in the relevant segment coordinate systems.

The knee kinematics constraints are based on virtual markers standing for the contact points and depending on the tibiofemoral extension/flexion angle θ.

The coordinates of the j^{th} virtual marker of the i^{th} segment about the three axes of the segment coordinate system are:

$$(r^s_{V_i^j})_{\mathbf{X}_i} = (a_n\theta^n)_{\mathbf{X}_i}$$
$$(r^s_{V_i^j})_{\mathbf{Y}_i} = (a_n\theta^n)_{\mathbf{Y}_i}$$
$$(r^s_{V_i^j})_{\mathbf{Z}_i} = (a_n\theta^n)_{\mathbf{Z}_i}$$

The coefficients of the polynomials for the three models are given in the following tables.

Model	Virtual marker	X			Y			Z		
		a_2	a_1	a_0	a_2	a_1	a_0	a_2	a_1	a_0
LCP	$r^s_{V_2^1}$	3.33E-06	4.65E-04	9.53E-03	2.88E-07	4.10E-05	-2.02E-02	-1.04E-20	-6.60E-19	-2.00E-02
	$r^s_{V_2^2}$	3.33E-06	4.65E-04	9.53E-03	2.88E-07	4.10E-05	-2.02E-02	1.04E-20	6.60E-19	2.00E-02
	$r^s_{V_4^1}$	6.04E-06	1.02E-03	9.53E-03	2.77E-06	-1.06E-04	-2.02E-02	-1.04E-20	-6.60E-19	-2.00E-02
	$r^s_{V_4^2}$	6.04E-06	1.02E-03	9.53E-03	2.77E-06	-1.06E-04	-2.02E-02	1.04E-20	6.60E-19	2.00E-02

Model	Virtual marker	X				Y				Z			
		a_3	a_2	a_1	a_0	a_3	a_2	a_1	a_0	a_3	a_2	a_1	a_0
SPP	$r^s_{V_2^1}$	-2.99E-08	-6.16E-06	-1.14E-04	-4.97E-03	4.74E-22	1.25E-20	6.56E-19	-2.02E-02	-1.11E-08	-1.00E-06	3.74E-05	-2.23E-02
	$r^s_{V_2^2}$	6.77E-08	9.08E-06	6.42E-04	4.96E-03	-1.57E-21	-1.47E-19	-1.31E-18	-2.02E-02	-3.84E-08	-4.21E-06	-7.15E-05	2.24E-02
	$r^s_{V_4^1}$	-1.82E-08	-4.65E-09	3.63E-04	-4.99E-03	1.18E-08	3.86E-06	6.60E-06	-2.02E-02	4.40E-09	1.05E-07	-8.11E-05	-2.23E-02
	$r^s_{V_4^2}$	-1.71E-08	-4.38E-09	3.42E-04	5.01E-03	1.11E-08	3.64E-06	6.22E-06	-2.02E-02	4.14E-09	9.89E-08	-7.65E-05	2.23E-02

Model	**Virtual marker**	**X**			**Y**			**Z**		
		a_2	**a_1**	**a_0**	**a_2**	**a_1**	**a_0**	**a_2**	**a_1**	**a_0**
PCP-N1	$r^s_{V_2^1}$	3.02E-06	3.92E-04	1.50E-02	1.38E-06	1.31E-04	-1.63E-02	2.09E-06	1.87E-04	-6.44E-03
	$r^s_{V_2^2}$	-1.44E-06	3.21E-05	3.24E-03	-4.38E-07	7.72E-05	-1.27E-02	5.64E-07	-2.39E-04	9.20E-03
	$r^s_{V_4^1}$	4.81E-06	7.44E-04	1.53E-02	1.78E-06	-4.90E-06	-1.99E-02	2.26E-06	2.74E-04	-5.99E-03
	$r^s_{V_4^2}$	2.38E-06	5.25E-04	6.01E-03	1.22E-06	-4.89E-06	-1.50E-02	1.20E-06	-1.18E-04	1.02E-02
PCP-N2	$r^s_{V_2^1}$	2.26E-06	3.11E-04	8.22E-03	-4.95E-07	-1.40E-05	-1.66E-02	1.28E-06	1.06E-04	-1.26E-02
	$r^s_{V_2^2}$	7.63E-06	6.22E-04	2.66E-04	-8.43E-07	-3.98E-05	-1.92E-02	5.00E-06	2.77E-04	2.28E-02
	$r^s_{V_4^1}$	3.07E-06	5.51E-04	8.42E-03	1.95E-06	-4.76E-05	-1.58E-02	1.79E-06	1.87E-04	-1.23E-02
	$r^s_{V_4^2}$	4.34E-06	6.04E-04	2.44E-03	1.02E-06	-8.52E-05	-1.73E-02	4.23E-06	2.85E-04	2.37E-02
PCP-N3	$r^s_{V_2^1}$	-3.48E-07	1.75E-05	1.38E-02	3.89E-07	2.72E-05	-1.71E-02	1.15E-06	6.33E-05	-9.64E-03
	$r^s_{V_2^2}$	1.50E-06	2.45E-04	1.00E-02	4.42E-07	1.04E-04	-1.35E-02	-1.47E-06	-3.22E-04	1.03E-02
	$r^s_{V_4^1}$	3.14E-06	6.05E-04	1.43E-02	2.73E-06	6.81E-05	-1.75E-02	1.35E-06	1.26E-04	-9.45E-03
	$r^s_{V_4^2}$	3.12E-06	5.90E-04	1.03E-02	1.94E-06	3.29E-05	-1.42E-02	-1.65E-06	-3.09E-04	1.04E-02

Model	Virtual marker	X			Y			Z		
		a_2	a_1	a_0	a_2	a_1	a_0	a_2	a_1	a_0
PCP-N4	$r^s_{V_2^1}$	6.25E-06	5.09E-04	1.79E-02	9.72E-08	2.85E-05	-1.95E-02	-1.69E-07	3.44E-05	-1.18E-02
	$r^s_{V_2^2}$	2.78E-06	4.27E-04	1.01E-02	-8.21E-07	-1.20E-06	-1.76E-02	4.13E-06	2.97E-04	2.75E-02
	$r^s_{V_4^1}$	4.87E-06	8.14E-04	1.79E-02	2.01E-06	1.31E-06	-1.97E-02	1.65E-07	5.40E-05	-1.26E-02
	$r^s_{V_4^2}$	-2.05E-06	3.08E-04	9.34E-03	3.75E-06	9.64E-05	-1.90E-02	4.90E-06	2.98E-04	2.67E-02
PCP-N5	$r^s_{V_2^1}$	-1.79E-06	1.11E-04	1.71E-02	-1.65E-06	-5.13E-05	-2.49E-02	-3.95E-06	-2.00E-04	-1.52E-02
	$r^s_{V_2^2}$	6.34E-06	5.60E-04	9.00E-03	1.80E-06	1.60E-04	-2.25E-02	-2.51E-06	-3.19E-04	2.47E-02
	$r^s_{V_4^1}$	-8.30E-09	5.43E-04	1.70E-02	6.91E-06	2.19E-04	-2.53E-02	-3.14E-06	-7.04E-05	-1.51E-02
	$r^s_{V_4^2}$	3.76E-06	6.67E-04	1.07E-02	2.10E-06	4.06E-05	-1.97E-02	-2.77E-06	-2.57E-04	2.51E-02
PCP-N6	$r^s_{V_2^1}$	1.34E-06	1.32E-04	8.63E-03	1.47E-07	1.04E-05	-2.18E-02	-9.98E-07	-6.11E-05	-1.88E-02
	$r^s_{V_2^2}$	4.94E-06	5.17E-04	6.37E-03	5.67E-07	6.03E-05	-1.85E-02	2.68E-07	4.85E-06	1.85E-02
	$r^s_{V_4^1}$	3.90E-06	6.59E-04	8.83E-03	1.56E-06	-1.01E-04	-2.33E-02	4.86E-07	1.46E-04	-1.73E-02
	$r^s_{V_4^2}$	3.71E-06	6.70E-04	5.86E-03	2.17E-06	1.94E-05	-1.78E-02	8.30E-07	1.20E-04	1.97E-02
PCP-N7	$r^s_{V_2^1}$	8.58E-07	1.13E-04	1.43E-02	1.66E-06	1.45E-04	-1.88E-02	3.57E-06	3.04E-04	-1.24E-02
	$r^s_{V_2^2}$	3.33E-07	2.80E-04	7.29E-03	-7.02E-07	6.56E-05	-1.64E-02	1.28E-06	-1.74E-04	1.55E-02
	$r^s_{V_4^1}$	3.43E-06	6.62E-04	1.33E-02	3.98E-06	1.37E-04	-1.80E-02	4.20E-06	4.17E-04	-1.29E-02
	$r^s_{V_4^2}$	7.12E-07	4.63E-04	7.33E-03	1.55E-06	1.38E-05	-1.65E-02	1.77E-06	-1.27E-04	1.51E-02

Model	Virtual marker	X			Y			Z		
		a_2	a_1	a_0	a_2	a_1	a_0	a_2	a_1	a_0
PCP-N8	$r^s_{V_2^1}$	1.11E-06	1.26E-04	1.22E-02	3.47E-07	4.35E-05	-1.82E-02	3.00E-07	4.71E-05	-1.21E-02
	$r^s_{V_2^2}$	8.53E-06	5.44E-04	1.07E-02	5.67E-06	3.83E-04	-1.56E-02	-1.39E-05	-9.69E-04	9.25E-03
	$r^s_{V_4^1}$	-3.68E-08	4.02E-04	1.22E-02	3.79E-06	1.26E-04	-1.89E-02	1.21E-06	1.08E-04	-1.14E-02
	$r^s_{V_4^2}$	6.08E-06	6.75E-04	1.05E-02	5.66E-06	2.76E-04	-1.58E-02	-1.37E-05	-9.53E-04	9.80E-03
PCP-N9	$r^s_{V_2^1}$	3.75E-06	4.58E-04	1.66E-02	6.11E-07	1.11E-04	-2.08E-02	8.80E-07	2.61E-04	-1.28E-02
	$r^s_{V_2^2}$	8.74E-06	8.41E-04	9.59E-03	1.24E-06	1.27E-04	-1.74E-02	-3.19E-06	-3.42E-04	2.08E-02
	$r^s_{V_4^1}$	6.66E-06	1.01E-03	1.74E-02	2.96E-06	-2.60E-05	-2.16E-02	2.23E-06	3.80E-04	-1.48E-02
	$r^s_{V_4^2}$	6.88E-06	9.27E-04	8.87E-03	2.33E-06	2.27E-05	-2.05E-02	-3.08E-06	-3.18E-04	1.89E-02
PCP-N10	$r^s_{V_2^1}$	5.66E-06	5.99E-04	1.58E-02	2.47E-07	3.49E-05	-2.06E-02	7.14E-07	1.08E-06	-1.47E-02
	$r^s_{V_2^2}$	-1.99E-07	1.46E-04	5.86E-03	-1.12E-06	-2.86E-05	-1.95E-02	2.91E-06	9.56E-05	2.08E-02
	$r^s_{V_4^1}$	8.19E-06	1.02E-03	1.57E-02	2.77E-06	-1.05E-05	-2.09E-02	1.54E-06	1.28E-04	-1.35E-02
	$r^s_{V_4^2}$	-1.55E-07	3.59E-04	6.17E-03	2.65E-06	4.08E-05	-1.78E-02	3.82E-06	2.23E-04	2.19E-02

This appendix also displays the trajectories of the contact points of all the OA and healthy subjects in the tibia transverse plane. For each subject, the medial and lateral contact point trajectories are plotted over the tibial plateau. The locations of contact points are marked at the following gait instances: The 1st and 2nd peaks of medial (Pk1 med, Pk2 med) and lateral (Pk1 lat, Pk2 lat) contact forces, heel strike (HS), toe off (TO), 0° (flx0) and 70° (flx70) knee flexions.

The contact point trajectories of all the subjects over the tibial plateau
PCP-N1 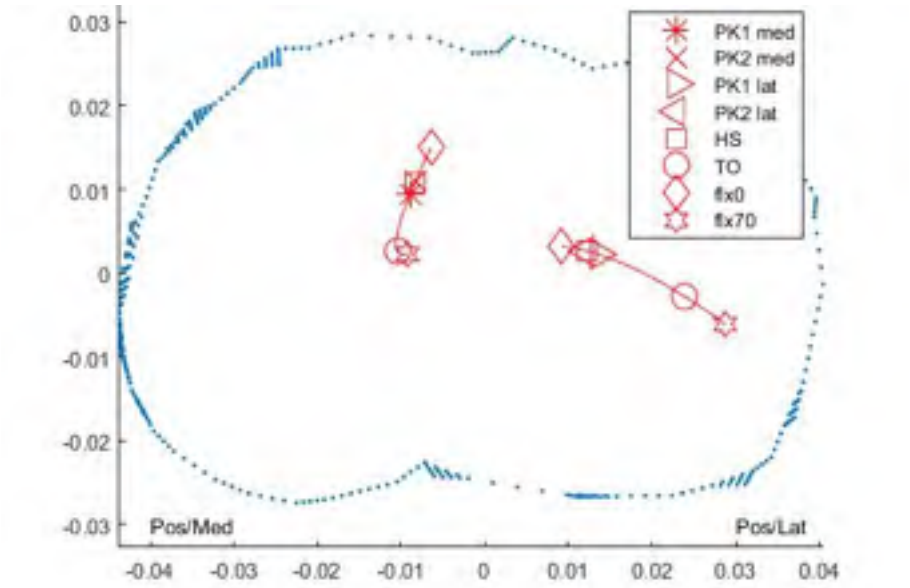

The contact point trajectories of all the subjects over the tibial plateau

PCP-N2

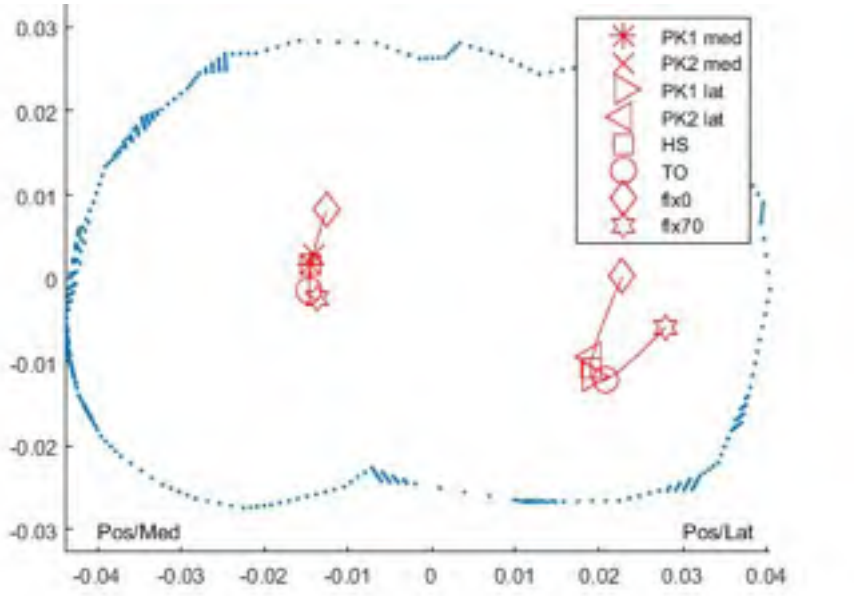

PCP-N3

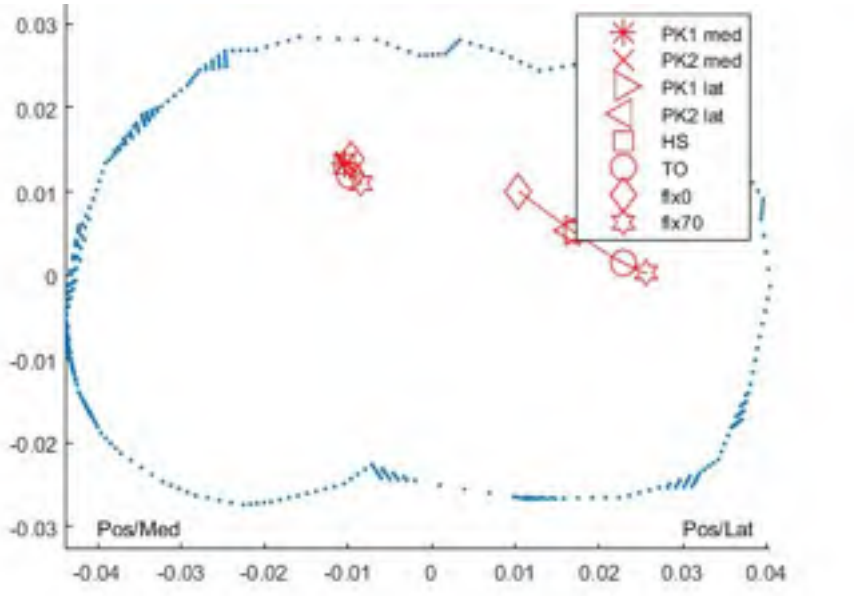

The contact point trajectories of all the subjects over the tibial plateau

PCP-N4

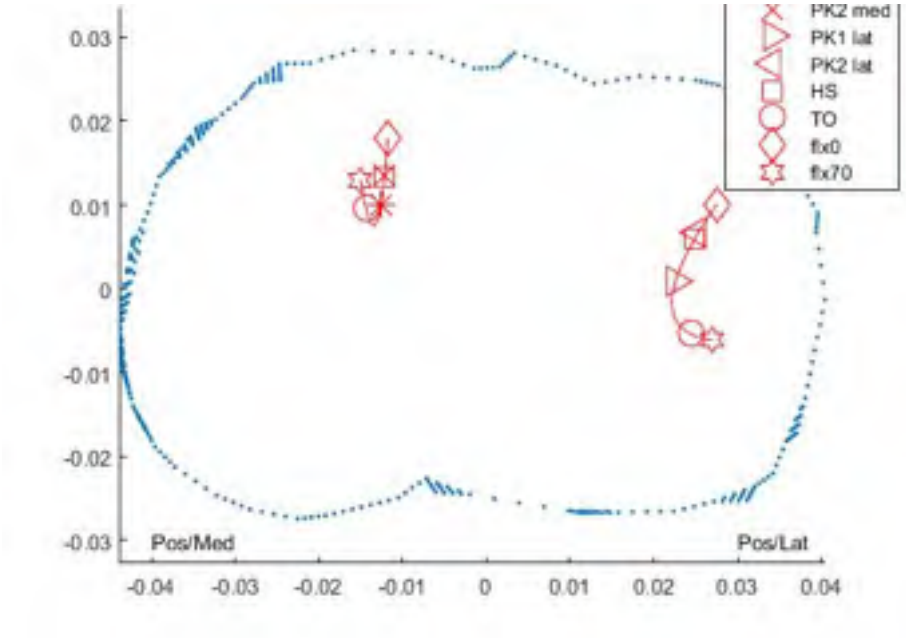

PCP-N5

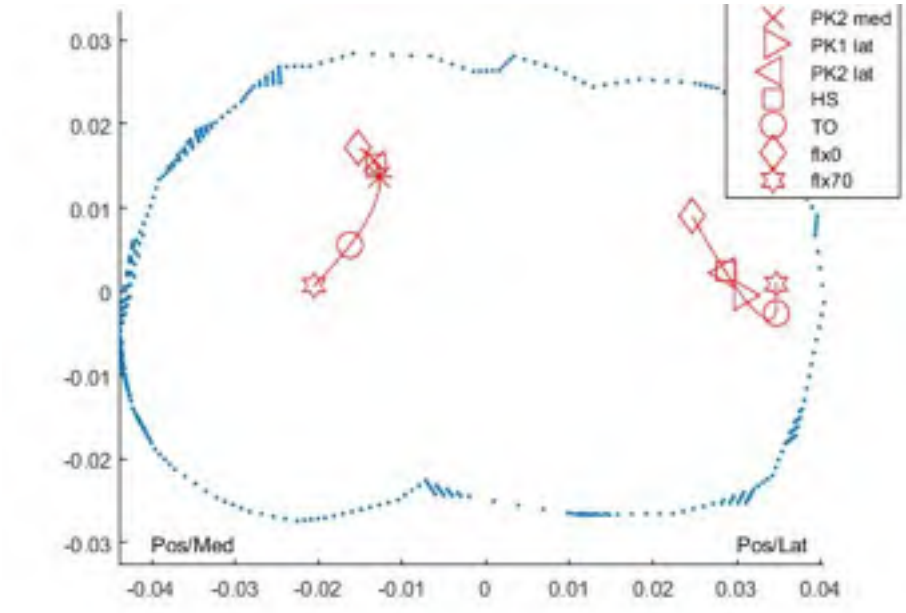

The contact point trajectories of all the subjects over the tibial plateau

PCP-N6

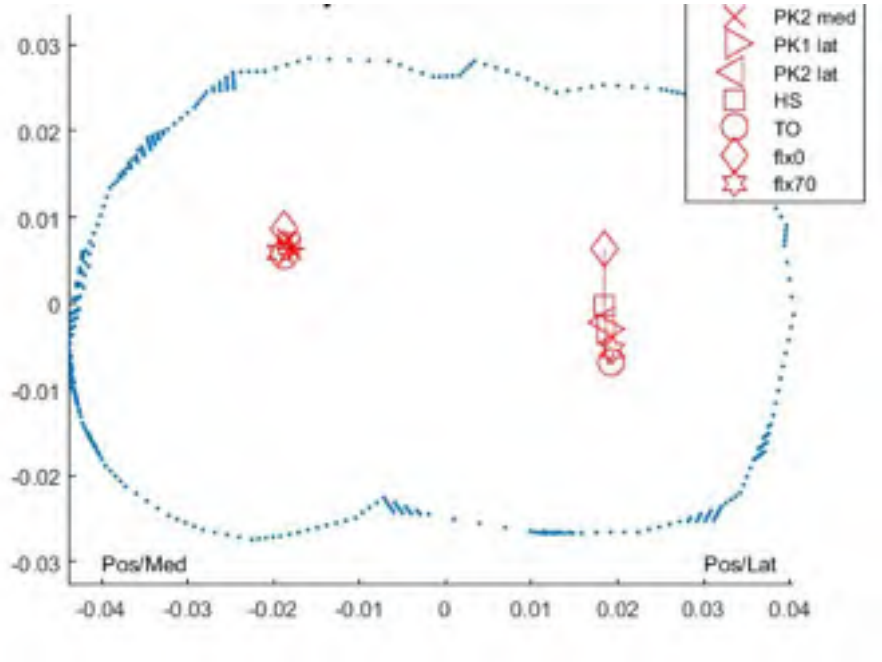

PCP-N7

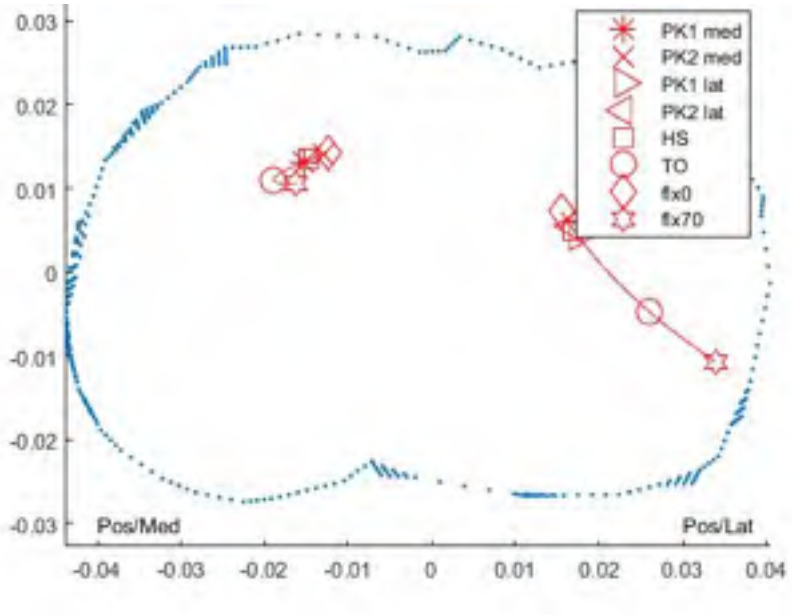

The contact point trajectories of all the subjects over the tibial plateau

PCP-N8

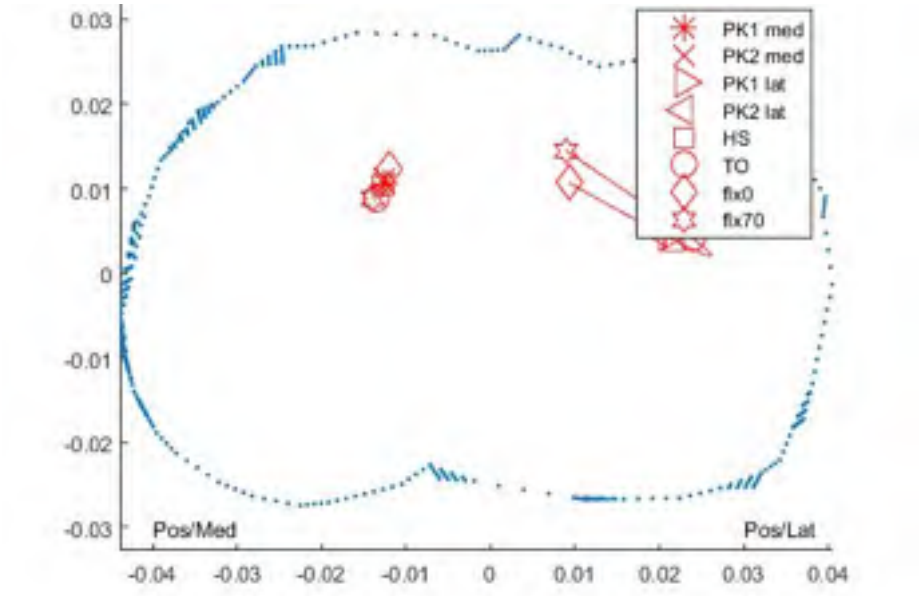

PCP-N9

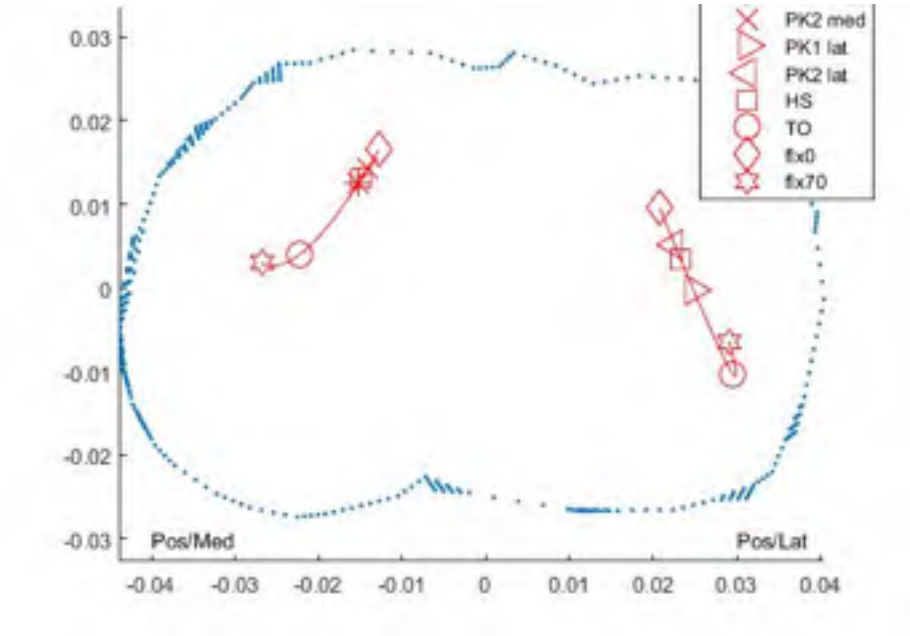

The contact point trajectories of all the subjects over the tibial plateau

PCP-N10

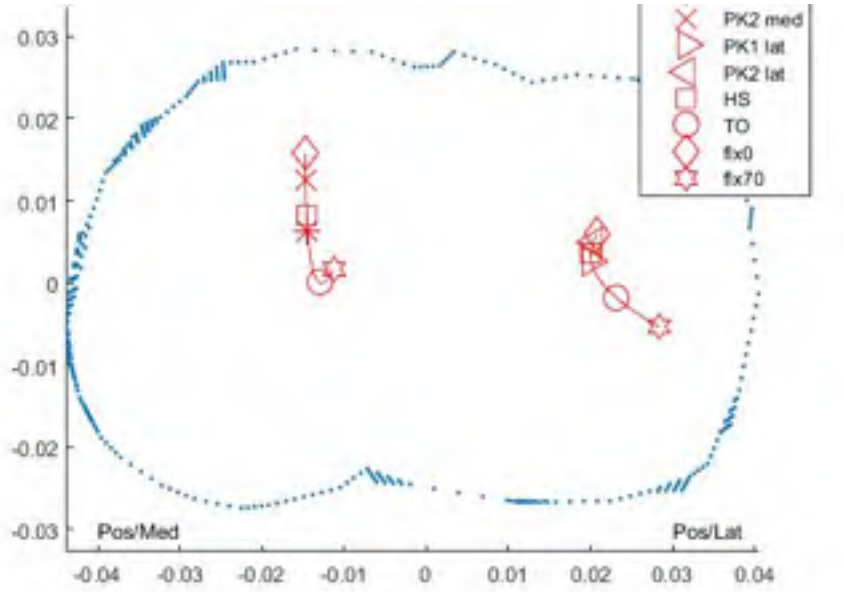

ANNEX II

INTERPOLATION MATRICES

This appendix provides interpolation matrices to express the polynomials of contact point trajectories presented in the annex I in the natural coordinate system to obtain the knee joint constraints as described in **chapter 5.**

The contact point trajectories $r^{s}_{V_i^j}$ as a function of θ in shank and thigh coordinate systems are presented in the annex (1). Once the $\mathbf{N}_i^{V_i^j}(\theta)$ are found, they would be replaced in Eq. (5.1) to form the five kinematic constraints.

$$\begin{pmatrix} \left(n_i^{V_i^j}(\theta)\right)_u \\ \left(n_i^{V_i^j}(\theta)\right)_v \\ \left(n_i^{V_i^j}(\theta)\right)_w \end{pmatrix} = \left[\mathbf{B}_i\right]^{-1} \mathbf{r}^{s}_{V_i^j}(\theta)$$

$$\mathbf{N}_i^{V_i^j}(\theta) = \left[\left(n_i^{V_i^j}(\theta)\right)_u \mathbf{E}_{3\times3} \quad \left(1+\left(n_i^{V_i^j}(\theta)\right)_v\right)\mathbf{E}_{3\times3} \quad -\left(n_i^{V_i^j}(\theta)\right)_v \mathbf{E}_{3\times3} \quad \left(n_i^{V_i^j}(\theta)\right)_w \mathbf{E}_{3\times3}\right]$$

with $\mathbf{E}_{3\times3}$ the identity matrix.

The other interpolation matrices in Eq (5.1) are built constant:

$$\mathbf{N}_i^{\mathbf{X}_i} = \left[\left(n_i^{\mathbf{X}_i}\right)_u \mathbf{E}_{3\text{x}3} \quad \left(n_i^{\mathbf{X}_i}\right)_v \mathbf{E}_{3\text{x}3} \quad -\left(n_i^{\mathbf{X}_i}\right)_v \mathbf{E}_{3\text{x}3} \quad \left(n_i^{\mathbf{X}_i}\right)_w \mathbf{E}_{3\text{x}3}\right]$$
$$\mathbf{N}_i^{\mathbf{Y}_i} = \left[\left(n_i^{\mathbf{Y}_i}\right)_u \mathbf{E}_{3\text{x}3} \quad \left(n_i^{\mathbf{Y}_i}\right)_v \mathbf{E}_{3\text{x}3} \quad -\left(n_i^{\mathbf{Y}_i}\right)_v \mathbf{E}_{3\text{x}3} \quad \left(n_i^{\mathbf{Y}_i}\right)_w \mathbf{E}_{3\text{x}3}\right],$$
$$\mathbf{N}_i^{\mathbf{Z}_i} = \left[\left(n_i^{\mathbf{Z}_i}\right)_u \mathbf{E}_{3\text{x}3} \quad \left(n_i^{\mathbf{Z}_i}\right)_v \mathbf{E}_{3\text{x}3} \quad -\left(n_i^{\mathbf{Z}_i}\right)_v \mathbf{E}_{3\text{x}3} \quad \left(n_i^{\mathbf{Z}_i}\right)_w \mathbf{E}_{3\text{x}3}\right]$$

$$\begin{bmatrix} \left(n_i^{\mathbf{X}_i}\right)_u & \left(n_i^{\mathbf{Y}_i}\right)_u & \left(n_i^{\mathbf{Z}_i}\right)_u \\ \left(n_i^{\mathbf{X}_i}\right)_v & \left(n_i^{\mathbf{Y}_i}\right)_v & \left(n_i^{\mathbf{Z}_i}\right)_v \\ \left(n_i^{\mathbf{X}_i}\right)_w & \left(n_i^{\mathbf{Y}_i}\right)_w & \left(n_i^{\mathbf{Z}_i}\right)_w \end{bmatrix} = \left[\mathbf{B}_i\right]^{-1}$$

The matrix $\mathbf{B}_i$ involved in the aforementioned interpolation matrix formulations stand for the orientation of the segment axes with respect to the axes of a non-orthonormal coordinate system based on the natural coordinates $\mathbf{Q}_i = \left[\mathbf{u}_i \quad \mathbf{r}_{P_i} \quad \mathbf{r}_{D_i} \quad \mathbf{w}_i\right]^T$ (R. Dumas et al., 2007):

$$\left[\mathbf{X}_i \quad \mathbf{Y}_i \quad \mathbf{Z}_i\right] = \left[\mathbf{u}_i \quad \underbrace{\mathbf{r}_{P_i} - \mathbf{r}_{D_i}}_{\mathbf{v}_i} \quad \mathbf{w}_i\right]\left[\mathbf{B}_i\right]^{-1}$$

$$\mathbf{B}_i = \begin{bmatrix} 1 & L_i \cos\gamma_i & \cos\beta_i \\ 0 & L_i \sin\gamma_i & \dfrac{\cos\alpha_i - \cos\beta_i \cos\gamma_i}{\sin\gamma_i} \\ 0 & 0 & \sqrt{1-\left(\cos\beta_i\right)^2 - \left(\dfrac{\cos\alpha_i - \cos\beta_i \cos\gamma_i}{\sin\gamma_i}\right)^2} \end{bmatrix},$$

with α_i, β_i, and γ_i the constant angles between the axes of the segment non-orthonormal coordinate system and L_i the constant length of the segment:

$$\begin{aligned} L_i &= \sqrt{\left(\mathbf{r}_{P_i} - \mathbf{r}_{D_i}\right)^2} \\ \alpha_i &= \cos^{-1}\left(\frac{\left(\mathbf{r}_{P_i} - \mathbf{r}_{D_i}\right)\cdot\mathbf{w}_i}{L_i}\right) \\ \beta_i &= \cos^{-1}\left(\mathbf{u}_i\cdot\mathbf{w}_i\right) \\ \gamma_i &= \cos^{-1}\left(\frac{\mathbf{u}_i\cdot\left(\mathbf{r}_{P_i} - \mathbf{r}_{D_i}\right)}{L_i}\right) \end{aligned}.$$

BIBLIOGRAPHY

Adouni, M., & Shirazi-Adl, A. (2014). Partitioning of knee joint internal forces in gait is dictated by the knee adduction angle and not by the knee adduction moment. *Journal of biomechanics, 47*(7), 1696-1703.

Ahmed, A., & Burke, D. (1983). In-vitro of measurement of static pressure distribution in synovial joints—Part I: Tibial surface of the knee. *Journal of Biomechanical Engineering, 105*(3), 216-225.

Aissaoui, R., Husse, S., Mecheri, H., Parent, G., & De Guise, J. (2006). Automatic filtering techniques for three-dimensional kinematics data using 3D motion capture system. Dans *Industrial Electronics, 2006 IEEE International Symposium on* (Vol. 1, pp. 614-619). IEEE.

Alton, F., Baldey, L., Caplan, S., & Morrissey, M. (1998). A kinematic comparison of overground and treadmill walking. *Clinical biomechanics, 13*(6), 434-440.

Amarantini, D., & Martin, L. (2004). A method to combine numerical optimization and EMG data for the estimation of joint moments under dynamic conditions. *Journal of biomechanics, 37*(9), 1393-1404.

Andersen, M. S., Benoit, D. L., Damsgaard, M., Ramsey, D. K., & Rasmussen, J. (2010). Do kinematic models reduce the effects of soft tissue artefacts in skin marker-based motion analysis? An in vivo study of knee kinematics. *Journal of biomechanics, 43*(2), 268-273.

Andersen, M. S., Damsgaard, M., & Rasmussen, J. (2009). Kinematic analysis of over-determinate biomechanical systems. *Computer methods in biomechanics and biomedical engineering, 12*(4), 371-384.

Anderst, W. J., & Tashman, S. (2003). A method to estimate in vivo dynamic articular surface interaction. *Journal of Biomechanics, 36*(9), 1291-1299.

Anderst, W. J., & Tashman, S. (2009). The association between velocity of the center of closest proximity on subchondral bones and osteoarthritis progression. *Journal of orthopaedic research, 27*(1), 71-77.

Andriacchi, T. P., Favre, J., Erhart-Hledik, J., & Chu, C. R. (2015). A systems view of risk factors for knee osteoarthritis reveals insights into the pathogenesis of the disease. *Annals of biomedical engineering, 43*(2), 376-387.

Andriacchi, T. P., Mündermann, A., Smith, R. L., Alexander, E. J., Dyrby, C. O., & Koo, S. (2004). A framework for the in vivo pathomechanics of osteoarthritis at the knee. *Annals of biomedical engineering, 32*(3), 447-457.

Arnold, E. M., Ward, S. R., Lieber, R. L., & Delp, S. L. (2010). A Model of the Lower Limb for Analysis of Human Movement. *Annals of biomedical engineering, 38*(2), 269-279.

Arokoski, J. P. A., Jurvelin, J. S., Väätäinen, U., & Helminen, H. J. (2000). Normal and pathological adaptations of articular cartilage. *Scand J Med Sci Sports,* (10), 186–198.

Asano, T., Akagi, M., Tanaka, K., Tamura, J., & Nakamura, T. (2001). In vivo three-dimensional knee kinematics using a biplanar image-matching technique. *Clinical Orthopaedics and Related Research, 388*, 157-166.

Astephen, J., & Deluzio, K. (2005). Changes in frontal plane dynamics and the loading response phase of the gait cycle are characteristic of severe knee osteoarthritis application of a multidimensional analysis technique. *Clinical biomechanics, 20*(2), 209-217.

Azmy, C., Guerard, S., Bonnet, X., Gabrielli, F., & Skalli, W. (2010). EOS® orthopaedic imaging system to study patellofemoral kinematics: Assessment of uncertainty. *Orthopaedics & Traumatology: Surgery & Research, 96*(1), 28-36.

Baliunas, A., Ryals, A., Hurwitz, D., Karrar, A., & Andriacchi, T. (2000). Gait adaptations associated with early radiographic tibiofemoral knee osteoarthritis. Dans *46th Annual Meeting Orthopaedic Research Society* (Vol. 260).

Baykan, M. A. (2009). Biologic Joint Reconstruction: Alternatives to Arthroplasty. *Journal of Sports Science and Medicine, 8*(2), 313-314.

Begon, M., Andersen, M. S., & Dumas, R. (2018). Multibody Kinematics Optimization for the Estimation of Upper and Lower Limb Human Joint Kinematics: A Systematized Methodological Review. *Journal of Biomechanical Engineering, 140*(3), 030801.

Bennell, K. L., Bowles, K.-A., Wang, Y., Cicuttini, F., Davies-Tuck, M., & Hinman, R. S. (2011). Higher dynamic medial knee load predicts greater cartilage loss over 12 months in medial knee osteoarthritis. *Annals of the rheumatic diseases, 70*(10), 1770-1774.

Benoit, D. L., Ramsey, D. K., Lamontagne, M., Xu, L., Wretenberg, P., & Renström, P. (2006). Effect of skin movement artifact on knee kinematics during gait and cutting motions measured in vivo. *Gait & posture, 24*(2), 152-164.

Beveridge, J. E., Shrive, N. G., & Frank, C. B. (2014). Repeatability and precision of a weighted centroid method for estimating dynamic in vivo tibiofemoral surface

interactions in sheep. *Computer methods in biomechanics and biomedical engineering, 17*(16), 1853-1863.

Bingham, J., Papannagari, R., Van de Velde, S., Gross, C., Gill, T., Felson, D., et al. (2008). In vivo cartilage contact deformation in the healthy human tibiofemoral joint. *Rheumatology, 47*(11), 1622-1627.

Blagojevic, M., Jinks, C., Jeffery, A., & Jordan, K. (2010). Risk factors for onset of osteoarthritis of the knee in older adults: a systematic review and meta-analysis. *Osteoarthritis and cartilage, 18*(1), 24-33.

Briem, K., Ramsey, D. K., Newcomb, W., Rudolph, K. S., & Snyder-Mackler, L. (2007). Effects of the amount of valgus correction for medial compartment knee osteoarthritis on clinical outcome, knee kinetics and muscle co-contraction after opening wedge high tibial osteotomy. *Journal of orthopaedic research, 25*(3), 311-318.

Butler, R. J., Marchesi, S., Royer, T., & Davis, I. S. (2007). The effect of a subject-specific amount of lateral wedge on knee mechanics in patients with medial knee osteoarthritis. *Journal of orthopaedic research, 25*(9), 1121-1127.

Chaibi, Y., Cresson, T., Aubert, B., Hausselle, J., Neyret, P., Hauger, O., et al. (2010). Fast 3D reconstruction of the lower limb using a parametric model and statistical inferences and clinical measurements calculation from biplanarX-rays. *Comput Methods Biomech Biomed Engin, 5*(15), 457-466.

Charlton, I., Tate, P., Smyth, P., & Roren, L. (2004). Repeatability of an optimised lower body model. *Gait & posture, 20*(2), 213-221.

Chav, R., Cresson, T., Kauffmann, C., & de Guise, J. A. (2009). Method for fast and accurate segmentation processing from prior shape: application to femoral head segmentation on x-ray images. Dans *SPIE Medical Imaging* (Vol. 7259, pp. 72594Y-72598). International Society for Optics and Photonics.

Chèze, L., Moissenet, F., & Dumas, R. (2015). State of the art and current limits of musculo-skeletal models for clinical applications. *Movement & Sport Sciences,* (4), 7-17.

Clément, J., de Guise, J. A., Fuentes, A., & Hagemeister, N. (2018). Comparison of soft tissue artifact and its effects on knee kinematics between non-obese and obese subjects performing a squatting activity recorded using an exoskeleton. *Gait & posture*.

Clément, J., Dumas, R., Hagemeister, N., & De Guise, J. A. (2015). Soft tissue artifact compensation in knee kinematics by multi-body optimization: performance of subject-specific knee joint models. *Journal of biomechanics, 48*(14), 3796-3802.

Clément, J., Dumas, R., Hagemeister, N., & De Guise, J. A. (2017). Can generic knee joint models improve the measurement of osteoarthritic knee kinematics during squatting activity? *Computer methods in biomechanics and biomedical engineering, 20*(1), 94-103.

Clément, J., Hagemeister, N., Aissaoui, R., & de Guise, J. A. (2014). Comparison of quasi-static and dynamic squats: A three-dimensional kinematic, kinetic and electromyographic study of the lower limbs. *Gait & Posture, 40*(1), 94-100.

Clements, K., Bee, Z., Crossingham, G., Adams, M., & Sharif, M. (2001). How severe must repetitive loading be to kill chondrocytes in articular cartilage? *Osteoarthritis and Cartilage, 9*(5), 499-507.

Collins, D. H. (1939). The pathology of osteoarthritis. *Br J Rheumatol,* (1), 248-262.

Creaby, M. (2015). It's not all about the knee adduction moment: the role of the knee flexion moment in medial knee joint loading. *Osteoarthritis and Cartilage, 23*(7), 1038-1040.

Cresson, T., Branchaud, D., Chav, R., Godbout, B., & de Guise, J. (2010). 3D shape reconstruction of bone from two x-ray images using 2D/3D non-rigid registration based on moving least-squares deformation. Dans *SPIE Medical Imaging* (pp. 76230F-76230F-76239). International Society for Optics and Photonics.

Cresson, T., Branchaud, D., Chav, R., Godbout, B., & de Guise, J. A. (2010). 3D shape reconstruction of bone from two x-ray images using 2D/3D non-rigid registration based on moving least-squares deformation. Dans *Medical Imaging: Image Processing* (pp. 76230F).

Cresson, T., Godbout, B., Branchaud, D., Chav, R., Gravel, P., & De Guise, J. A. (2008). Surface reconstruction from planar x-ray images using moving least squares. Dans *Engineering in Medicine and Biology Society, 2008. EMBS 2008. 30th Annual International Conference of the IEEE* (pp. 3967-3970). IEEE.

Crowninshield, R. D. (1978). Use of Optimization Techniques to Predict Muscle Forces. *Journal of Biomechanical Engineering, 100*(2), 88-92. doi: 10.1115/1.3426197.

da Luz, S. B., Modenese, L., Sancisi, N., Mills, P. M., Kennedy, B., Beck, B. R., et al. (2017). Feasibility of using MRIs to create subject-specific parallel-mechanism joint models. *Journal of biomechanics, 53*, 45-55.

De Jalon, J. G., & Bayo, E. (2012). *Kinematic and dynamic simulation of multibody systems: the real-time challenge*. Springer Science & Business Media.

DeFrate, L. E., Sun, H., Gill, T. J., Rubash, H. E., & Li, G. (2004). In vivo tibiofemoral contact analysis using 3D MRI-based knee models. *Journal of biomechanics, 37*(10), 1499-1504.

Delp, S. L., Loan, J. P., Hoy, M. G., Zajac, F. E., Topp, E. L., & Rosen, J. M. (1990). An interactive graphics-based model of the lower extremity to study orthopaedic surgical procedures. *IEEE Transactions on Biomedical engineering, 37*(8), 757-767.

DeMers, M. S., Pal, S., & Delp, S. L. (2014). Changes in tibiofemoral forces due to variations in muscle activity during walking. *Journal of orthopaedic research, 32*(6), 769-776.

Dennis, D. A., Mahfouz, M. R., Komistek, R. D., & Hoff, W. (2005). In vivo determination of normal and anterior cruciate ligament-deficient knee kinematics. *Journal of biomechanics, 38*(2), 241-253.

Deschênes, S., Charron, G., Beaudoin, G., Labelle, H., Dubois, J., Miron, M.-C., et al. (2010). Diagnostic imaging of spinal deformities: reducing patients radiation dose with a new slot-scanning X-ray imager. *Spine, 35*(9), 989-994.

Draganich, L., Andriacchi, T., & Andersson, G. (1987). Interaction between intrinsic knee mechanics and the knee extensor mechanism. *Journal of orthopaedic research, 5*(4), 539-547.

Dubousset, J., Charpak, G., Dorion, I., Skalli, W., Lavaste, F., Deguise, J., et al. (2005). A new 2D and 3D imaging approach to musculoskeletal physiology and pathology with low-dose radiation and the standing position: the EOS system. *Bulletin de l'Académie nationale de médecine, 189*(2), 287-297; discussion 297-300.

Dufour, M. (2007). Anatomie de l'appareil locomoteur: Tome 1, Membre inférieur. *Édition: 2e édition. Issy-les-Moulineaux: Elsevier Masson*.

Dumas, R., Aissaoui, R., Mitton, D., Skalli, W., & de Guise, J. A. (2005). Personalized body segment parameters from biplanar low-dose radiography. *IEEE Transactions on Biomedical engineering, 52*(10), 1756-1763.

Dumas, R., & Chèze, L. (2007). 3D inverse dynamics in non-orthonormal segment coordinate system. *Medical & Biological Engineering & Computing, 45*(3), 315-322. doi: 10.1007/s11517-006-0156-8.

Dumas, R., Cheze, L., & Moissenet, F. (2018). Multibody optimisations: from kinematic constraints to knee contact forces and ligament forces. Dans *Biomechanics of Anthropomorphic Systems*. Springer.

Duprey, S., Cheze, L., & Dumas, R. (2010). Influence of joint constraints on lower limb kinematics estimation from skin markers using global optimization. *Journal of biomechanics, 43*(14), 2858-2862.

El Habachi, A., Duprey, S., Cheze, L., & Dumas, R. (2015). A parallel mechanism of the shoulder—application to multi-body optimisation. *Multibody System Dynamics, 33*(4), 439-451.

Erdemir, A., McLean, S., Herzog, W., & van den Bogert, A. J. (2007). Model-based estimation of muscle forces exerted during movements. *Clinical biomechanics, 22*(2), 131-154.

Erhart, J. C., Dyrby, C. O., D'Lima, D. D., Colwell, C. W., & Andriacchi, T. P. (2010). Changes in in vivo knee loading with a variable-stiffness intervention shoe correlate with changes in the knee adduction moment. *Journal of orthopaedic research, 28*(12), 1548-1553.

Esculier, J.-F., Willy, R. W., Baggaley, M. W., Meardon, S. A., & Willson, J. D. (2017). Sex-specific kinetic and kinematic indicators of medial tibiofemoral force during walking and running. *The Knee, 24*(6), 1317-1325.

Farrokhi, S., Voycheck, C. A., Gustafson, J. A., Fitzgerald, G. K., & Tashman, S. (2016). Knee joint contact mechanics during downhill gait and its relationship with varus/valgus motion and muscle strength in patients with knee osteoarthritis. *The Knee, 23*(1), 49-56.

Farrokhi, S., Voycheck, C. A., Klatt, B. A., Gustafson, J. A., Tashman, S., & Fitzgerald, G. K. (2014). Altered tibiofemoral joint contact mechanics and kinematics in patients with knee osteoarthritis and episodic complaints of joint instability. *Clinical biomechanics, 29*(6), 629-635.

Favre, J., Erhart-Hledik, J. C., Blazek, K., Fasel, B., Gold, G. E., & Andriacchi, T. P. (2017). Anatomically Standardized Maps Reveal Distinct Patterns of Cartilage Thickness With Increasing Severity of Medial Compartment Knee Osteoarthritis. *Journal of orthopaedic research*.

Feikes, J., O'Connor, J., & Zavatsky, A. (2003). A constraint-based approach to modelling the mobility of the human knee joint. *Journal of biomechanics, 36*(1), 125-129.

Fiacchi, F., Zambianchi, F., Digennaro, V., Ricchiuto, I., Mugnai, R., & Catani, F. (2014). In vivo kinematics of medial unicompartmental osteoarthritic knees during activities of daily living. *The Knee, 21*, S10-S14.

Fox, A. J. S., Bedi, A., & Rodeo, S. A. (2009). The Basic Science of Articular Cartilage: Structure, Composition, and Function. *J of Sports health*, 461-468.

Fregly, B. J., D'Lima, D. D., & Colwell, C. W. (2009). Effective gait patterns for offloading the medial compartment of the knee. *Journal of orthopaedic research, 27*(8), 1016-1021.

Ganjikia, S., Duval, N., Yahia, L. H., & de Guise, J. (2000). Three-dimensional knee analyzer validation by simple fluoroscopic study. *The Knee, 7*(4), 221-231.

Gasparutto, X., Moissenet, F., Lafon, Y., Chèze, L., & Dumas, R. (2017). Kinematics of the Normal Knee during Dynamic Activities: A Synthesis of Data from Intracortical Pins and Biplane Imaging. *Applied Bionics and Biomechanics, 2017*.

Gasparutto, X., Sancisi, N., Jacquelin, E., Parenti-Castelli, V., & Dumas, R. (2015). Validation of a multi-body optimization with knee kinematic models including ligament constraints. *Journal of biomechanics, 48*(6), 1141-1146.

Gerus, P., Sartori, M., Besier, T. F., Fregly, B. J., Delp, S. L., Banks, S. A., et al. (2013). Subject-specific knee joint geometry improves predictions of medial tibiofemoral contact forces. *Journal of biomechanics, 46*(16), 2778-2786.

Giroux, M., Moissenet, F., & Dumas, R. (2013). EMG-based validation of musculo-skeletal models for gait analysis. *Computer methods in biomechanics and biomedical engineering, 16*(sup1), 152-154.

Grood, E. S., & Suntay, W. J. (1983). A Joint Coordinate System for the Clinical Description of Three-Dimensional Motions: Application to the Knee. *Journal of Biomechanical Engineering, 105*(2), 136-144.

Hagemeister, N., Parent, G., Van de Putte, M., St-Onge, N., Duval, N., & de Guise, J. (2005). A reproducible method for studying three-dimensional knee kinematics. *Journal of Biomechanics, 38*(9), 1926-1931.

Hamai, S., Moro-oka, T. a., Miura, H., Shimoto, T., Higaki, H., Fregly, B. J., et al. (2009). Knee kinematics in medial osteoarthritis during in vivo weight-bearing activities. *Journal of Orthopaedic Research, 27*(12), 1555-1561.

Herzog, W., & Federico, S. (2006). Considerations on joint and articular cartilage mechanics. *Biomechanics and modeling in mechanobiology, 5*(2), 64-81.

Higginson, J. S., Ramsay, J. W., & Buchanan, T. S. (2012). Hybrid models of the neuromusculoskeletal system improve subject-specificity. *Proceedings of the Institution of Mechanical Engineers, Part H: Journal of Engineering in Medicine, 226*(2), 113-119.

Hoshino, Y., & Tashman, S. (2012). Internal tibial rotation during in vivo, dynamic activity induces greater sliding of tibio-femoral joint contact on the medial compartment. *Knee Surgery, Sports Traumatology, Arthroscopy, 20*(7), 1268-1275.

Hurwitz, D., Ryals, A., Case, J., Block, J., & Andriacchi, T. (2002). The knee adduction moment during gait in subjects with knee osteoarthritis is more closely correlated with static alignment than radiographic disease severity, toe out angle and pain. *Journal of orthopaedic research, 20*(1), 101-107.

Jerbi, T., Burdin, V., Stindel, E., & Roux, C. (2011). A 2D 3D registration with low dose radiographic system for in vivo kinematic studies. Dans *Engineering in Medicine and Biology Society, EMBC, 2011 Annual International Conference of the IEEE* (pp. 8070-8073). IEEE.

Johal, P., Williams, A., Wragg, P., Hunt, D., & Gedroyc, W. (2005). Tibio-femoral movement in the living knee. A study of weight bearing and non-weight bearing knee kinematics using 'interventional'MRI. *Journal of Biomechanics, 38*(2), 269-276.

Johnson, F., Scarrow, P., & Waugh, W. (1981). Assessments of loads in the knee joint. *Medical and Biological Engineering and Computing, 19*(2), 237-243.

Jung, Y., Phan, C.-B., & Koo, S. (2016). Intra-Articular Knee Contact Force Estimation During Walking Using Force-Reaction Elements and Subject-Specific Joint Model. *Journal of Biomechanical Engineering, 138*(2), 021016.

Kanhonou, M. (2017). *Méthode d'évaluation fonctionnelle de la gonarthrose par étude de la pseudo-cinématique d'accroupissement* (École de technologie supérieure).

Kanhonou, M., Cresson, T., Clement, J., Lavoie, F., Hagemeister, N., & De Guise, J. A. (2014). 2D/3D registration of personalized knee 3D models on biplane radiographs for morpho-functional study. *International Journal of Computer Assisted Radiology and Surgery, 9*(1), 31-34.

Kaufman, K. R., Hughes, C., Morrey, B. F., Morrey, M., & An, K.-N. (2001). Gait characteristics of patients with knee osteoarthritis. *Journal of biomechanics, 34*(7), 907-915.

Kazemi, M., Dabiri, Y., & Li, L. P. (2013). Recent Advances in Computational Mechanics of the Human Knee Joint. *Computational and Mathematical Methods in Medicine*, 27 pages.

Kellgren, J., & Lawrence, J. (1957). Radiological assessment of osteo-arthrosis. *Annals of the rheumatic diseases, 16*(4), 494.

Kemp, G., Crossley, K. M., Wrigley, T. V., Metcalf, B. R., & Hinman, R. S. (2008). Reducing joint loading in medial knee osteoarthritis: shoes and canes. *Arthritis Care & Research, 59*(5), 609-614.

Kia, M., Stylianou, A. P., & Guess, T. M. (2014). Evaluation of a musculoskeletal model with prosthetic knee through six experimental gait trials. *Medical Engineering & Physics, 36*(3), 335-344.

Kim, H. J., Fernandez, J. W., Akbarshahi, M., Walter, J. P., Fregly, B. J., & Pandy, M. G. (2009). Evaluation of predicted knee-joint muscle forces during gait using an instrumented knee implant. *Journal of orthopaedic research, 27*(10), 1326-1331.

Kinney, A. L., Besier, T. F., Silder, A., Delp, S. L., D'Lima, D. D., & Fregly, B. J. (2013). Changes in in vivo knee contact forces through gait modification. *Journal of orthopaedic research, 31*(3), 434-440.

Kleemann, R. U., Krocker, D., Cedraro, A., Tuischer, J. N., & Duda, G. (2005). Altered cartilage mechanics and histology in knee osteoarthritis: relation to clinical assessment (ICRS Grade). *Osteoarthritis and Cartilage,* (13), 958-963.

Koo, S., Dyrby, C., & Andriacchi, T. (2007). Abnormal ambulation after ACL rupture affects knee articular cartilage spatial thinning pattern. Dans *Annual Meeting of the Orthopaedic Research Society* (pp. 11-14).

Koo, S., Rylander, J. H., & Andriacchi, T. P. (2011). Knee joint kinematics during walking influences the spatial cartilage thickness distribution in the knee. *Journal of biomechanics, 44*(7), 1405-1409.

Kumar, D., Manal, K. T., & Rudolph, K. S. (2013). Knee joint loading during gait in healthy controls and individuals with knee osteoarthritis. *Osteoarthritis and Cartilage, 21*(2), 298-305.

Kutzner, I., Küther, S., Heinlein, B., Dymke, J., Bender, A., Halder, A. M., et al. (2011). The effect of valgus braces on medial compartment load of the knee joint–in vivo load measurements in three subjects. *Journal of biomechanics, 44*(7), 1354-1360.

Kutzner, I., Trepczynski, A., Heller, M. O., & Bergmann, G. (2013). Knee adduction moment and medial contact force–facts about their correlation during gait. *PLoS One, 8*(12), e81036.

Leardini, A., Belvedere, C., Nardini, F., Sancisi, N., Conconi, M., & Parenti-Castelli, V. (2017). Kinematic models of lower limb joints for musculo-skeletal modelling and optimization in gait analysis. *Journal of biomechanics, 62*, 77-86.

Lemieux, P.-O., Cresson, T., & Aissaoui, R. (2016). Simultaneous estimation of the path, magnitude and orientation of the femorotibial contact forces using bone geometry constraints: an exploratory numerical study for the stance phase of gait. *Multibody System Dynamics*, 1-21.

Lenhart, R. L., Kaiser, J., Smith, C. R., & Thelen, D. G. (2015). Prediction and validation of load-dependent behavior of the tibiofemoral and patellofemoral joints during movement. *Annals of biomedical engineering, 43*(11), 2675-2685.

Lenhart, R. L., Smith, C. R., Vignos, M. F., Kaiser, J., Heiderscheit, B. C., & Thelen, D. G. (2015). Influence of step rate and quadriceps load distribution on patellofemoral cartilage contact pressures during running. *Journal of biomechanics, 48*(11), 2871-2878.

Lerner, Z. F., DeMers, M. S., Delp, S. L., & Browning, R. C. (2015). How tibiofemoral alignment and contact locations affect predictions of medial and lateral tibiofemoral contact forces. *Journal of biomechanics, 48*(4), 644-650.

Lerner ZF, D. M., Delp SL, Browning RC. (2015 Feb 26). How tibiofemoral alignment and contact locations affect predictions of medial and lateral tibiofemoral contact forces. *Journal of Biomechanics, 4*(48), 644-650.

Li, C., Hosseini, A., Tsai, T. Y., Kwon, Y. M., & Li, G. (2015). Articular contact kinematics of the knee before and after a cruciate retaining total knee arthroplasty. *Journal of orthopaedic research, 33*(3), 349-358.

Li, G., DeFrate, L. E., Park, S. E., Gill, T. J., & Rubash, H. E. (2005). In Vivo Articular Cartilage Contact Kinematics of the Knee An Investigation Using Dual-Orthogonal Fluoroscopy and Magnetic Resonance Image–Based Computer Models. *The American journal of sports medicine, 33*(1), 102-107.

Li, G., Lopez, O., & Rubash, H. (2001). Variability of a three-dimensional finite element model constructed using magnetic resonance images of a knee for joint contact stress analysis. *Journal of Biomechanical Engineering,* (123), 341–346.

Li, G., Wuerz, T. H., & DeFrate, L. E. (2004). Feasibility of using orthogonal fluoroscopic images to measure in vivo joint kinematics. *Journal of Biomechanical Engineering, 126*(2), 313-318.

Lin, Y.-C., Walter, J. P., Banks, S. A., Pandy, M. G., & Fregly, B. J. (2010). Simultaneous prediction of muscle and contact forces in the knee during gait. *Journal of biomechanics, 43*(5), 945-952.

Liu, M. Q., Anderson, F. C., Schwartz, M. H., & Delp, S. L. (2008). Muscle contributions to support and progression over a range of walking speeds. *Journal of biomechanics, 41*(15), 3243-3252.

Lloyd, D., & Buchanan, T. (1996). A model of load sharing between muscles and soft tissues at the human knee during static tasks. *TRANSACTIONS-AMERICAN SOCIETY OF MECHANICAL ENGINEERS JOURNAL OF BIOMECHANICAL ENGINEERING, 118*, 367-376.

Lloyd, D. G., & Besier, T. F. (2003). An EMG-driven musculoskeletal model to estimate muscle forces and knee joint moments in vivo. *Journal of biomechanics, 36*(6), 765-776.

Lohmander, L. S., Englund, P. M., Dahl, L. L., & Roos, E. M. (2007). The long-term consequence of anterior cruciate ligament and meniscus injuries: osteoarthritis. *The American journal of sports medicine, 35*(10), 1756-1769.

Lu, T.-W., & O'connor, J. (1999). Bone position estimation from skin marker co-ordinates using global optimisation with joint constraints. *Journal of biomechanics, 32*(2), 129-134.

Lucchetti, L., Cappozzo, A., Cappello, A., & Della Croce, U. (1998). Skin movement artefact assessment and compensation in the estimation of knee-joint kinematics. *Journal of biomechanics, 31*(11), 977-984.

Lundberg, H. J., Foucher, K. C., & Wimmer, M. A. (2009). A parametric approach to numerical modeling of TKR contact forces. *Journal of biomechanics, 42*(4), 541-545.

Lustig, S., Magnussen, R. A., Cheze, L., & Neyret, P. (2012). The KneeKG system: a review of the literature. *Knee Surgery, Sports Traumatology, Arthroscopy, 20*(4), 633-638.

Mainil-Varlet, P., Aigner, T., Brittberg, M., Bullough, P., Hollander, A., & Hunziker, E. (2003). Histological assessment of cartilage repair: a report by the Histology Endpoint Committee of the International Cartilage Repair Society (ICRS). *J Bone Joint Surg,* (4).

Manal, K., & Buchanan, T. S. (2013). An electromyogram-driven musculoskeletal model of the knee to predict in vivo joint contact forces during normal and novel gait patterns. *Journal of Biomechanical Engineering, 135*(2), 021014.

Manal, K., Gardinier, E., Buchanan, T. S., & Snyder-Mackler, L. (2015). A more informed evaluation of medial compartment loading: the combined use of the knee adduction and flexor moments. *Osteoarthritis and Cartilage, 23*(7), 1107-1111.

Mankin, H. J., Dorfman, H., Lippiello, L., & Zarins, A. (1971). Biochemical and metabolic abnormalities in articular cartilage from osteoarthritic human hips. II. Correlation of morphology with biochemical and metabolic data. *J Bone Joint Surg, 53A*(3), 523-537.

Marouane, H., Shirazi-Adl, A., & Adouni, M. (2016). Alterations in knee contact forces and centers in stance phase of gait: a detailed lower extremity musculoskeletal model. *Journal of biomechanics, 49*(2), 185-192.

Marra, M. A., Vanheule, V., Fluit, R., Koopman, B. H. F. J. M., Rasmussen, J., Verdonschot, N., et al. (2015). A Subject-Specific Musculoskeletal Modeling Framework to Predict In Vivo Mechanics of Total Knee Arthroplasty. *Journal of Biomechanical Engineering, 137*(2), 020904-020904-020912.

Martin, T. J., Medicine, C. o. S., & Fitness. (2001). Technical report: knee brace use in the young athlete. *Pediatrics, 108*(2), 503-507.

Matsuno, H., Kadowaki, K. M., & Tsuji, H. (1997). Generation II knee bracing for severe medial compartment osteoarthritis of the knee. *Archives of physical medicine and rehabilitation, 78*(7), 745-749.

Meireles, S., De Groote, F., Reeves, N., Verschueren, S., Maganaris, C., Luyten, F., et al. (2016). Knee contact forces are not altered in early knee osteoarthritis. *Gait & posture, 45*, 115-120.

Meyer, A. J., D'Lima, D. D., Besier, T. F., Lloyd, D. G., Colwell, C. W., & Fregly, B. J. (2013). Are external knee load and EMG measures accurate indicators of internal knee contact forces during gait? *Journal of orthopaedic research, 31*(6), 921-929.

Miyazaki, T., Wada, M., Kawahara, H., Sato, M., Baba, H., & Shimada, S. (2002). Dynamic load at baseline can predict radiographic disease progression in medial compartment knee osteoarthritis. *Annals of the rheumatic diseases, 61*(7), 617-622.

Moissenet, F., Cheze, L., & Dumas, R. (2017). Individual muscle contributions to ground reaction and to joint contact, ligament and bone forces during normal gait. *Multibody System Dynamics, 40*(2), 193-211.

Moissenet, F., Chèze, L., & Dumas, R. (2012). Anatomical kinematic constraints: consequences on musculo-tendon forces and joint reactions. *Multibody System Dynamics, 28*(1), 125-141.

Moissenet, F., Chèze, L., & Dumas, R. (2014). A 3D lower limb musculoskeletal model for simultaneous estimation of musculo-tendon, joint contact, ligament and bone forces during gait. *Journal of biomechanics, 47*(1), 50-58.

Moissenet, F., Chèze, L., & Dumas, R. (2014). Introduction of a set of EMG-based muscular activations in a multi-objective optimisation when solving the muscular redundancy problem during gait. *Computer methods in biomechanics and biomedical engineering, 17*(sup1), 132-133.

Moissenet, F., Chèze, L., & Dumas, R. (2016a). Contribution of individual musculo-tendon forces to the axial compression force of the femur during normal gait. *Movement & Sport Sciences,* (3), 63-69.

Moissenet, F., Chèze, L., & Dumas, R. (2016b). Influence of the level of muscular redundancy on the validity of a musculoskeletal model. *Journal of Biomechanical Engineering, 138*(2), 021019.

Moissenet, F., Giroux, M., Chèze, L., & Dumas, R. (2015). Validity of a musculoskeletal model using two different geometries for estimating hip contact forces during normal walking. *Computer methods in biomechanics and biomedical engineering, 18*(sup1), 2000-2001.

Moro-oka, T.-a., Hamai, S., Miura, H., Shimoto, T., Higaki, H., Fregly, B. J., et al. (2007). Can magnetic resonance imaging–derived bone models be used for accurate motion measurement with single-plane three-dimensional shape registration? *Journal of Orthopaedic Research, 25*(7), 867-872.

Moro-oka, T. a., Hamai, S., Miura, H., Shimoto, T., Higaki, H., Fregly, B. J., et al. (2008). Dynamic activity dependence of in vivo normal knee kinematics. *Journal of Orthopaedic Research, 26*(4), 428-434.

Morrison, J. (1970). The mechanics of the knee joint in relation to normal walking. *Journal of biomechanics, 3*(1), 51-61.

Moyer, R., Birmingham, T., Bryant, D., Giffin, J., Marriott, K., & Leitch, K. (2015). Biomechanical effects of valgus knee bracing: a systematic review and meta-analysis. *Osteoarthritis and Cartilage, 23*(2), 178-188.

Murray, M. P., Drought, A. B., & Kory, R. C. (1964). Walking patterns of normal men. *JBJS, 46*(2), 335-360.

Nisell, R., Németh, G., & Ohlsén, H. (1986). Joint forces in extension of the knee: analysis of a mechanical model. *Acta Orthopaedica Scandinavica, 57*(1), 41-46.

Nissan, M. (1980). Review of some basic assumptions in knee biomechanics. *Journal of biomechanics, 13*(4), 375-381.

Norkin, C. C., & White, D. J. (2016). *Measurement of joint motion: a guide to goniometry*. FA Davis.

Parenti-Castelli, V., & Sancisi, N. (2013). Synthesis of spatial mechanisms to model human joints. Dans *21st century kinematics* (pp. 49-84). Springer.

Pritzker, K. P. H., S, G., Jimenez, S. A., & Ostergaard, K. (2005). Osteoarthritis cartilage histopathology: grading and staging. *Osteoarthritis and Cartilage*.

Prodromos, C., Andriacchi, T., & Galante, J. (1985). A relationship between gait and clinical changes following high tibial osteotomy. *JBJS, 67*(8), 1188-1194.

Prodromos, C. C., Andriacchi, T., & Galante, J. (1985). A relationship between gait and clinical changes following high tibial osteotomy. *The Journal of bone and joint surgery. American volume, 67*(8), 1188-1194.

Qi, W., Hosseini, A., Tsai, T.-Y., Li, J.-S., Rubash, H. E., & Li, G. (2013). In vivo kinematics of the knee during weight bearing high flexion. *Journal of biomechanics, 46*(9), 1576-1582.

Saliba, C. M., Brandon, S. C., & Deluzio, K. J. (2017a). Sensitivity of medial and lateral knee contact force predictions to frontal plane alignment and contact locations. *Journal of biomechanics*.

Saliba, C. M., Brandon, S. C., & Deluzio, K. J. (2017b). Sensitivity of medial and lateral knee contact force predictions to frontal plane alignment and contact locations. *Journal of biomechanics, 57*, 125-130.

Sancisi, N., Gasparutto, X., Parenti-Castelli, V., & Dumas, R. (2017). A multi-body optimization framework with a knee kinematic model including articular contacts and ligaments. *Meccanica, 52*(3), 695-711.

Sartori, M., Farina, D., & Lloyd, D. G. (2014). Hybrid neuromusculoskeletal modeling to best track joint moments using a balance between muscle excitations derived from electromyograms and optimization. *Journal of biomechanics, 47*(15), 3613-3621.

Sati, M., de Guise, J. A., Larouche, S., & Drouin, G. (1996). Quantitative assessment of skin-bone movement at the knee. *The Knee, 3*(3), 121-138.

Scheys, L., Desloovere, K., Spaepen, A., Suetens, P., & Jonkers, I. (2011). Calculating gait kinematics using MR-based kinematic models. *Gait & posture, 33*(2), 158-164.

Schiphof, D., Boers, M., & Bierma-Zeinstra, S. M. (2008). Differences in descriptions of Kellgren and Lawrence grades of knee osteoarthritis. *Annals of the rheumatic diseases, 67*(7), 1034-1036.

Schipplein, O., & Andriacchi, T. (1991). Interaction between active and passive knee stabilizers during level walking. *Journal of orthopaedic research, 9*(1), 113-119.

Schnitzer, T. J., Popovich, J. M., Andersson, G. B., & Andriacchi, T. P. (1993). Effect of piroxicam on gait in patients with osteoarthritis of the knee. *Arthritis & Rheumatology, 36*(9), 1207-1213.

Setton, L. A., Elliott, D. M., & Mow, V. C. (1999). Altered mechanics of cartilage with osteoarthritis: human osteoarthritis and an experimental model of joint degeneration. *J of Osteoarthritis and Cartilage, 7*(1), 2-14.

Sharma, L., Lou, C., & Dunlop, D. D. (2000). The mechanism of the effect of obesity in knee osteoarthritis: the mediating role of malalignment. *Arthritis & Rheumatology, 43*(3), 568-575.

Shelburne, K. B., Torry, M. R., & Pandy, M. G. (2005). Muscle, ligament, and joint-contact forces at the knee during walking. *Medicine & Science in Sports & Exercise, 37*(11), 1948-1956.

Shelburne, K. B., Torry, M. R., & Pandy, M. G. (2006). Contributions of muscles, ligaments, and the ground-reaction force to tibiofemoral joint loading during normal gait. *Journal of orthopaedic research, 24*(10), 1983-1990.

Sholukha, V., Leardini, A., Salvia, P., Rooze, M., & Jan, S. V. S. (2006). Double-step registration of in vivo stereophotogrammetry with both in vitro 6-DOFs electrogoniometry and CT medical imaging. *Journal of biomechanics, 39*(11), 2087-2095.

Sophia Fox, A. J., Bedi, A., & Rodeo, S. A. (2009). The basic science of articular cartilage: structure, composition, and function. *Sports health, 1*(6), 461-468.

Sritharan, P., Lin, Y. C., Richardson, S. E., Crossley, K. M., Birmingham, T. B., & Pandy, M. G. (2017). Musculoskeletal loading in the symptomatic and asymptomatic knees of middle-aged osteoarthritis patients. *Journal of orthopaedic research, 35*(2), 321-330.

Stauffer, R. N., Chao, E. Y., & GyÖry, A. N. (1977). Biomechanical gait analysis of the diseased knee joint. *Clinical orthopaedics and related research, 126*, 246-255.

Strathy, G., Chao, E., & Laughman, R. (1983). Changes in knee function associated with treadmill ambulation. *Journal of biomechanics, 16*(7), 517521-519522.

Südhoff, I. (2007). *Modélisation géométrique et mécanique personnalisée de l'appareil locomoteur* (École de technologie supérieure).

Südhoff, I., Van Driessche, S., Laporte, S., de Guise, J. A., & Skalli, W. (2007). Comparing three attachment systems used to determine knee kinematics during gait. *Gait & posture, 25*(4), 533-543.

Tashman, S., & Anderst, W. (2003). In-Vivo Measurement of Dynamic Joint Motion Using High Speed Biplane Radiography and CT: Application to Canine ACL Deficiency. *J Biomech Eng, 2*(125), :238-245.

Thorp, L., Wimmer, M., Foucher, K., Sumner, D., Shakoor, N., & Block, J. (2010). The biomechanical effects of focused muscle training on medial knee loads in OA of the knee: a pilot, proof of concept study. *J Musculoskelet Neuronal Interact, 10*(2), 166-173.

Thorp, L. E., Sumner, D. R., Block, J. A., Moisio, K. C., Shott, S., & Wimmer, M. A. (2006). Knee joint loading differs in individuals with mild compared with moderate medial knee osteoarthritis. *Arthritis & Rheumatology, 54*(12), 3842-3849.

Thoumie, P., Sautreuil, P., & Mevellec, E. (2001). Orthèses de genou. Première partie: Évaluation des propriétés physiologiques à partir d'une revue de la littérature. Dans *Annales de réadaptation et de médecine physique* (Vol. 44, pp. 567-580). Elsevier.

Trepczynski, A., Kutzner, I., Bergmann, G., Taylor, W. R., & Heller, M. O. (2014). Modulation of the relationship between external knee adduction moments and medial joint contact forces across subjects and activities. *Arthritis & Rheumatology, 66*(5), 1218-1227.

Tsai, T.-Y., Li, J.-S., Wang, S., Li, P., Kwon, Y.-M., & Li, G. (2015). Principal component analysis in construction of 3D human knee joint models using a statistical shape model method. *Computer methods in biomechanics and biomedical engineering, 18*(7), 721-729.

Valente, G., Pitto, L., Stagni, R., & Taddei, F. (2015). Effect of lower-limb joint models on subject-specific musculoskeletal models and simulations of daily motor activities. *Journal of biomechanics, 48*(16), 4198-4205.

Vincent, K. R., Conrad, B. P., Fregly, B. J., & Vincent, H. K. (2012). The pathophysiology of osteoarthritis: a mechanical perspective on the knee joint. *PM&R, 4*(5), S3-S9.

Walker, P., Kurosawa, H., Rovick, J., & Zimmerman, R. (1985). External knee joint design based on normal motion. *J Rehabil Res Dev, 22*(1), 9-22.

Walter, J. P., D'Lima, D. D., Colwell, C. W., & Fregly, B. J. (2010). Decreased knee adduction moment does not guarantee decreased medial contact force during gait. *Journal of orthopaedic research, 28*(10), 1348-1354.

Walter, J. P., Korkmaz, N., Fregly, B. J., & Pandy, M. G. (2015). Contribution of tibiofemoral joint contact to net loads at the knee in gait. *Journal of orthopaedic research, 33*(7), 1054-1060.

Wang, J.-W., Kuo, K., Andriacchi, T., & Galante, J. (1990). The influence of walking mechanics and time on the results of proximal tibial osteotomy. *JBJS, 72*(6), 905-909.

Warabi, T., Kato, M., Kiriyama, K., Yoshida, T., & Kobayashi, N. (2005). Treadmill walking and overground walking of human subjects compared by recording sole-floor reaction force. *Neuroscience research, 53*(3), 343-348.

Winby, C. R., Lloyd, D. G., Besier, T. F., & Kirk, T. B. (2009). Muscle and external load contribution to knee joint contact loads during normal gait. *Journal of biomechanics, 42*(14), 2294-2300.

Yao, J., Lancianese, S. L., Hovinga, K. R., Lee, J., & Lerner, A. L. (2008). Magnetic resonance image analysis of meniscal translation and tibio-menisco-femoral contact in deep knee flexion. *Journal of Orthopaedic Research, 26*(5), 673-684.

Yue, B., Varadarajan, K. M., Moynihan, A. L., Liu, F., Rubash, H. E., & Li, G. (2011). Kinematics of medial osteoarthritic knees before and after posterior cruciate ligament retaining total knee arthroplasty. *Journal of Orthopaedic Research, 29*(1), 40-46.

Zeighami, A., Aissaoui, R., & Dumas, R. (2018). Knee medial and lateral contact forces in a musculoskeletal model with subject-specific contact point trajectories. *Journal of biomechanics*, 69, 138-145.

Zeighami, A., Dumas, R., & Aissaoui, R. (2016). Medial and lateral knee joint contact forces during gait in normal and osteoarthritic subjects. Dans *Virtual Physiological Human Conference VPH2016*.

Zeighami, A., Dumas, R., Kanhonou, M., Hagemeister, N., Lavoie, F., De Guise, J., et al. (2017). Tibio-femoral joint contact in healthy and osteoarthritic knees during quasi-static squat: A bi-planar X-ray analysis. *Journal of biomechanics, 53*, 178-184.

Zhao, D., Banks, S. A., Mitchell, K. H., D'Lima, D. D., Colwell, C. W., & Fregly, B. J. (2007). Correlation between the knee adduction torque and medial contact force for a variety of gait patterns. *Journal of orthopaedic research, 25*(6), 789-797.

Zheng, G., Gollmer, S., Schumann, S., Dong, X., Feilkas, T., & Ballester, M. A. G. (2009). A 2D/3D correspondence building method for reconstruction of a patient-specific 3D bone surface model using point distribution models and calibrated X-ray images. *Medical image analysis, 13*(6), 883-899.

Zheng, L., Li, K., Shetye, S., & Zhang, X. (2014). Integrating dynamic stereo-radiography and surface-based motion data for subject-specific musculoskeletal dynamic modeling. *Journal of biomechanics, 47*(12), 3217-3221.